INTERACTIONS BETWEEN WEAR MECHANISMS IN A WC-CO / TI-6AL-4V MACHINING TRIBOSYSTEM

A Thesis

by

QIONG BAI

Submitted to the Office of Graduate and Professional Studies of
Texas A&M University
in partial fulfillment of the requirements for the degree of

MASTER OF SCIENCE

Chair of Committee, Jyhwen Wang
Co-Chair of Committee, Mathew Kuttolamadom
Committee Member, Hong Liang
Head of Department, Andreas Polycarpou

December 2014

Major Subject: Mechanical Engineering

ABSTRACT

The objective of this research work is to identify and analyze the interactions between wear mechanisms in a machining tribosystem, and to confirm the fundamental physicochemical material interaction behavior through tribometric tests. The machining tribosystem under study involves dry turning of a grade-5 titanium alloy (Ti-6Al-4V) with uncoated tungsten carbide-cobalt (WC-Co) cutting tools. The interactions being investigated involve both individual and combinations of macro and microstructural wear mechanisms that are predominantly force or temperature controlled. The worn surface obtained with different operational parameters was examined by scanning electron microscopy (SEM) and the elemental composition analyzed by energy dispersive spectroscopy (EDS). In addition, the topology of worn tools was characterized through scanning by a 3D optical surface profiler. The following major interactions were observed. At low cutting speeds, adhesion of Ti alloy and minor diffusion of C was observed (which increases with feed). At medium and high cutting speeds, the increased diffusion of Co led to WC grain pullout forming a crater, followed by the adhesion of Ti alloy. Also, at low feed rates C pullout and deposition was observed. Machining process conditions were appropriately represented in ball-on-disc tribometric bench tests to study the associated material behavior – two of the above interactions were confirmed. These led to recommendations to increase productivity by enabling selective wear mechanism interactions (though parameter selection) thus providing a better understanding of how the final worn tool surface is generated.

ACKNOWLEDGEMENTS

First of all, I would like to express my deepest appreciation and gratitude to my advisor, Dr. Mathew Kuttolamadom, for guiding me into the areas of tribology and providing instructions and encouragement throughout my research. I also acknowledge Dr. Jyhwen Wang for being committee chair, and Dr. Hong Liang for being my committee member and discussion on my thesis. I specially thank Dr. Liang to provide experiment apparatus for my research.

I would also like to acknowledge my current group members, Rubens Schatz, and my friend, Zhujian Feng, for their assistance, support and friendship. I am always grateful to our graduate advisor, Dr. Daniel McAdams, and our department secretary, Tandilyn Phillips. I appreciate their help and patience during my graduate study in TAMU.

Finally, I devote my deepest appreciation to my parents, my brother, and all my cousins. Without their love, support and understanding, this thesis would have been impossible.

TABLE OF CONTENTS

Page

Page

Page

LIST OF FIGURES

FIGURE Page

FIGURE Page

FIGURE Page

FIGURE Page

FIGURE Page

FIGURE Page

FIUGRE Page

LIST OF TABLES

1. INTRODUCTION

1.1 OBJECTIVE

The objective of this research work is to identify and analyze the interactions between wear mechanisms in a machining tribosystem, and to confirm the major fundamental physicochemical material interaction behavior through tribometric bench tests. The machining tribosystem under study involves dry turning of a grade-5 titanium alloy (Ti-6Al-4V) with uncoated tungsten carbide-cobalt (WC-Co) cutting tools. Machining process conditions are appropriately represented in tribometric bench tests to study the associated fundamental material behavior. The interactions being investigated involve both individual and combinations of macro and microstructural wear mechanisms that are predominantly force or temperature controlled. This investigation is expected to provide a better understanding of how major wear mechanisms interact so as to generate the final worn tool surface.

1.2 MOTIVATION

The motivation for this work is to truly understand the interactions between wear mechanisms and how they affect the final wear state of a surface within a machining tribosystem. Traditionally, investigators have studied wear mechanisms individually [1, 2]. However, different wear mechanisms occur simultaneously in a tribosystem and they interact with each other. Therefore, studying the interactions between wear mechanisms is necessary to truly understand the wear process as a function of operational parameters - this will help predict and control the cumulative wear state of tool materials effectively. Figure 1-1 shows

the worn surface of a WC-Co tool used to turn Ti-6Al-4V which illustrates multiple wear mechanism interactions. A crater seems to have formed first due to the Co-binder leaving with the chips leading to WC grain pullout. A deficiency of C in the crater (and deposition on the tool surface) suggests high temperature dissolution. Additionally, Ti was found adhered over the crater, as well as C build-up over this adhered layer possibly due to C being "chemically-pulled" out of the tool body.

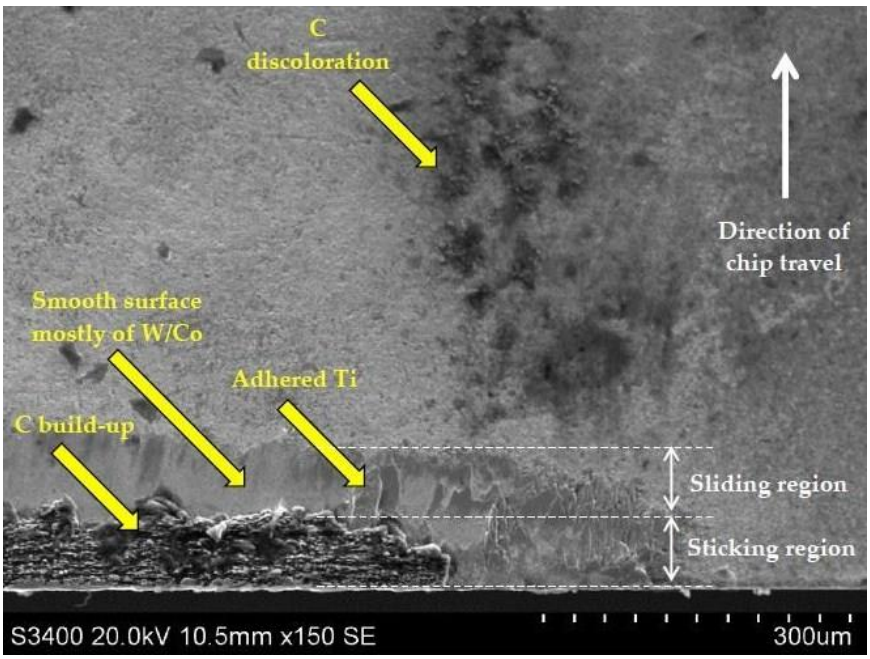

Figure 1-1 Worn surface of a WC-Co tool used to turn Ti-6Al-4V showing wear mechanism interactions. A crater was formed due to the Co-binder leaving with the chips, & eventual WC-grain pullout. C seems to have left the crater due to high temperature dissolution (and deposited on the surface). Further, Ti was found adhered as well as C built-up over the crater.

Thus, such complex wear mechanism interactions need to be thoroughly investigated to fundamentally understand the synergistic wear process. Tribometric bench tests will help investigate physicochemical material behavior in a simpler setting at the model-level test [3].

1.3 METHODOLOGY

From previously conducted machining experiments, the worn surface of cutting tools were analyzed by Scanning Electron Microscopy (SEM), Energy Dispersive Spectroscopy (EDS), and a 3D optical surface profiler to identify the dominant wear mechanisms at different process conditions. Then, the major interactions between them were identified and characterized as a function of process parameters. Finally, these mechanisms and interactions were mapped onto a feed rate vs. cutting speed plot.

For the associated tribometric tests, the machining tribosystem operational parameters were first scales as suitable for the pin-on-disc tribometer. After conducting tribometric tests, the worn surfaces of the ball were analyzed by SEM, EDS, and the 3D surface profiler. The observed wear mechanism interactions between the machining tribosystem (field-level test) and tribometric bench tests (model-level test) were compared to confirm the fundamental material physics. These analyses led to recommendations to increase productivity by enabling selective wear mechanism interactions (though parameter selection) thus providing better understanding of how the final worn tool surface is generated as a result of major wear mechanism interactions.

2. BACKGROUND AND LITERATURE REVIEW

This chapter covers the relevant background and literature review for this work. The topics are grouped into seven sections for organization:

1. The Machining Tribosystem
2. Tool Material: WC-Co
3. Types of Wear Mechanisms
4. Transitions in Wear Rate/Mechanisms and Interaction of Wear Mechanisms
5. Wear Testing and Selection of Testing Method

2.1 THE MACHINING TRIBOSYSTEM

The machining process can be analyzed as a tribosystem with a number of inputs and outputs, which are affected by disturbances as well as experience some losses. The machining tribosystem involves the turning of Ti-6Al-4V by WC-Co tools, where the region of interest is interface between the rake face of the cutting tool and the chip flowing over it.

Machining is one of the most popular manufacturing processes. It is used for primary processing and finishing of simple and complex profiles for low/high production volumes with good finishes. It is a complex process with two simultaneous operations: large strain plastic deformation in a concentrated shear zone and material transport with the chip flow [4]. As a result, the cutting tool experiences high forces which can be resolved into cutting force and thrust force on the tool or normal force and friction force on the tool/chip interface. Further, the tools also experience high temperatures (with increasing speed), often exceeding 1000°F. Figure 2-1 shows the typical turning operation. Figure 2-2 shows the schematic illustration of orthogonal turning where the chip is formed during the process.

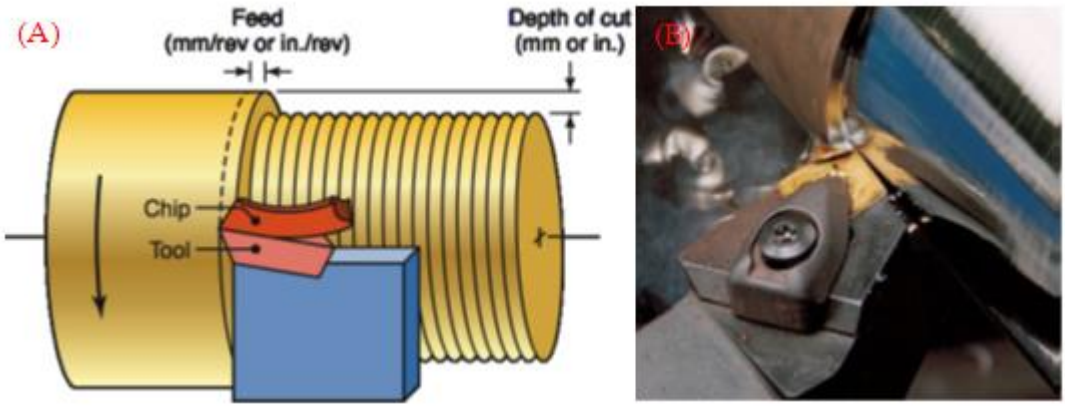

Figure 2-1 (A) Typical turning operation on a lathe [5]. (B) Image of an actual bar turning operation [6].

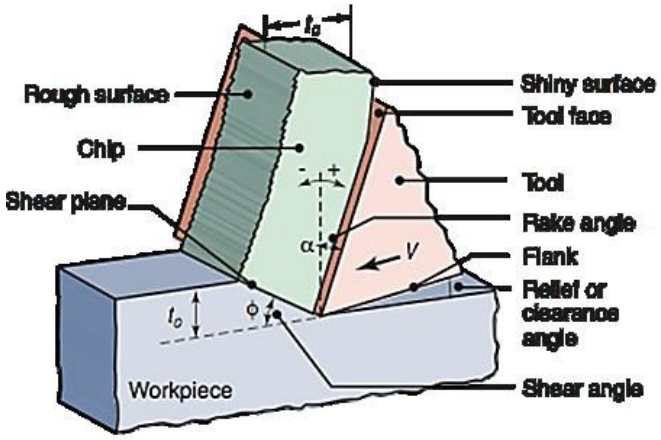

Figure 2-2 Schematic illustration of orthogonal turning where the chip formation process can be considered to be two-dimensional [5]

WC-Co tools can usually be classified into two categories, which are ISO K-type for non-ferrous metals and ISO P-type for ferrous metals. The K-type WC-Co is used in this study, which contains hard WC grains and about 4-12% Co binder. The important parameters of interest of WC-Co tool include Co concentration, carbide grain size, distribution of mean carbide grain size, bonding layer thickness, etc. which determine their hardness (decreases

with temperature) and transverse rupture strength. For instance, the increase of Co content will decrease the hardness and increase its transverse rupture strength (within limits).

Ti-6Al-4V is an alloy which has high fracture and corrosion resistance, and can maintain high strength at elevated temperatures. Thus, it is a good candidate material for the aerospace industry. However, titanium alloys also have some disadvantages, such as low modulus of elasticity, high chemical reactivity and low thermal conductivity [7]. The low thermal conductivity of Ti-6Al-4V results in the majority of the generated heat flowing into the tool edge (about 80%) [8], rather than the chip or the stock, thereby wearing out the cutting tool faster.

When a WC-Co tool cuts Ti-6Al-4V, common wear mechanisms observed are adhesive wear due to Ti-adhesion, diffusion of Co to the chips, loss of C, and WC grain pull-out. High cutting speed (and hence high temperatures) will accelerate the wear. By using coolant, one can effectively reduce the frictional force and the temperature and mitigate wear to an extent [9]. High pressure coolant application is recommended rather than flood coolant. Other common measures to mitigate wear include controlling the hard impurities/inclusions which contribute to abrasion, applying thermal spray coating on the tool surface [10], find the optimum cutter diameter to width of cut ratio, set range of recommended cutting speeds, feeds, spindle specifications [11], etc.

2.2 TOOL MATERIAL: WC-CO

Tungsten carbide (WC-Co) is a composite, which consists ceramic and metal. It is being regarded as one of the most commonly used carbide. Figure 2-3 shows the microstructure of WC-Co. The grains with different shapes are the WC grains and the white part is the Co.

WC-Co tools have been divided into two categories, which are the ISO K-type for non-ferrous metals and the ISO P-type for ferrous metals. The K-type tool substrates contain hard WC-grains and about 4-12% of the softer or ductile Co-binder [12].

It is common for cemented carbide tools to have a carbide grain size of less than l μm. There are two main phases in a WC-Co, which are the tungsten carbide phase, and the binder phase. Tungsten carbide has a highly anisotropic structure. With the crystal growth, the shapes of anisotropic crystal develop into flat triangular prisms or polygonal shapes with clear boundaries. WC has a quantitatively low crystal defect densities. This is because that the residual stresses during sintering are accommodated by plastic deformation. Figure 2-3 [13] shows the microstructure of WC displaying the straight faceted WC grain. Cobalt is the most commonly used bonding metal or binder, which separates the carbide particles. Unlike the WC grain, the Cobalt phase has relatively high dislocation density and stacking faults. The ductility from this cobalt phase and the strength provided by the harder WC phase give the high toughness of WC-Co [14]. A cobalt skeleton forms in the microstructure when the content of Co is high. Relevant physical and chemical properties of WC-Co are shown in Table 2-1.

Table 2-1 The physical and chemical properties of WC-Co [12, 15, 16]

	WC-Co	
Grain size	H10A (0.54μm)	H13A (0.61μm)
Composition	10.2% Co, 89.8% WC	10.2% Co, 89.8% WC
Density (g/cm3)	14.96	
Hardness (HV)	1675	1580
Young's Modulus (GPa)	580 [16]	
Ultimate Tensile Strength (MPa)	1440	

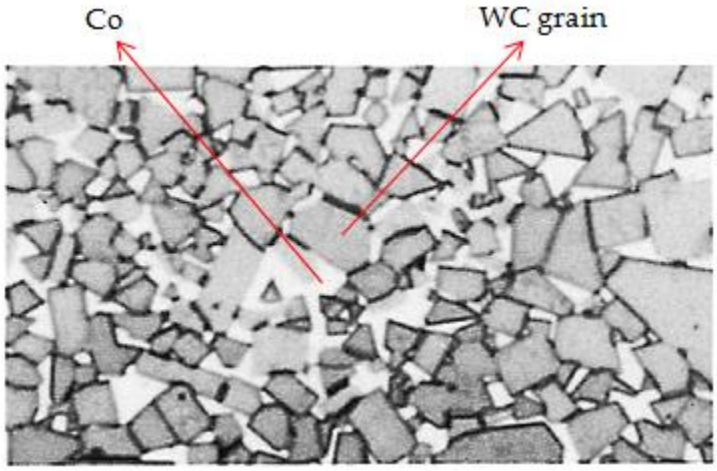

Figure 2-3 Typical microstrucute of WC-Co [13]

The typical mechanical properties of interest for WC-Co tool as a function of the percentage of Co content is shown in Figure 2-4 [5]. The important parameters of interest of WC-Co tools include cobalt concentration, carbide grain size, distribution of mean carbide grain size, and bonding layer thickness. These parameters determine their hardness (strength) and transverse rupture strength (TRS), which is a measure of its toughness, or the amount of

energy it can absorb until fracture. From Figure 2-4, the hardness decreases with the increase of the Co content. On the other side, the TRS increases with the increase of Co content.

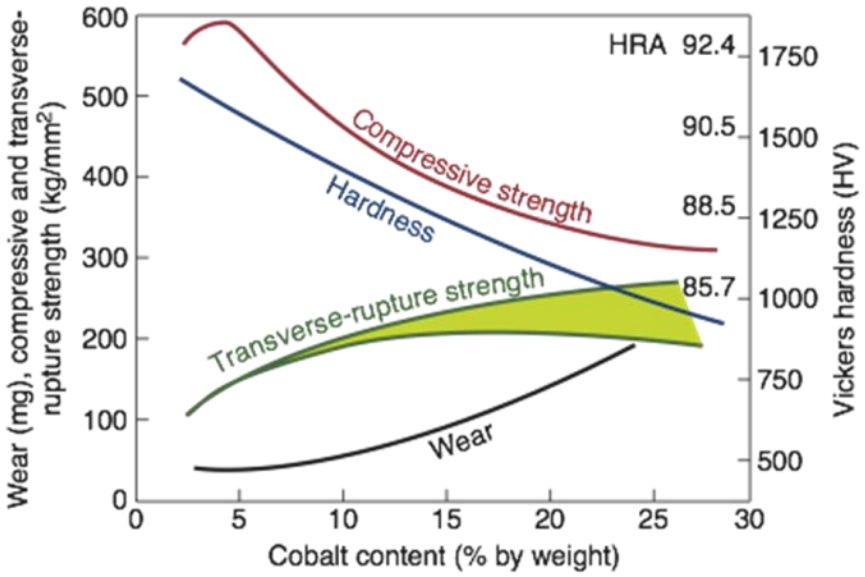

Figure 2-4 The effect of Cobalt content on the mechanical properties of WC-Co cutting tools [5].

Temperature is another factor affects the hardness of WC-Co cutting tool, in which the hardness of WC-Co decreases as the temperature increases. WC tools are generally usable until about 800 °C, beyond which the hot-hardness is unsatisfactory [5].

2.3 TYPES OF WEAR MECHANISMS

Common classifications of major wear mechanism include the following:

2.3.1 Adhesive Wear

Adhesive wear occurs when two materials rub together with sufficient force to cause the removal of material from the less wear resistant surface [17]. Adhesive wear refers to a type of wear generated by the sliding of one solid surface along another surface, as shown in

Figure 2-5 Schematic images of adhesive wear [19]. Adhesive wear denotes a wearing action in which no specific agency can be identified as the cause of the wear [18].

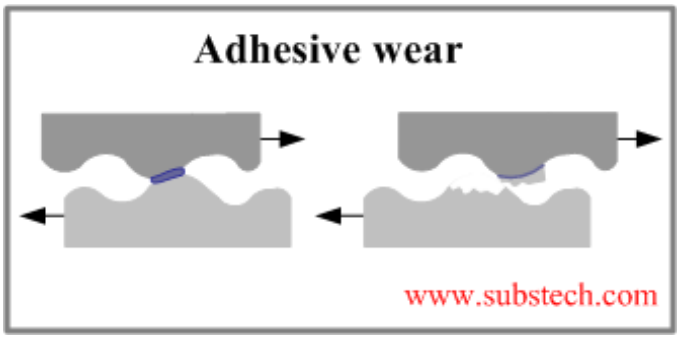

Figure 2-5 Schematic images of adhesive wear [19]

The wearing process involves many variables, which include bonding between substrates, materials dependence, conformity of contacting surface, few of which have been studied sufficiently to formulate wear equations that can be used by designers. Until now, the most widely publicized equation is Archard equation [20], which is

$$V = K_{ad}\frac{WL}{H} \qquad (2.1)$$

Where V is the wear volume, K_{ad} is called the wear coefficient for adhesive wear. W is the total normal load, L is the sliding distance, and H is the hardness of the softest contacting surfaces. The physical meaning of K_{ad} is the wear volume fraction at the plastic contact zone, and it is strongly affected by the material properties and the geometry of the zone in compression and shearing. In the adhesive wear of metals wear coefficient K_{ad} varies between 10^{-7} and 10^{-2} depending on the operating conditions and materials properties.

Adhesive wear mechanisms are analyzed separately for metals and polymers. In 60-40 brass versus tool steel, adhesive wear was observed via two different mechanisms, which produce two effects. One is local adherence of brass to steel, and the other is continuous film formed by zinc oxide. Also, it is indicated that transition between severe ear and mild wear is affected by sliding speed, applied load, and ambient temperature. Hard metals do not wear soft metals away. In the rubbing of polymers on metals, a thin film of polymer is established on the metal surface. The formation of this film can be divided by three steps, which are break-in regime, steady-state wear regime and severe wear regime. In this process, there are two factors in controlling the formation of transfer film. One is the surface finish orientation to sliding direction and the other surface cleanliness.

Some measures to prevent the adhesive wear, such as avoiding sliding similar material together. Also, comparison of the relative hardness of materials is needed considered before working. Lubrication is another way to reduce wear.

2.3.2 Abrasive Wear

According to the definition of ASTM [21], abrasive wear is due to the hard particles or hard protuberances that are forced against and move along a solid surface.

According to different types of contact, abrasion can be categorized two-body and three-body wear, which is as shown in Figure 2-6 [19]. Contact environments are classified as either free or constrained. From Blickensderfer test, the measurements of the loss in closed systems are higher than that in open system due to the higher loads in closed systems. Abrasion can be further categorized as being low stress, high stress, or gouging.

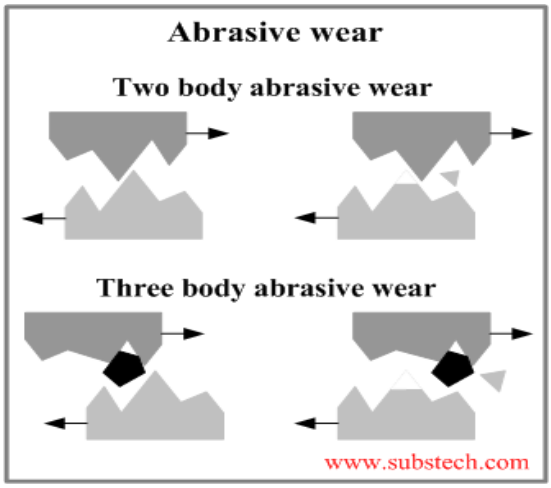

Figure 2-6 Schematic images of abrasive wear [19]

There is no single one mechanism can be used to completely clarify the loss during abrasion. The commonly proposed mechanisms include fracture, fatigue and melting. The abrasive wear is affected by many material properties, which include hardness of material, work harden, crystal structure and orientation, microstructure, fracture toughness, and alloying. For example, the harnesses were inverse linearly related to abrasive wear. The materials with constant hardness and different fracture toughness also shows different wear rate. The one with higher toughness shows a smaller wear rate. Alloying is another method to improve abrasion resistance.

The environment is also very critical to abrasive wear. The environmental factors include the type of abrasive and its characteristic, humidity speed of contact and corrosive effect. For instance, the hardness of the abrasive particles affects the abrasion rate of the subject materials. There is one analytical model [22] to explain the abrasive wear, which is expressed as the following.

$$V_g = \frac{2l\tan\alpha}{\pi H} W_g \qquad (2.2)$$

Where V_g is the volume of removed material, l is the distance travelling, α is the angle, H is the material's yield stress under indentation (hardness) and W_g is the individual load. It shows that the abrasive wear is proportional to the load, following the Archard equation [20], which was derived for adhesive wear and also very useful for abrasive wear.

2.3.3 Oxidative Wear

Oxidative wear refers to wear affected by material surface reaction with oxygen [22]. Oxidative wear has the surprising characteristic that although wear might be severe it is usually accompanied by a diminished coefficient of friction. Temperature and sliding speed are two critical factors in determining the rate of oxidative wear. It was found that when the temperature and sliding speed are high enough to increase the contact temperature by several hundred, the debris will change from iron to iron oxides. Archard [23] proposes an assumption that when the thick oxidative film was formed, the mild oxidative wear prevailed and if the thick film was broken down or worn away severe wear would happen. Figure 2-7 shows the formation of thick oxidative wear on piercing tools. The thickness is related to the temperature. Usually, the thickness of the oxidation thin film is larger at high temperature.

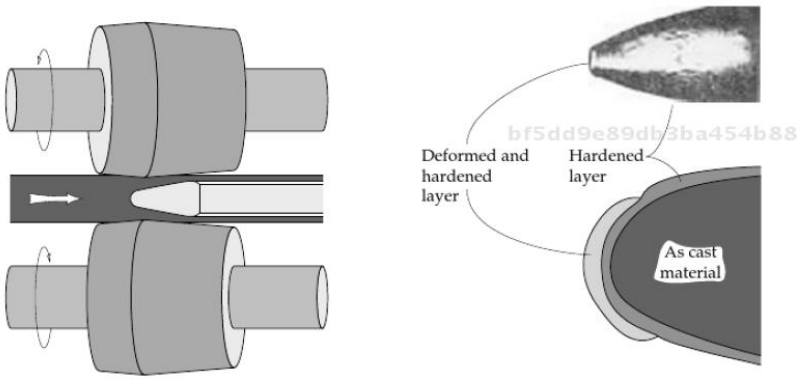

Figure 2-7 Thick oxidative wear scales formation on piercing tools [24]

2.3.4 Diffusive Wear

When two opposing surfaces maintain true contact at a high interface temperature, significant diffusion of chemical elements from one body to another can occur [22]. The rake face of a cutting tool close to the cutting edge in high-speed machining is a typical example. In this situation, there is almost the perfect contact between the tool and the metal chip due to the extreme contact stresses and very high temperatures, reaching 700°C or more [25]. The metal chip represents a continually refreshed supply of relatively pure metal while the tool is a high concentration mixture of some radically different elements, such as tungsten and carbon. Therefore, some elements in the tool have a trend to diffuse into the chip. When the surface material of the tool loses a vital alloying element it becomes soft and is very soon worn away by the chip [25]. Figure 2-8 shows the diffusion mechanism in cutting titanium alloys with tungsten carbide cutting tool. The diffusive wear rate of cutting tools depends on the tool material solubility limits in the workpiece. The rate of diffusive wear can be expressed as the following [26]:

$$W = (2C_s/\rho)(VD_0'/\pi x)^{\frac{1}{2}} \exp\left(-\frac{Q'}{2RT}\right) \quad (2.3)$$

Here, C_s is the concentration of Cobalt in the chip at the chip-tool interface (assumed equal to the original Cobalt concentration in the tool; ρ is the density of the diffusing substance; V is the velocity of the chip; x is the distance along the rake face, measured from the tip of the tool and D_0' and Q' are, respectively, the pre-exponential coefficient and the activation energy for the diffusion of Cobalt inside the Titanium alloy [26].

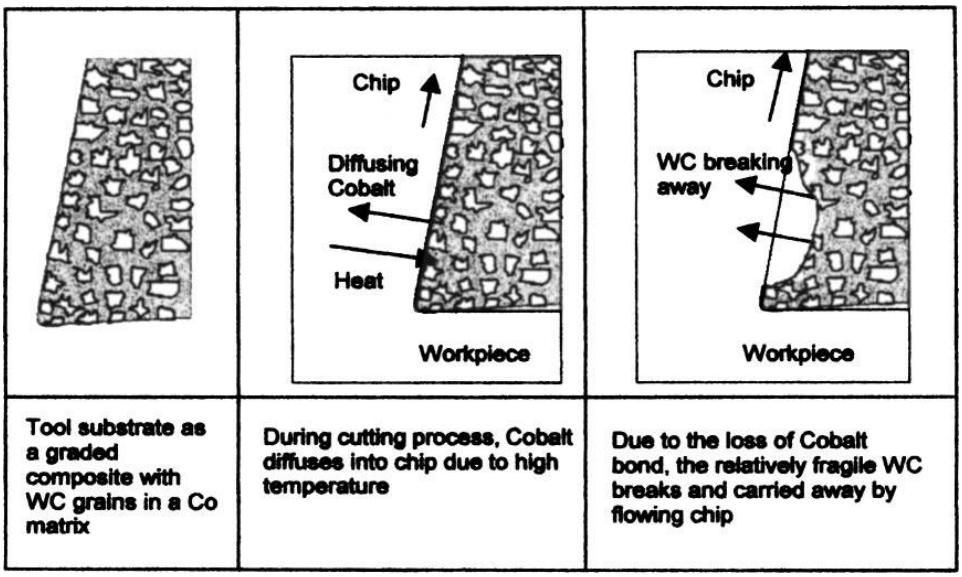

Figure 2-8 Diffusion mechanism in cutting titanium alloys with tungsten carbide tool [1]

Also, dissolution wear occurs when two materials with different chemical potentials are in contact with each other. To some extent, dissolution wear can be considered as a superset of diffusive wear and dissociation into elements [27, 28]. It is to be noted that there are a series of chemically driven mechanisms such as diffusion, dissolution and chemical reaction happening during the formation of a crater. All these chemically driven mechanisms can be

grouped together as "generalized dissolution." For a WC-Co tool machining a Ti-6Al-4V workpiece, this consists of the following processes:

- Dissociation of tool material into WC, and Co,
- Chemical reaction of these dissociated species with Ti-6Al-4V stock material,
- Atomic transport across the tool-chip interface (in both directions), and
- Diffusion of the dissociated species that have not been consumed.

2.3.5 Other Chemically Driven Wear Mechanisms

Besides the wear mechanisms above, other chemically driven wear mechanisms exist such as corrosive wear. Corrosive wear is the degradation of materials in which both corrosion and wear mechanisms are involved [18], which usually occurs in a corrosive environment caused by the chemical reaction. Figure 2-9 shows an example of corrosive wear, in which a corrosive layer is formed by the chemical reaction between Fe and H_2SO_4. When corrosive attack exists on the surfaces and the sliding action wears off the corroded surface film, corrosive wear occurs. If the corroded compounds formed are harder than the original material and it is loose particles, the wear rate accelerates. If the corroded compounds formed are softer, this acts to reduce the wear rate [29].

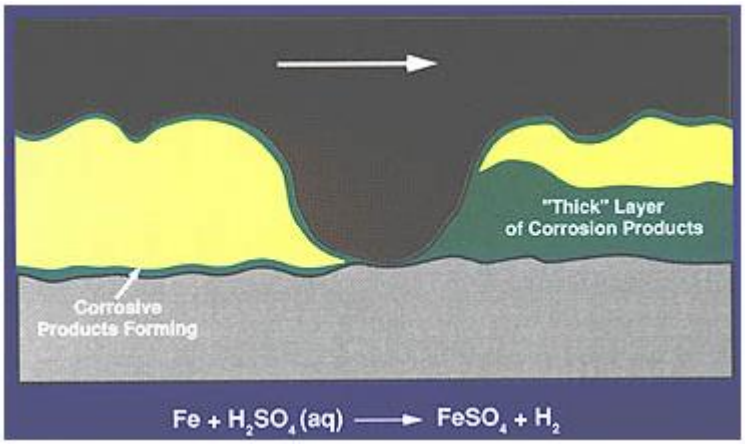

Figure 2-9 Schematic figure of corrosive wear,in which the corrosive products formed by chemical reaction [29].

2.4 TRANSITIONS IN WEAR RATE/MECHANISMS AND INTERACTIONS

Numerous researchers have studied the transition of wear mechanisms, which include (1) the transition in the dominance from one wear mechanism to another, and, (2) the transition (or change) of wear rate of one particular wear mechanism.

Relevant investigations on dominance transition from one wear mechanism to another include the following. Sasada [30] reported that the abrasive grain size has an effect on the transition between abrasive and adhesive wear. Okonkwo [31] reported that temperature affects the wear mechanism transition from adhesive wear to material removal by ploughing. Kagnaya [32] pointed out that the wear mechanisms of WC-Co tools cutting steels change from plastic deformation and micro-cracking of WC grain, to diffusive wear when increasing the sliding speed. At low sliding speeds, plastic deformation and micro-cracking of WC grain occurred, while diffusive wear occurred at high sliding speeds. Generally, the transitions of wear mechanisms are described by wear maps; and an example is shown in Figure 2-10. This wear map is for uncoated WC cutting tools when dry turning steel.

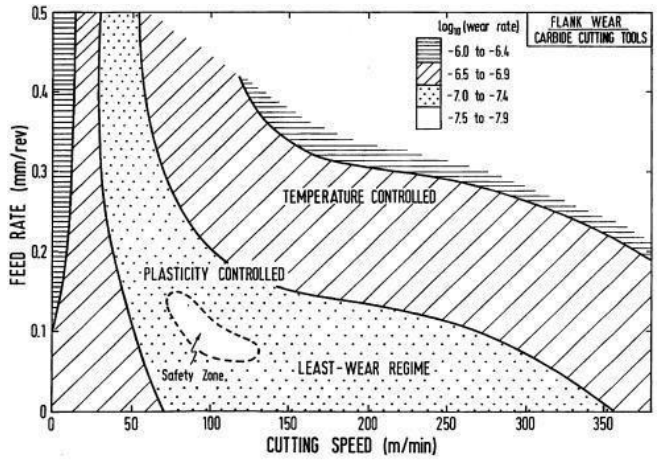

Figure 2-10 Wear map for uncoated WC cutting tools when dry turning steel [33].

Similarly, some relevant investigations on transition in wear rate include the following. For steel / tool steel pairs, Wang [34] and So [35] reported that increase in the load affects the rate of oxidative wear in steels from mild wear to severe wear in dry sliding. Okonkwo [31] reported that temperature is also a critical factor on change of rate of sliding wear of steel / tool steel pairs. For WC-Co, the wear rate decreases by decreasing the binder (Co) content and increasing the hardness [2]. For WC-Co, the wear rate increases by increasing the binder (Co) content [2] and increasing grain size [36]. Hsu [37], Xu [38], and Cho [39] investigated the effects of temperature and cutting speed on the wear rate transition of alumina. Figure 2-11 shows the plots of transitioning wear rate versus sliding time under different applied loads for alumina.

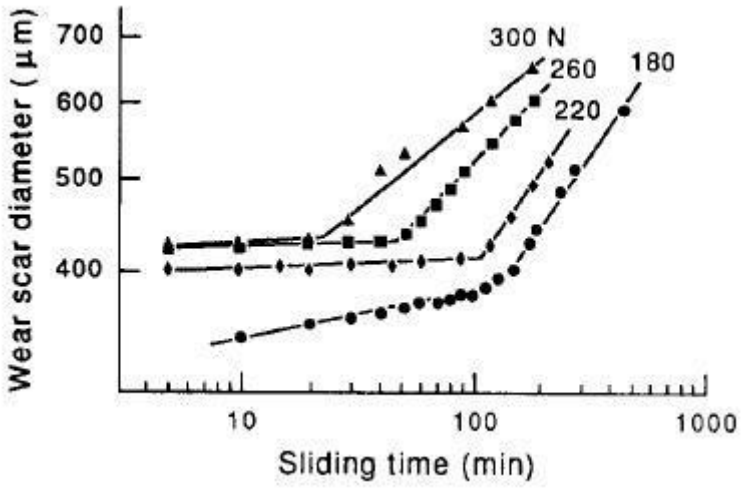

Figure 2-11 Log plot of wear scar diameter VS sliding time for 4 μm grain sized alumina under different applied loads [39].

However, there are no reports on the interactions among and between wear mechanisms. In reality, the final wear state of a surface is the result of a number of wear mechanisms occurring and synergistically interacting simultaneously. For instance, after the dominant wear mechanism changes from one to another, the former dominant wear mechanism may still be in effect. This means that more than one wear mechanisms may exist simultaneously. This research work will focus on addressing interactions between these wear mechanisms.

In order to analyze the interactions between wear mechanisms, these can be divided into force-controlled wear and temperature-controlled wear [40]. Force-controlled wear describes wear mainly governed by the process of deformation and fracturing. The deformation process has a substantial role in the overall wear process of ductile materials, and the fracturing process has a major role in the wear process of brittle materials. Force-controlled wear can be also called “mechanical wear”, which include adhesive wear, abrasive wear, etc. On the other hand, temperature-controlled wear describes the wear related to the change of

temperature. It can also refer to the wear became noticeable at high temperature, such as diffusive wear. In addition to diffusive wear, temperature-controlled wear include chemical wear, thermal wear, oxidation wear and so on.

When studying the collective wear of WC-Co tools, the interactions and dependency of each of these wear mechanisms with each other needs to be considered as well. The two main factors that affect chemically driven wear in machining are temperature and relative chemical affinity of the tool and workpiece material constituents. It is not straight forward to explicitly differentiate between force and temperature-controlled wear mechanisms as they occur simultaneously. This research is an attempt to investigate the interactions among and between them.

2.5 WEAR TESTINGS AND SELECTION OF TESTING METHODS

Wear testing is usually conducted by tribometer, which is an instrument that measures tribological quantities, such as coefficient of friction, friction force, and wear volume. Tribometers are often referred to the specific contact arrangement they simulate. Several arrangements exist, such as four ball [41, 42], pin-on-disc [43], block on ring [44], bouncing ball, SRV testing machine, reciprocal sliding wear test [45], twin disc, etc. The most common ones, such as four-ball method, pin-on-disc, block-on-ring and reciprocal testing, are briefly explained.

2.5.1 Common Wear Testing Methods

2.5.1.1 Four-Ball Method

Four-ball method is usually used to determine the measurement of properties of the most popular oil additive, such as lubricating grease. There are two arrangements for this test, which are Precision Scientific Company Four-Ball Test Arrangement and Falex Corporation (Roxanna) Four-Ball Test Arrangement, as shown in Figure 2-12 [41].

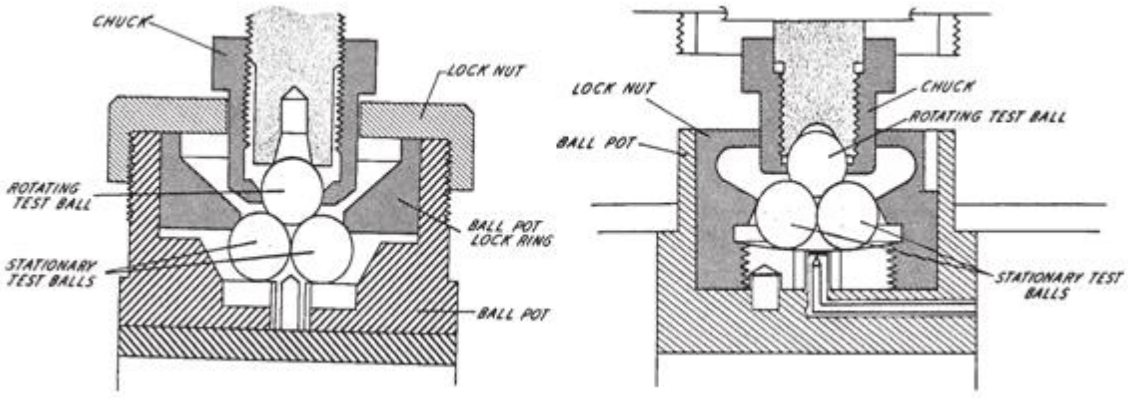

Figure 2-12 (left) Precision scientific company four ball test arrangement and (right) Falex corporation Four-ball test arrangement [41]

In each of the above two four-ball test arrangements, three 12.7 mm diameter steel balls are fixed together and the lubricant is covered on them to be evaluated. A fourth 12.7 mm diameter steel ball on the top is pressed with a force of 392 N into the cavity formed by the three clamped balls for three-point contact. The temperature of the lubricating grease specimen is regulated at 75°C and then the top ball is rotated at 1200 rpm for 60 min. Lubricants are compared by using the average size of the scar diameters worn on the three lower clamped balls [42].

2.5.1.2 Pin-on-Disc Method

Pin-on-Disc test [43] is used to determine the wear of materials during sliding. In pin-on-disc wear test, a pin with a tip is positioned perpendicular to a flat circular disk. In this test, either the disk specimen or the pin specimen is set to revolve about the disk center and the pin is pressed against the disk at a selected load. This test is conducted at a specified value of sliding distance, load and speed. The wear result is reported as volume loss.

Figure 2-13 shows a schematic drawing of pin-on-disc test arrangement, where F is applied normal load, R is radius of the wear track that is produced, d is diameter of the spherical top of the pin, D is Diameter of the disk and w is rotational speed.

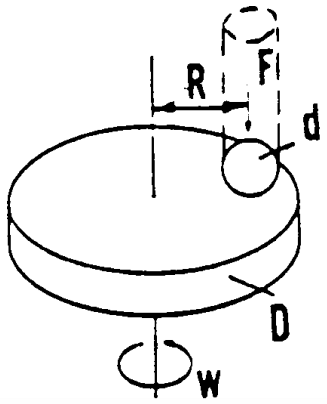

Figure 2-13 Arrangement of ball-on-disc test. The pin is stationary and the disc is rotating. [43]

The precision of this test depends on the test parameters chosen. The reproducibility of repeated tests on the same material will depend on material homogeneity and the interaction between machine and material.

2.5.1.3 Ball-on-Disc Wear Test

The ball-on-Disc apparatus tests the sliding wear and friction of the coatings. It consists mainly of a ball, and a horizontally rotating disc at the bottom of the ball as shown in Figure 2-14 [46]. The stationary ball was loaded by a dead weight on the top of the ball. The rotating disc was driven by a d.c. motor. The tangential force originated from the normal force was measured by a strain gauge. The experimental data were collected and displayed graphically using a microcomputer via an analogue-digital converter.

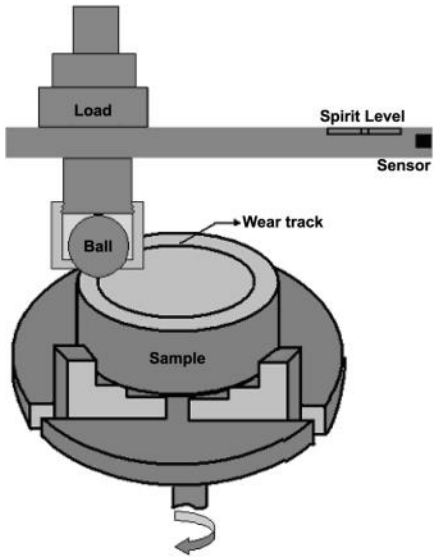

Figure 2-14 Schematic illustration of ball-on-disc test. The ball is stationary and the disc is rotating. [46]

2.5.1.4 Block-on-Ring Wear Test

Block-on-Ring test is used to determine sliding wear of various materials. The stationary block specimen is stationary and is applied a constant force while the ring specimen is rotating at a direction perpendicular to the ring's axis of rotation [44].Friction between these two specimen leads to the loss of material from both surfaces. This block-on-ring test is mainly used for metals. The test may be run at the loads, velocities, and temperatures which

simulate the service conditions with various lubricants and liquids. The volume loss in cubic millimeters for both the block and ring is used as the wear test results. The following is a typical test setup, as shown in Figure 2-15.

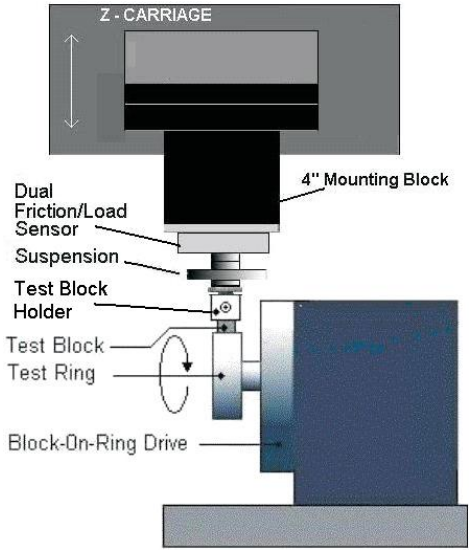

Figure 2-15 Arrangement of block-on-ring test [44]

2.5.1.5 Reciprocal Sliding Wear Test

The reciprocal sliding wear test [45] utilizes a flat lower specimen and a ball-shaped upper specimen are utilized and the ball-shaped upper specimen slides against the flat specimen in a linear, back and forth way under a prescribed set of conditions. In this test method, the load is applied vertically downward through the ball specimen against the horizontally mounted flat specimen. The normal load, stroke length, frequency of oscillation, test temperature, lubricant, and test duration are selected from one of two procedures given in Table 2-2.

Table 2-2 Parameters used for reciprocal sliding wear test

Procedure	Lube	Temp.	Applied load	Stroke length	Oscillating frequency	Duration
A	No	Ambient	25 N	10.0 mm	5.0 Hz	16min40sec
B	Yes	150 °C	200 N	10.0 mm	10.0 Hz	30min20sec

2.5.1.6 Pin-on-Drum Abrasive Wear Test

Pin-on-Drum test is used to study the wear that occurs during crushing and grinding of ore [47]. The test rig is shown in Figure 2-16Figure 2-16 Arrangement of pin-on-drum wear test [47]. A cylindrical pin specimen is moved over abrasive paper with sufficient load to abrade material from the specimen and crush the fixed abrasive grains. The sample pin also rotates while moving. In this high-stress abrasion test, the load is sufficient to fracture the abrasive particles.

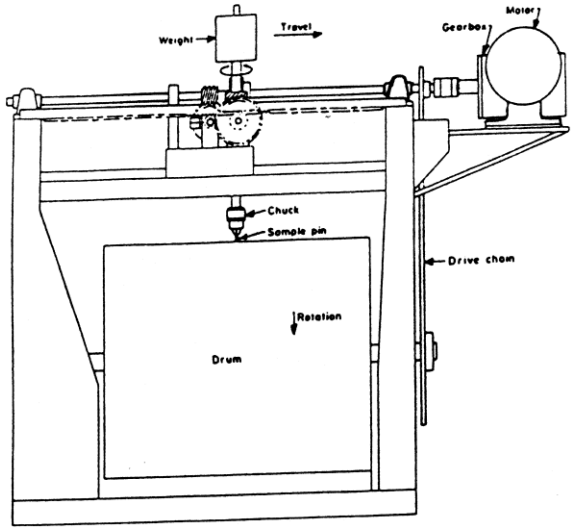

Figure 2-16 Arrangement of pin-on-drum wear test [47]

2.5.1.7 Taber Abraser Test

The Taber Abraser, which is shown in Figure 2-17, is designed to test abrasive wear. In Taber Abraser, a specimen is mounted on a rotating turntable and subjected to the wearing action of two abrasive wheels applied at a specific load. The rotating turntable will drive the wheels. In this process, abrasive wear is produced by the sliding-rotation of the two abrading wheels against the specimen. The resulting abrasion marks form a circle on the specimen surface. The resistance of abrasive wear is described by this circle.

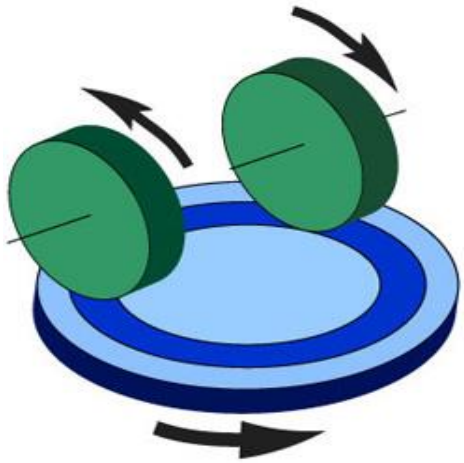

Figure 2-17 Schematic diagram of Taber Abraser [47]

2.5.1.8 Ball-on-Three-Discs Wear Test

The Ball on Three Disks tester is a bench test to measure diesel fuel lubricity [48], which is shown in Figure 2-18. In this tester, it consists of a ceramic ball that revolves for 45 minutes against 3 metal disks that are pressed against the ball whilst being immersed in a test fuel sample. The final wear scar diameter (WSD) on the ceramic ball determines the lubricity of fuel sample. A low WSD indicates a good lubricity fuel sample and a high WSD indicates

a poor lubricity fuel sample. This test is a new test. This test and the result of test have been sent to ASTM by the Falex Corporation.

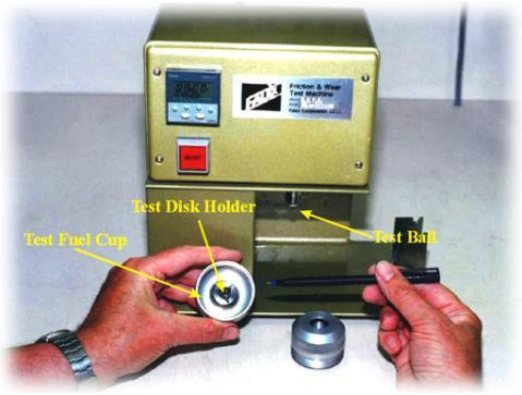

Figure 2-18 Ball on Three Disc tester with original fuel test cup disc holder and fuel test cup lid [48]

2.5.1.9 Particle Erosion Wear Test

The particle erosion wear test is usually used to test the erosion resistance of materials and coatings. This erosion test machine, which is shown in Figure 2-19, controls a repeated impact erosion approach which involves a small nozzle delivering gas stream containing abrasive particles. These particles impact the surface of a test specimen and erosion wear occurs. The erosion rate can be expressed by the amount of weight loss per unit of time. The Test System may be used to rank the erosion resistance of different materials.

Figure 2-19 Picture of Erosion Test Machine [49]

2.5.1.10 Fretting Wear Test

The fretting wear test is usually used to test the fretting wear of the materials. Fretting wear occurs where there is oscillatory motion with a small displacement of the contacting surfaces under load. The fretting wear test rig is shown in Figure 2-20 [50]. In this rig, the research object is two rolling bearings and the fretting wear of bearings is studied. An eccentric cam and crank mechanism were used to minutely oscillate the bearings to cause the fretting wear on them.

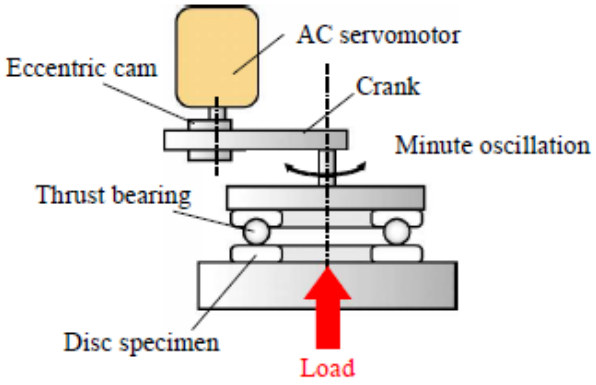

Figure 2-20 Schematic diagram of Fretting Wear Test [50]

2.5.1.11 Ball Cratering Test

The Ball Cratering Test is used to test the mild abrasive wear resistance of the coatings [51] and to measure the coating thickness of coatings [52]. The schematic diagram is shown in Figure 2-21, which is three-body abrasion test. This apparatus consists of a hard steel ball being rotated by drive shaft against to the sample at certain speed. The contact between ball and sample is fed with abrasive slurry. After some cycles, a crater will be formed on the sample.

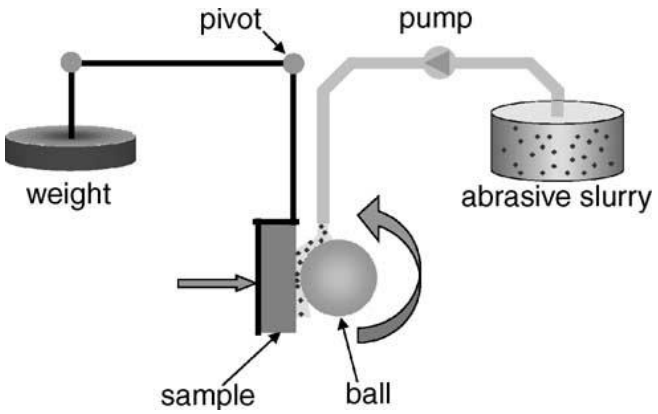

Figure 2-21 Schematic diagram of Ball Cratering Test [51]

2.5.2 Selection of Wear Test Methods

The bench tests described above are used for quality control functions such as thickness of coating, porosity, adhesion, strength, hardness, ductility, and wear resistance of coating and bulk materials. These bench tests serve for replicating and investigating real-world wear problems. The transition from the real-world wear problem to the bench test solution needs to be explored. Extracting the necessary key information in the field problem is very important for the following steps of bench test. This transition sometimes is a very difficult process, and in some case it involves some compromises due to the lack of information, availability of the bench test equipment and the economic reasons.

Voitik [53] generalized a procedure to select the wear test method, as follows. First, the characteristics of the field problem is evaluated, which include recording characteristics of contact velocity, contact area, contact pressure, and entry angle. An appropriate bench test is then selected from Tribology Aspect Number (TAN) tables [53]. Then, the test conditions need to be established. The test conditions must be based on the field conditions, which include contact pressure, speed, lubricants, materials, hardness and surface finishes. Finally,

the temperature is set to represent the field condition. The bench test is usually run for lower cycle times compared to the real-world scenario for economic reasons.

In this research, we focus on the wear mechanisms of WC-Co. We need to know the conditions and relative parameters during the real manufacturing process. Then we determine which test method is feasible and also can provide the similar conditions as that of machining process for a more accurate simulation. Next, we need to determine the variables to be used in the experiment, which affect our objective. For the wear, the cutting speed, feed rate, and cutting time will affect the wear. Also, we need know how to measure our objective and find the best way to get our objective. For example, the simplest way to measure the wear is to measure the weight loss during and after a test. To measure the weight loss, we can measure the volume loss, the crater height if crater occurred after the experiment. We can also measure the wear coefficient.

Currently, the methods used to test the wear properties of WC-Co include the Pin-on-Disc test, Ball Cratering test, Ball-on-Disc. Zhao [54] studied the friction and wear properties of WC-Co sliding against Ti-6Al-4V alloy by Rotating Pin-on-Disc test. He found a distinct difference in wear mechanism between the pin and disc. For Ti-6Al-4V disc, severe grooved wear, squeezing, adhering and tearing interactions are the main mechanisms. For WC-Co pin, abrasion, adhesion and WC grain pulling out are the main mechanisms. Acker [51] studied the influence of tungsten carbide particle size and distribution on the wear resistance of laser clad WC/Ni coatings by Ball-on-Disc and Ball Cratering test. The Ball-on-Disc test shows that an increase in concentration of the carbides and a decrease in their size are both favorable for the wear resistance. In Ball Cratering test, wear coefficient decreases with increasing carbide concentration. Xu [55] studied the friction and wear properties of

Ti6Al4V/WC-Co friction pair were studied using an autonomous atmospheric pressure bare electrode cold plasma jet generating device and Block-on-Ring wear tester, respectively. Kagnaya [32] used Pin-on-Disc wear test to study the friction and wear of WC-Co cemented carbide. The WC-Co is the pin and the steel is served as disc. The pin experienced different wear mechanisms at different speeds. At low sliding speeds, the wear mechanisms of the pin deal with plastic deformation and micro-cracking of WC grains, fragmentation and debonding of WC grains and polishing of the pin contact surface. At high sliding speeds, a supplementary wear mechanism is observed. It deals with transfer of iron oxide.

3. RESEARCH METHODOLOGY

This chapter briefly describes the research methodology that was used to attain the objective of this work. As stated before, the objective of this research work is to identify and analyze the interactions between wear mechanisms in a machining tribosystem, and to confirm the fundamental physicochemical material interaction behavior through tribometric tests.

3.1 RESEARCH QUESTIONS, TASKS AND OUTPUTS

- **RQ 1: What are the major interactions among wear mechanisms in the Ti-6Al-4V / WC-Co turning tribosystem, and how do these change as a function of process conditions?**

To answer RQ 1, the dominant wear mechanisms observed on the rake face of the cutting tool were identified and mapped as a function of feed rate and cutting speed. Following this the major interactions between these were identified and mapped as well.

- **Methodology:** SEM images, EDS elemental distribution maps, and the 3D surface profile (from the white light interferometer) of the worn cutting tool surfaces were analyzed to identify the dominant wear mechanisms. Following this, these dominant wear mechanisms as a function of the controllable process parameters were mapped. Then, the evolution of the major interactions among dominant wear mechanisms were identified and charted at different process parameters. Finally, the major wear mechanism interactions as a function of the feed rate and cutting speed were mapped.
- **Outputs:** The major outputs from these tasks are maps of dominant wear mechanisms

and interactions between them as a function of process parameters.

- **RQ 2: How do the wear mechanism interactions in tribometric testing compare with (field-level) machining tests?**

To answer RQ 2, the operating parameters were calculated for appropriately reproducing the tribometric conditions experienced by the rake face of the tool by suitable tribometric bench tests. The major interactions among the dominant wear mechanisms in (field-level) machining tribosystem and the idealized tribometric bench tests were compared.

- **Methodology:** Published guidelines for appropriately representing field-level tribosystem conditions by model-level bench tests [18, 56] were used. Based on the general rule that the contact stress in tribometric testing should closely match the contact stress in machining, the normal stress was converted appropriately. Also, the relative surface speed on the rake face of the tool (chip velocity) was converted to the appropriate velocity parameter in the bench tests. Finally, the major wear mechanisms interactions in bench tests by a combination of SEM, EDS, and 3D surface profiler results were identified and compared.
- **Outputs:** The output of this task will be analyses of wear mechanisms and interactions between the field and model-level tests to characterize fundamental material wear interaction behavior.

- **RQ 3: How can the operational parameters in the machining process be controlled to manipulate wear mechanism interactions so as to increase the life of the cutting tool?**

To answer RQ 3, the wear mechanism interactions at different process conditions were qualitatively ranked in terms of the total material worn away from the tool (and from the tribometric testing component). Then, strategies were devised to minimize collective wear on the tool for each process condition.

- **Methodology:** The collective material loss that occurred due to each interaction process was approximated by the 3D surface profiler and the mechanism interactions were ranked accordingly. Then, strategies were devised by recommending process parameters so as to obtain a competitive material removal rate (MRR).
- **Outputs:** The outputs of this task are strategies to increase tool life by controlling process conditions based on ranked wear mechanism interactions.

3.2 OUTLINE

An outline of this research work is shown in Table 3. 1.

Table 3. 1 Outline of this study

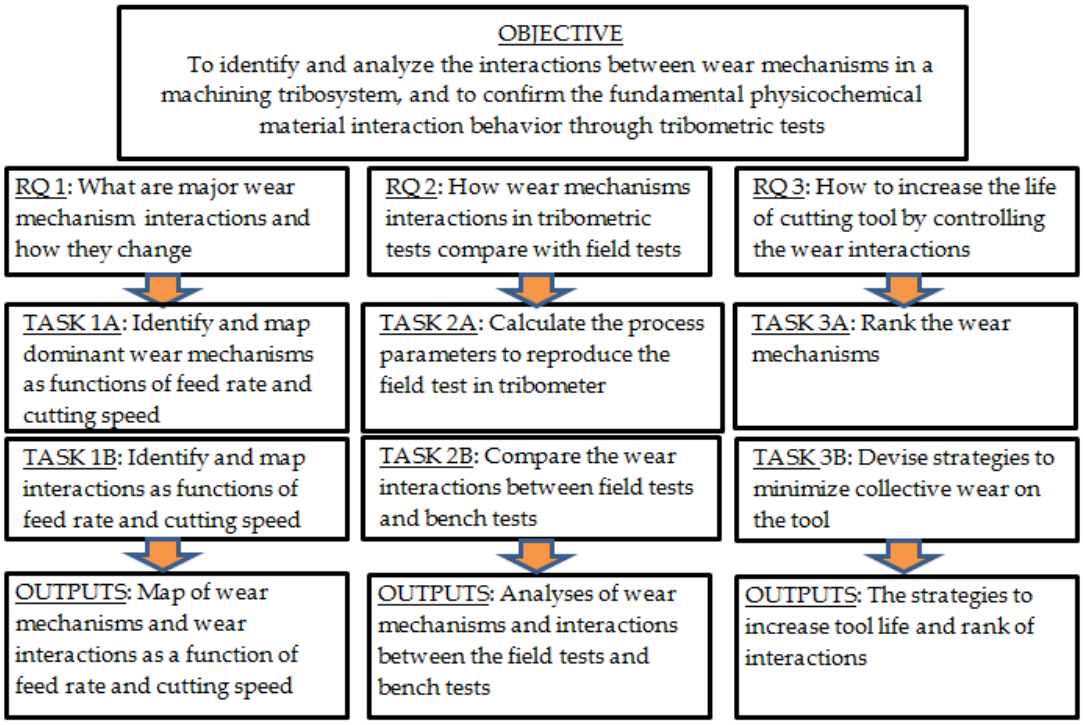

4. IDENTIFICATION AND MAPPING OF WEAR MECHANISMS INTERACTIONS (RQ1)

4.1 EXPERIMENTAL SETUP

The cutting tool used in this study is a WC-Co insert tool (Sandvik CNGP 12 04 08 H10A). The workpiece material used here is Ti-6Al-4V. Ti-6Al-4V is a material with poor machinability, which is due to the low thermal conductivity and elastic modulus, and high chemical reactivity and temperature strength. The low thermal conductivity results in the majority of the generated heat flowing into the tool edge (about 80%) [8].

Worn WC-Co cutting tools from turning tests conducted on Ti-6Al-4V are analyzed in this research work. The design of experiment for cutting inserts H10A consists of 3 combinations of feed rates and cutting speeds [12], which is shown in Table 4-1. The depth of cutting is 2 mm. The turning test setup is shown in Figure 4-1.

Table 4-1 Machining test conditions

Tests	Feed rate (mm/rev)	Cutting speed (m/min)	Duration of test (s)	MRR (mm^3/min)
1	0.05	30	200	3000
2	0.05	60	100	6000
3	0.05	120	50	12000
4	0.15	30	66.7	9000
5	0.15	60	33.3	18000
6	0.15	120	16.7	36000
7	0.30	30	33.3	18000
8	0.30	60	16.7	36000
9	0.30	120	8.3	72000

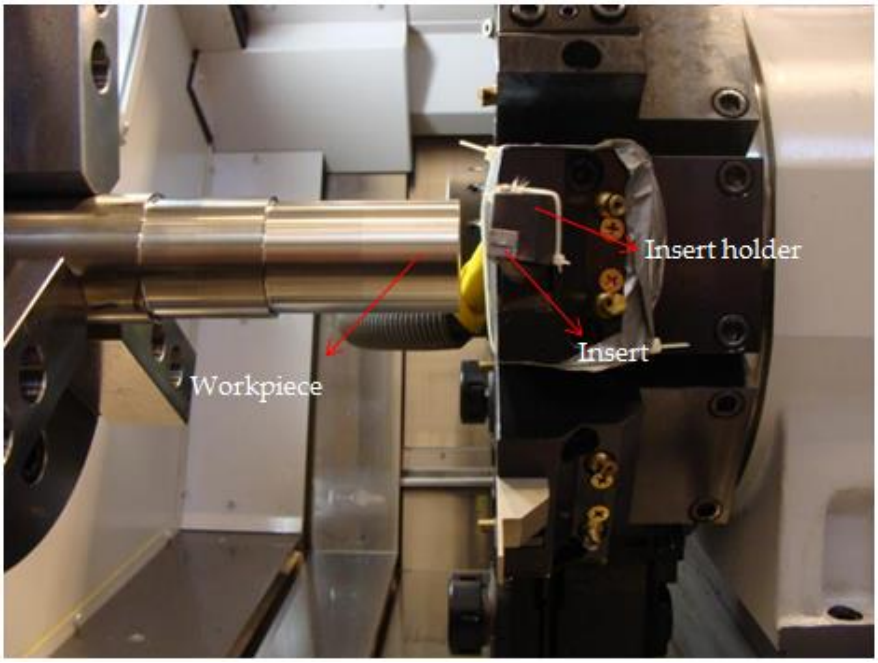

Figure 4-1 Setup of the Ti-6Al-4V turning test

H10A Grade WC-Co Insert has good abrasive wear resistance and large toughness for the medium to rough turning of heat resistant steels and titanium alloys [6]. H10A WC-Co inset is suitable for machining heat resistant super alloys and titanium alloys. The specification of the H10A insert [57] is listed below.

Item: Carbide Turning Insert

Relief Angle: 0° Ground

Insert Shape: 80° Diamond

Style: CNGP

Inset Size: 432

Chip-Breaker: Groove

Grade: H10A

Application: Finishing

Workpiece Material: Non-Ferrous

Inscribed Circle: 1/2 inch (12.7 mm)

Insert Thickness: 0.1875 inch (4.7625 mm)

Nose Radius: 0.0315 inch (0.8 mm)

Coating: Uncoated

Cutting Direction: Neutral

Mounting Hole Diameter: 0.203 inch (5.1562 mm)

Mounting Style: Top and Hole Clamping

Rake: Negative

No. of Edges: 4

ISO Number:CNGP 12 04 08 h10a

ANSI Number: CNGP 432 H10A

Weigth: 0.01

The worn cutting tool after each run is characterized by SEM, EDS, and 3D surface profiler. Some general guidelines were used to identify the wear mechanisms [58-60], which

include that micro-chipping or indications of "chunks" of material pulled away as indicators for adhesive wear, wear scars or grooves on the tool caused by harder particles (or inclusions) as indicators for abrasive wear, discolorations for oxidation or chemical wear, and smooth surfaces on the tool for diffusive wear.

4.2 OBSERVED WEAR MECHANISMS

From the machining experiments, the major observed wear mechanisms on the WC-Co tool surface are explained below:

4.2.1 After Machining 10-cm^3 of Ti-6Al-4V Workpiece Stock (Volume-1)

4.2.1.1 Cutting Speed at 30 m/min (Volume 1)

The SEM images of cutting tool H10A at cutting speed 30 m/min are shown in Figure 4-2 and Figure 4-3. Figure 4-2 (left) is the image at the feed rate of 0.05 mm/rev and Figure 4-2 (right) is the image at the feed rate of 0.15 mm/rev. Figure 4-3 (left) is the image at the feed rate of 0.30 mm/rev and Figure 4-3 (right) is the amplified part of the wear area of Figure 4-3 (left). The dark grey area is the adhesion area. As shown in Figure 4-2 and Figure 4-3, only adhesive wear occurs. Also, it is obvious that when the feed rate increases, the area of adhered Ti become larger. When feed rate is 0.05 mm/rev, only small amounts of adhered Ti were found at the outer edge. When the feeding rate increases to 0.15 mm/rev, there is an increase in the amount of adhered Ti area. Figure 4-4 shows EDS image of composition of element in cutting tool when cutting speed is 30m/min and feed rate is 0.30 mm/rev. From the EDS images, it can be seen the elements at the adhered area are Ti, V and Al. Ti is the primary adhered element since Ti is the primary element in Ti-6Al-4V.

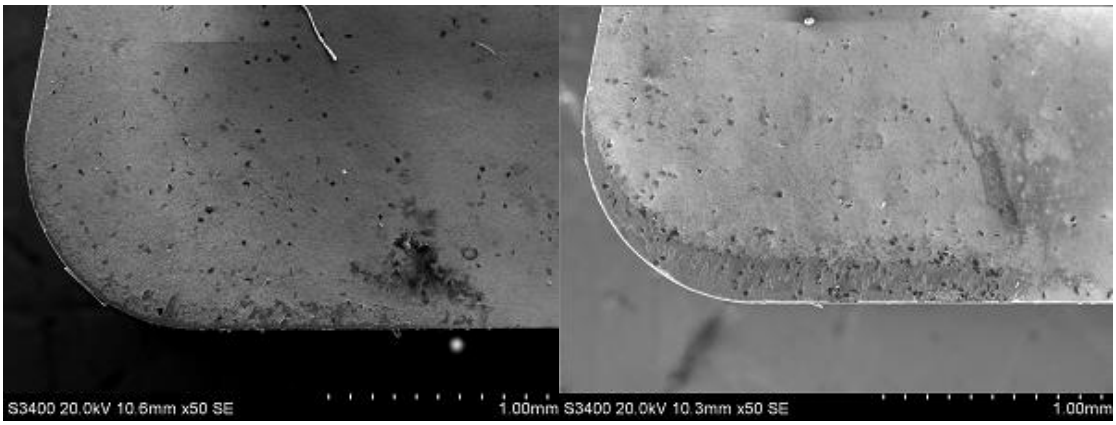

Figure 4-2 SEM images of tool at a cutting speed of 30m/min and feed of 0.05 mm/rev (left), 0.15 mm/rev (right) after machining 10 cm^3

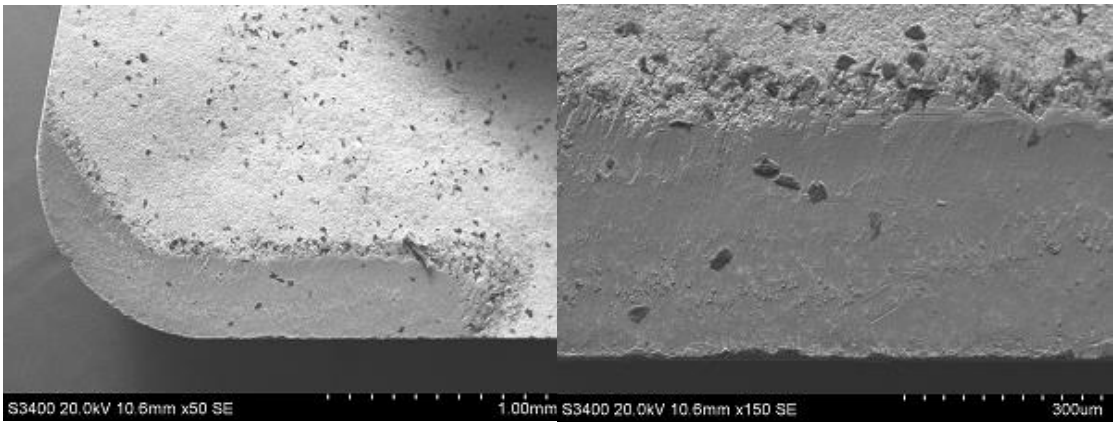

Figure 4-3 SEM images of cutting tool when cutting speed is 30m/min and feed rate is 0.30 mm/rev (left) and amplified part (right) after machining 10 cm^3

Figure 4-4 EDS images of composition of elements in cutting tool when cutting speed is 30m/min and feed rate is 0.30 mm/rev after machining 10 cm^3. The elements are Ti, V, Al, C, and W from left to right.

4.2.1.2 Cutting Speed at 60 m/min (Volume 1)

The SEM images of cutting tool H10A at cutting speed 60 m/min are shown in Figure 4-5 and Figure 4-6. Figure 4-5 (left) is the image at the feed rate of 0.05 mm/rev, and Figure 4-5 (right) is the image at the feed rate of 0.30 mm/rev. Figure 4-6 (left) is the image at the feed rate of 0.15 mm/rev and Figure 4-6 (right) is the amplified part of the wear area. The adhesion of Ti occur at all different feed rates. From the figures, it is obvious that when the feed rate increases, the area of adhered Ti becomes larger qualitatively, which follows the trend at cutting speed 30 m/min. Also, a smooth surface appears at feed rate 0.15 mm/rev, which is the crater. The formation mechanism of crate will be given in the discussion part. One feature in Figure 4-6 (left) is carbon discoloration, which is due to the diffusion of C. In Figure 4-6 (right), the Ti BUE (built-up edge) is also formed due to the inhomogeneity of Ti adhesion distribution. Figure 4-7 shows EDS image of composition of elements when feed rate is 0.15 mm/rev. From the EDS image, the primary element at the adhered area is Ti.

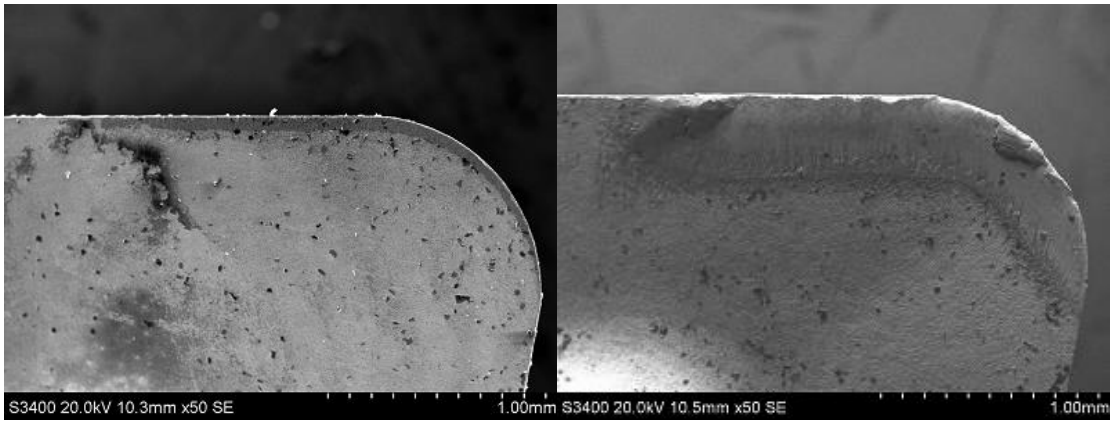

Figure 4-5 SEM images of cutting tool when cutting speed is 60m/min and feed rate is 0.05 mm/rev (left) and 0.30 mm/rev (right) after machining 10 cm^3

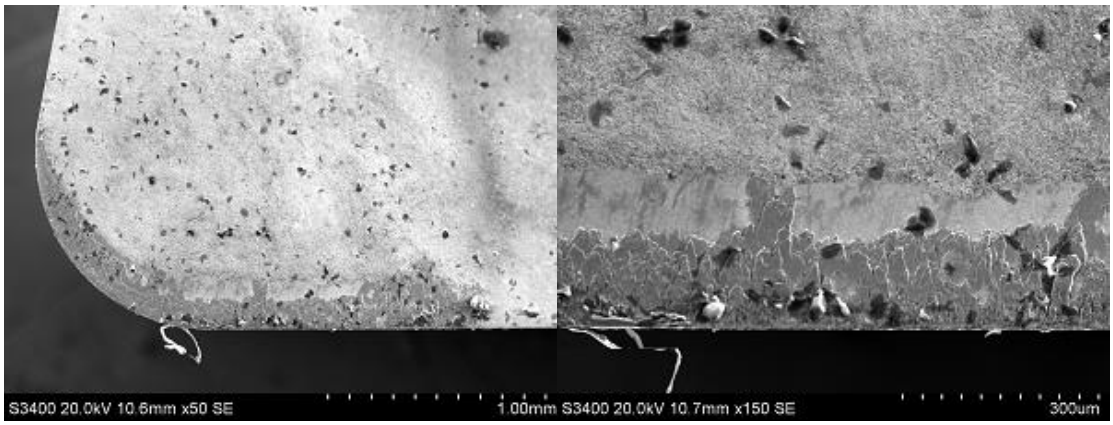

Figure 4-6 SEM images of cutting tool when cutting speed is 60m/min and feed rate is 0.15 mm/rev (left) and amplified part (right) after machining 10 cm^3

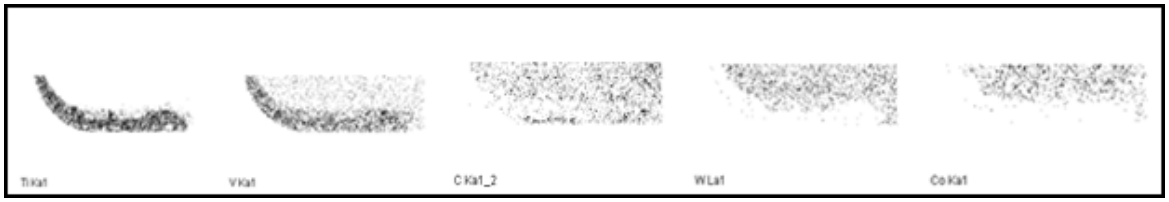

Figure 4-7 EDS images of composition of elements in cutting tool when cutting speed is 60m/min and feed rate is 0.15 mm/rev after machining 10 cm^3. The elements are Ti, V, C, W, and Co from left to right.

4.2.1.3 Cutting Speed at 120 m/min (Volume 1)

The SEM images of cutting tool H10A at cutting speed 120 m/min are shown in Figure 4-8 and Figure 4-9. Figure 4-8 (left) is the image at the feed rate 0.05 mm/rev and Figure 4-8 (right) is the image at the feed rate 0.30 mm/rev. Figure 4-9 (left) is the image at the feed rate 0.15 mm/rev and Figure 4-9 (right) is the amplified part. At cutting speed 120 m/min, the adhesion of Ti occurs in all cases. In Figure 4-8 (left), the carbon build-up can be seen at the tool edge. Figure 4-10 shows EDS image of composition of element when feed rate is 0.15

mm/rev. From the EDS image, it can be learned that the adhered area is mainly composed of Ti. And there is no Co on the smooth area.

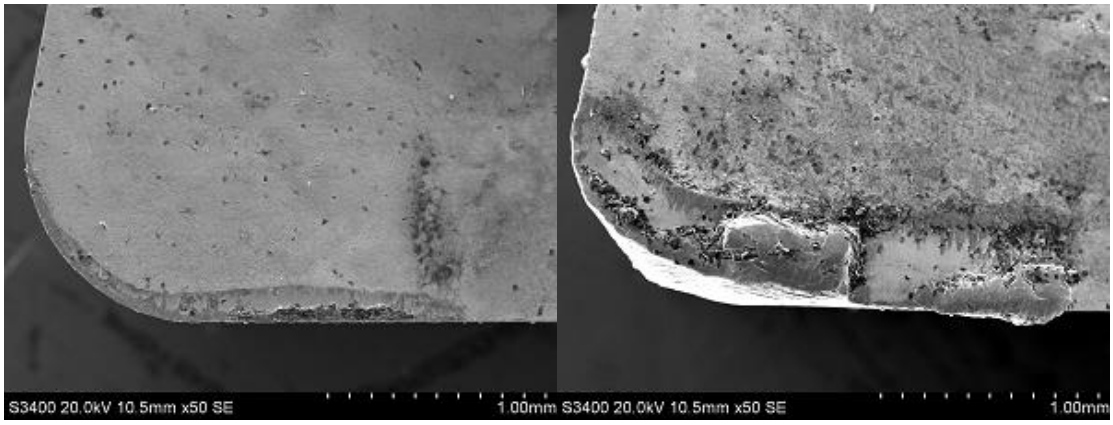

Figure 4-8 SEM images of cutting tool when cutting speed is 120m/min and feed rate is 0.05 mm/rev (left) and 0.30 mm/rev (right) after machining 10 cm^3

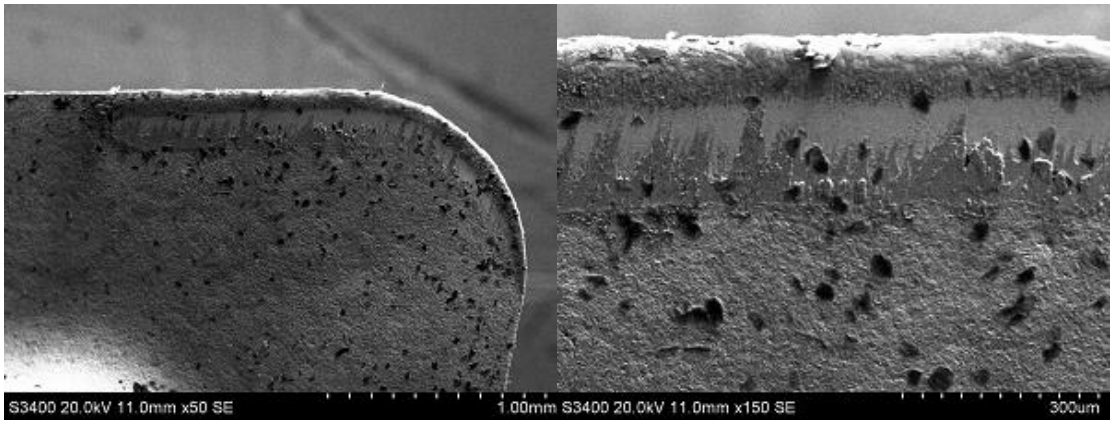

Figure 4-9 SEM images of cutting tool when cutting speed is 120m/min and feed rate is 0.15 mm/rev (left) and amplified part (right) after machining 10 cm^3

Figure 4-10 EDS images of composition of elements in cutting tool when cutting speed is 120m/min and feed rate is 0.15 mm/rev after machining 10 cm^3. The elements are Ti, V, C, W, and Co from left to right.

4.2.2 After Machining 20-cm^3 of Ti-6Al-4V Workpiece Stock (Volume-2)

4.2.2.1 Cutting Speed at 30 m/min (Volume 2)

The SEM images of cutting tool H10A at cutting speed 30 m/min are shown in Figure 4-11 and Figure 4-12. Figure 4-11 (left) is the image at the feed rate of 0.05 mm/rev and Figure 4-11 (right) is the image at the feed rate of 0.15 mm/rev. Figure 4-12 (left) is the image at the feed rate of 0.30 mm/rev and Figure 4-12 (right) is the amplified part of the wear area. The area of adhesion increases as the feed rate increases from 0.05 to 0.30 mm/rev. At feed rate 0.30 mm/rev, some adhered Ti layer are worn way and the new smooth area appears. This is different from that at same cutting speed and feed rate in Volume 1. This is due to the increase of cutting volume and some area with Ti adhesion is worn away. Figure 4-13 shows EDS image of composition of element when feed rate is 0.30 mm/rev. From the EDS images, it is obvious that the adhesion area mainly composed by Ti.

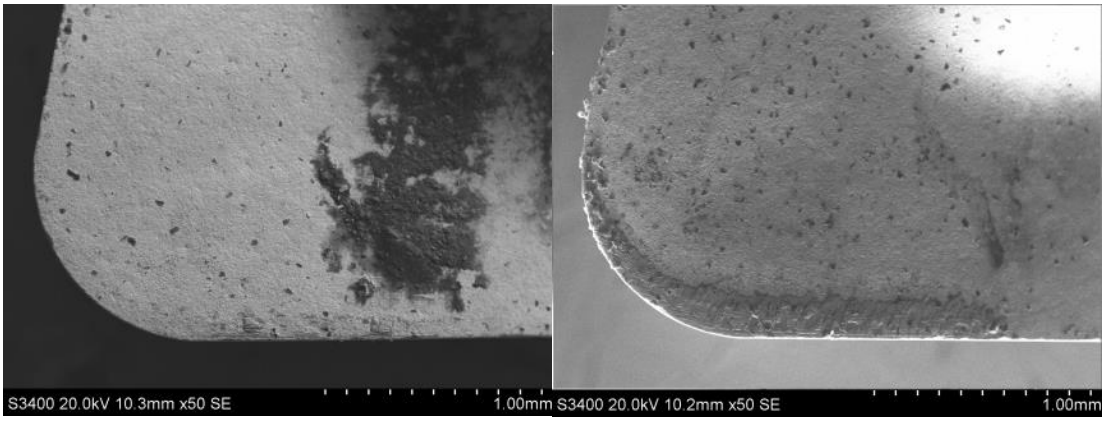

Figure 4-11 SEM images of cutting tool when cutting speed is 30m/min and feed rate is 0.05 mm/rev (left) and 0.15 mm/rev (right) after machining 20 cm^3

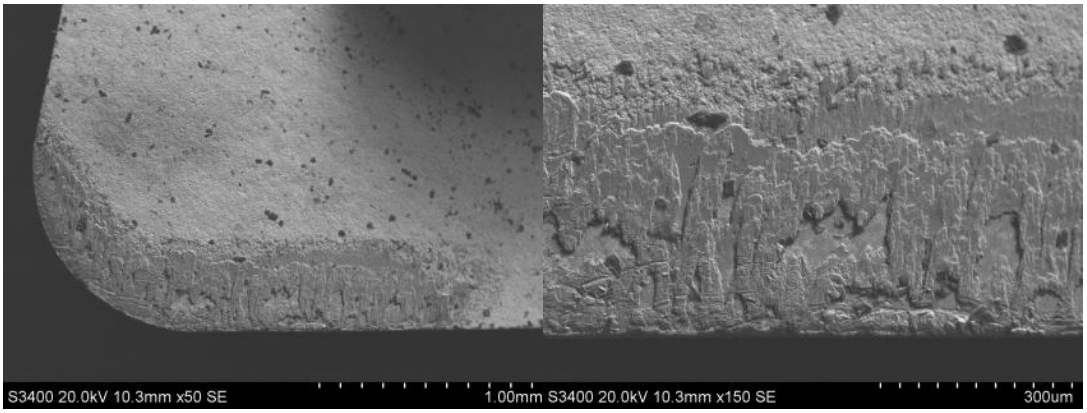

Figure 4-12 SEM images of cutting tool when cutting speed is 30m/min and feed rate is 0.30 mm/rev (left) and amplified part (right) after machining 20 cm^3

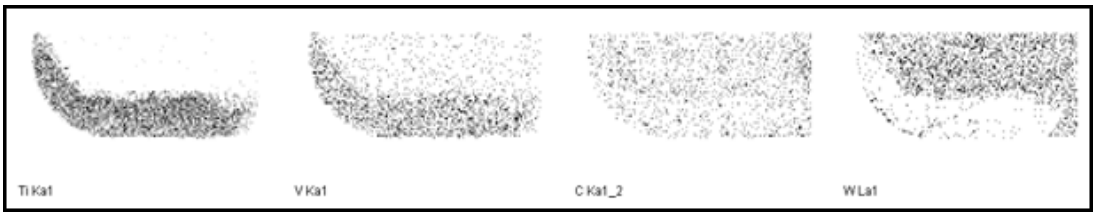

Figure 4-13 EDS images of composition of elements in cutting tool when cutting speed is 30m/min and feed rate is 0.30 mm/rev after machining 20 cm^3. The elements are Ti, V, C, and W from left to right.

4.2.2.2 Cutting Speed at 60 m/min (Volume 2)

The SEM images of cutting tool H10A at cutting speed 60 m/min are shown in Figure 4-14 and Figure 4-15. Figure 4-14 (left) is the image at the feed rate of 0.05 mm/rev and Figure 4-14 (right) is the image at the feed rate of 0.30 mm/rev. Figure 4-15 (left) is the image at the feed rate of 0.15 mm/rev and Figure 4-15 (right) is the amplified part of the wear area. The adhesion of Ti occur at all different feed rates. From the figures, it is obvious that when the feed rate increases, the area of adhered Ti becomes larger qualitatively. At feed rate 0.15 mm/rev, some adhered Ti is worn away and the smooth area appears. This is due to the increase of cutting volume, which leads some area with Ti adhesion worn away. Figure 4-16 shows EDS image of composition of elements when feed rate is 0.15 mm/rev. From the EDS image, the primary element at the adhered area is Ti. The carbon discoloration can be seen on EDS image.

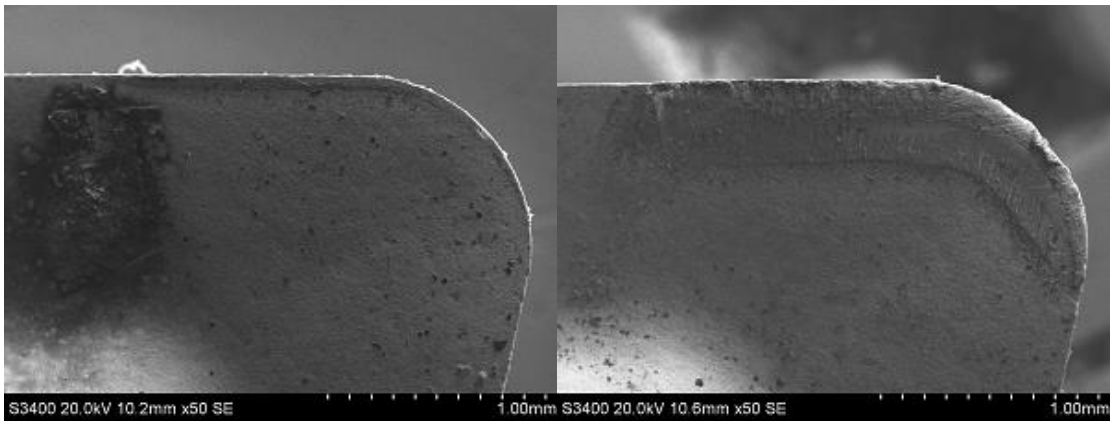

Figure 4-14 SEM images of cutting tool when cutting speed is 60m/min and feed rate is 0.05 mm/rev (left) and 0.30 mm/rev (right) after machining 20 cm^3

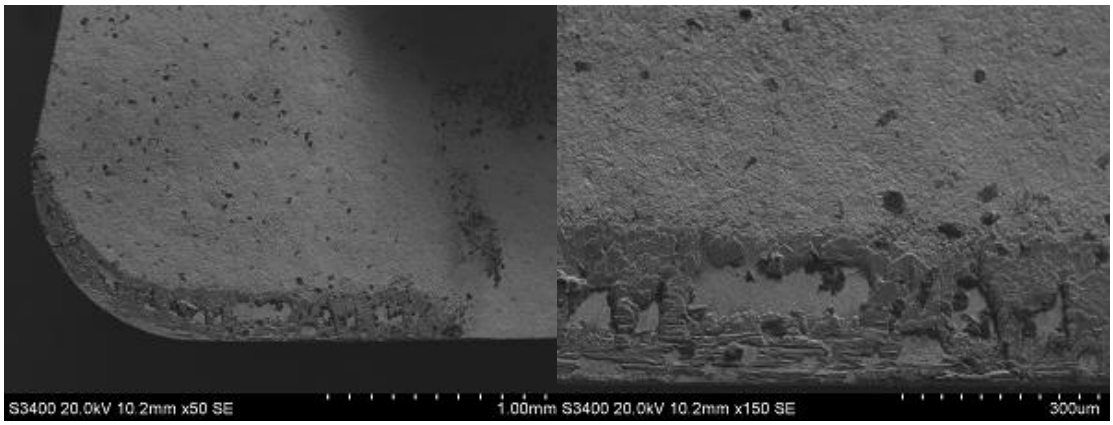

Figure 4-15 SEM images of cutting tool when cutting speed is 60m/min and feed rate is 0.15 mm/rev (left) and amplified part (right) after machining 20 cm^3

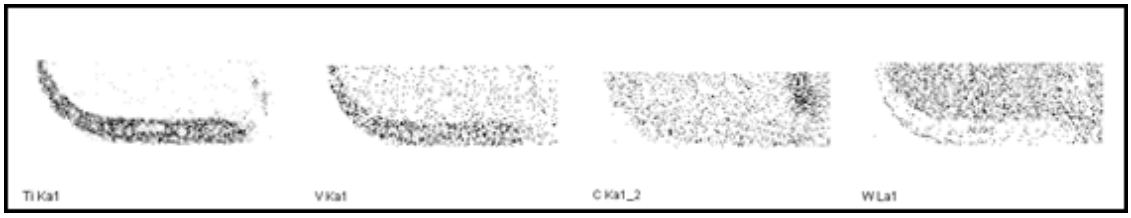

Figure 4-16 EDS images of composition of elements in cutting tool when cutting speed is 60m/min and feed rate is 0.15 mm/rev after machining 20 cm^3. The elements are Ti, V, C, W, and Co from left to right.

4.2.2.3 Cutting Speed at 120 m/min (Volume 2)

The SEM images of cutting tool H10A at cutting speed 120 m/min are shown in Figure 4-17 and Figure 4-18. Figure 4-17 (left) is the image at the feed rate 0.05 mm/rev and Figure 4-17 (right) is the image at the feed rate 0.15 mm/rev. Figure 4-18 (left) is the image at the feed rate 0.30 mm/rev and Figure 4-18 (right) is the amplified part of the wear area. Compared to that at cutting speed 30 m/min, more adhered Ti is worn away, which is due to larger abrasive wear and high temperature wear. When the feed rate increases to 0.30 mm/rev, most of the adhesion layer disappears. On the left side of the worn area, the fracture appears.

When the chip flows over the tool surface, the chip begins to adhere to some region of the cutting tool. Then the afterward movement of the chip may induce the plastic deformation of the welded joint and finally lead to the fracture of cutting tool. Figure 4-19 shows EDS image of composition of element when feed rate is 0.15 mm/rev.

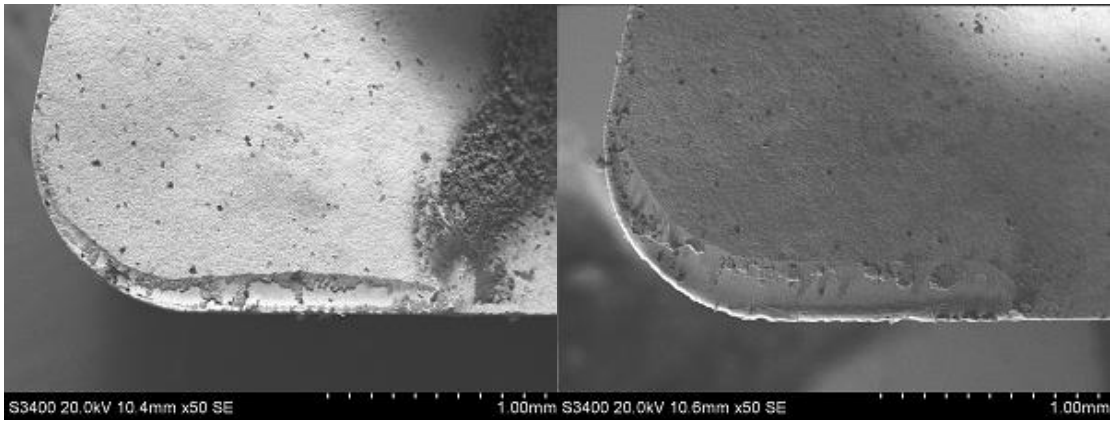

Figure 4-17 SEM image of tool for a speed of 120m/min and feed is 0.05 mm/rev (left) and 0.15 mm/rev (right) after machining 20 cm^3

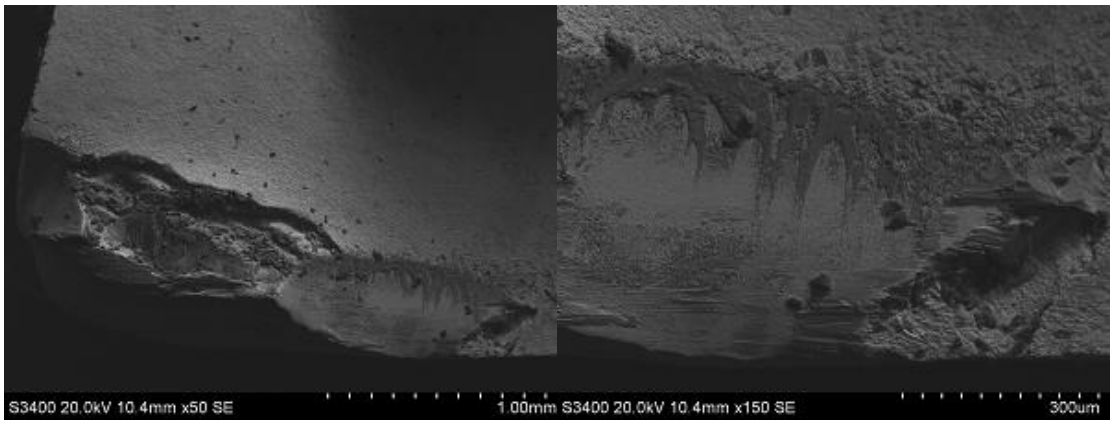

Figure 4-18 SEM image of cutting tool when cutting speed is 120m/min and feed rate is 0.30 mm/rev (left) and amplified part (right) after machining 20 cm^3

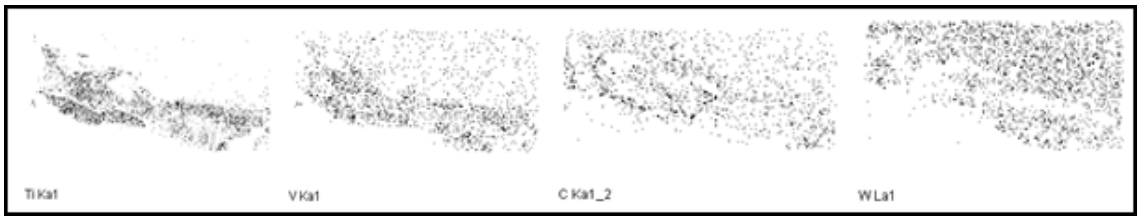

Figure 4-19 EDS image of composition of element in cutting tool when cutting speed is 120m/min and feed rate is 0.15 mm/rev after machining 20 cm^3. The elements are Ti, V, C, W, and Co from left to right.

4.2.3 After Machining 30-cm^3 of Ti-6Al-4V Workpiece Stock (Volume-3)

4.2.3.1 Cutting Speed at 30 m/min (Volume 3)

The SEM images of cutting tool H10A at cutting speed 30 m/min are shown in Figure 4-20 and Figure 4-21. Figure 4-20 (left) is the image at the feed rate 0.05 mm/rev and Figure 4-20 (right) is the image at the feed rate 0.15 mm/rev. Figure 4-21 (left) is the image at the feed rate 0.30 mm/rev and Figure 4-21 (right) is the amplified part of the wear area. The area of adhesion increases as the feed rate increase from 0.05 to 0.30 mm/rev. When the feed rate increases to 0.30 mm/rev, some smooth area appears. This is different from that for Volume 1 and Volume 2. This is due to the increase of cutting volume, which leads some area with Ti adhesion worn away. Figure 4-22 shows EDS images of composition of element when feed rate is 0.30 mm/rev. From the EDS images, Ti is the primary adhered element.

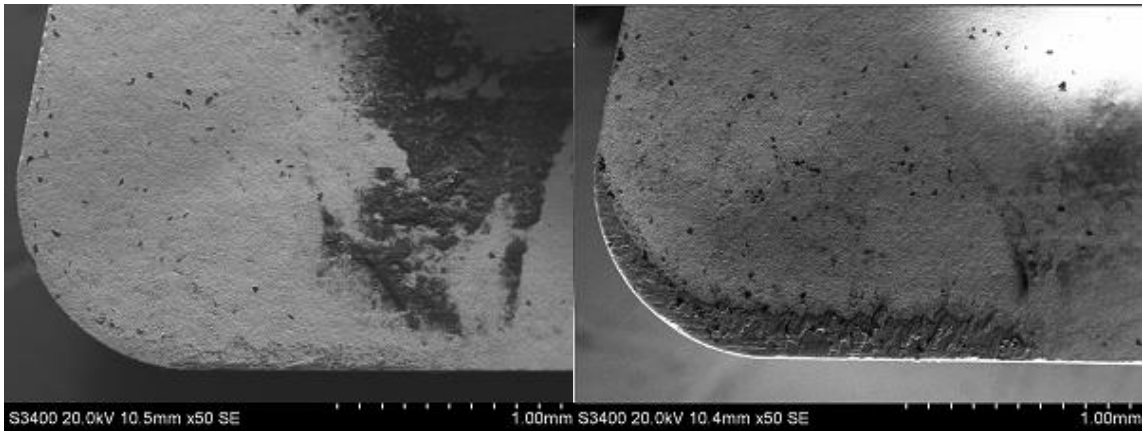

Figure 4-20 SEM images of cutting tool when cutting speed is 30m/min and feed rate is 0.05 mm/rev (left) and 0.15 mm/rev (right) after machining 30 cm^3.

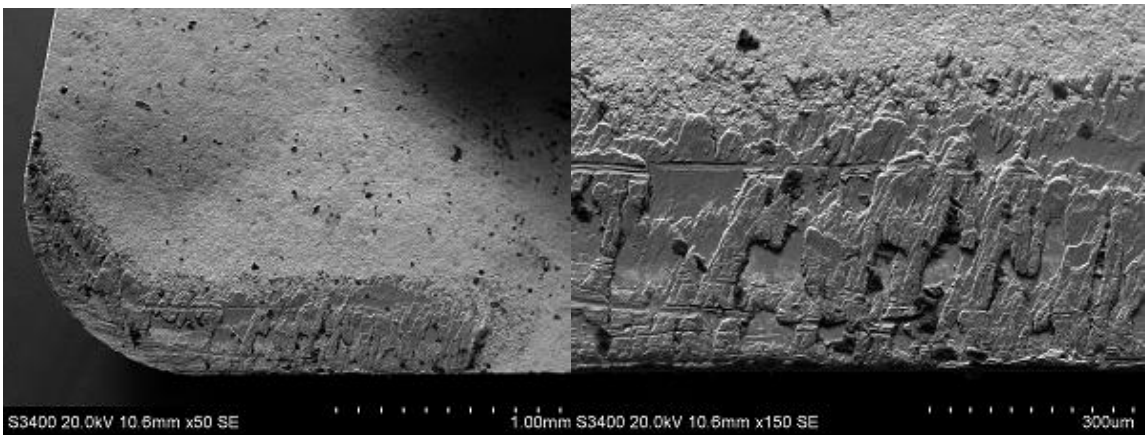

Figure 4-21 SEM images of cutting tool when cutting speed is 30m/min and feed rate is 0.30 mm/rev (left) and amplified part (right) after machining 30 cm^3

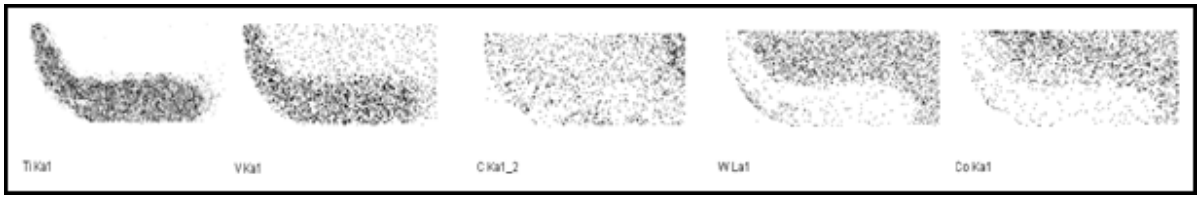

Figure 4-22 EDS images of composition of elements in cutting tool when cutting speed is 30m/min and feed rate is 0.30 mm/rev after machining 30 cm^3. The elements are Ti, V, C, W, and Co from left to right.

4.2.3.2 Cutting Speed at 60 m/min (Volume 3)

The SEM images of cutting tool H10A at cutting speed 30 m/min are shown in Figure 4-23 and Figure 4-24. Figure 4-23 (left) is the image at the feed rate 0.05 mm/rev and Figure 4-23 (right) is the image at the feed rate 0.15 mm/rev. Figure 4-24 (left) is the image at the feed rate 0.30 mm/rev and Figure 4-24 (right) is the amplified part of the wear area. From Figure 4-23 and Figure 4-24, some adhesive layer is worn way and the smooth area appears when the feed rate increases to 0.15 mm/rev. Figure 4-25 shows EDS image of composition of elements when feed rate is 0.15 mm/rev. From the EDS image, the primary element on the adhered area is Ti.

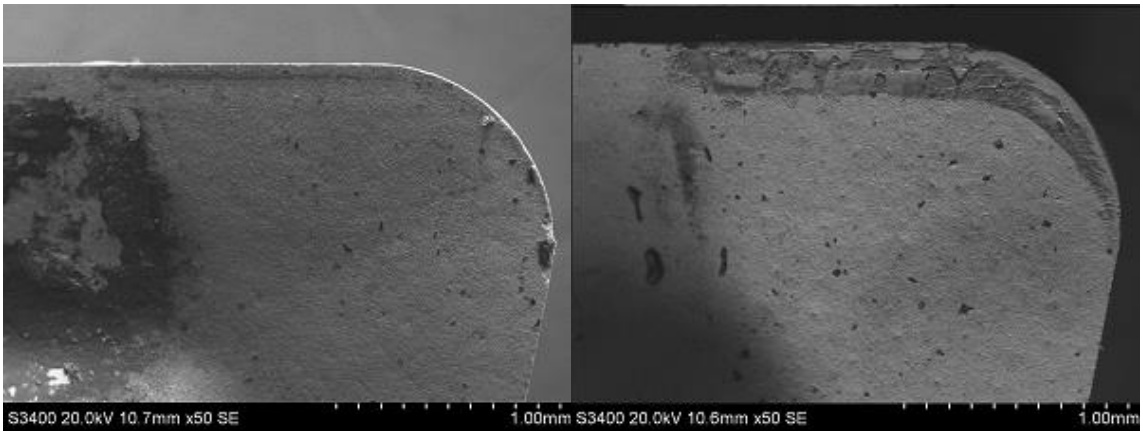

Figure 4-23 SEM images of cutting tool when cutting speed is 60m/min and feed rate is 0.05 mm/rev (left) and 0.15 mm/rev (right) after machining 30 cm^3

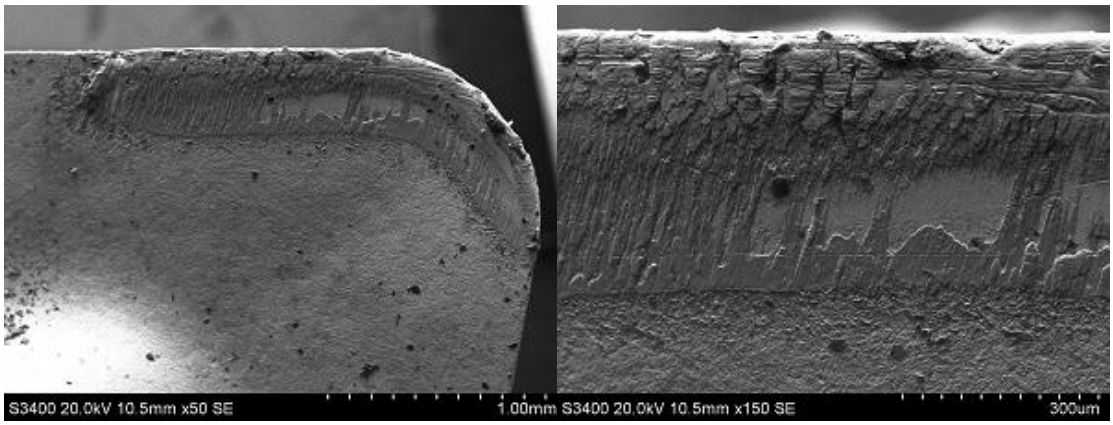

Figure 4-24 SEM images of cutting tool when cutting speed is 60m/min and feed rate is 0.30 mm/rev (left) and amplified part (right) after machining 30 cm^3

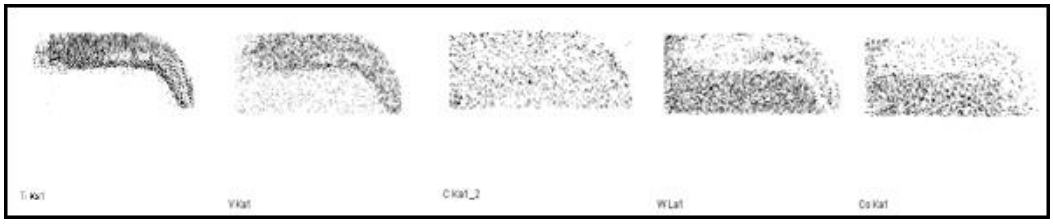

Figure 4-25 EDS images of composition of elements in cutting tool when cutting speed is 60m/min and feed rate is 0.30 mm/rev after machining 30 cm^3. The elements are Ti, V, C, W, and Co from left to right.

4.2.3.3 Cutting Speed at 120 m/min (Volume 3)

The SEM images of cutting tool H10A at cutting speed 120 m/min are shown in Figure 4-26 and Figure 4-27. Figure 4-26 (left) is the image at the feed rate 0.05 mm/rev and Figure 4-26 (right) is the image at the feed rate 0.15 mm/rev. Figure 4-27 (left) is the image at the feed rate 0.30 mm/rev and Figure 4-27 (right) is the amplified part of the wear area. At these three feeding rates, some adhered layer is worn way and the smooth area appears. When the feed rate increases to 0.30 mm/rev, the left edge of cutting tool begins to crack. Figure 4-28 shows EDS image of composition of element when feed rate is 0.15 mm/rev.

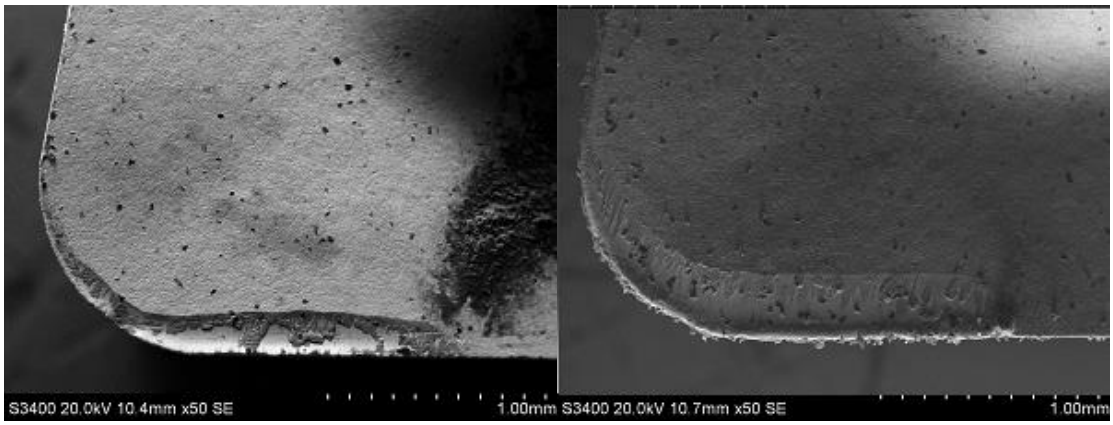

Figure 4-26 SEM image of cutting tool when cutting speed is 120 m/min and feed rate is 0.05 mm/rev (left) and 0.15 mm/rev (right) after machining 30 cm^3

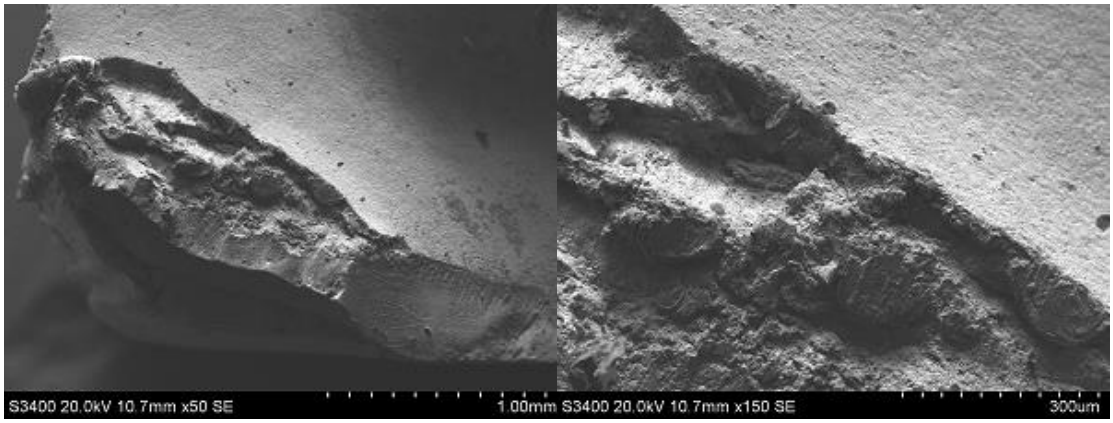

Figure 4-27 SEM image of cutting tool when cutting speed is 120m/min and feed rate is 0.30 mm/rev (left) and amplified part (right) after machining 30 cm^3

Figure 4-28 EDS image of composition of element in cutting tool when cutting speed is 120m/min and feed rate is 0.15 mm/rev after machining 30 cm^3. The elements are Ti, V, C, W, and Co from left to right.

4.3 DISCUSSION OF RESULTS

From the above experiments for Volume 1, when the cutting speed is low (30 m/min) and the feed rate increase from 0.05 to 0.30 mm/rev, the only wear mechanism is the Ti adhesion and the area of Ti adhesion increases. When the cutting speed is medium (60 m/min), both of the crater and Ti adhesion are observed at all three feed rates. When the cutting speed is high (120 m/min), the wear mechanisms are similar as that at medium cutting speed (60 m/min).

In the experiments for Volume 2, when the cutting speed is low (30 m/min) and the feed rate increases from 0.05 to 0.30 mm/rev, the only wear mechanism is the Ti adhesion. When the cutting speed is medium and high, the characteristic features of surface are the same as that in Volume 1. Some of Ti adhesion is worn away and some new adhesion area is observed on the top of crater. When the cutting speed is 120 m/min and feed rate is 0.30 mm/rev, the failure of cutting tool happens.

In the experiments for Volume 3, the characteristic features of the surface of cutting tool follow the trends in Volume 2. The failure and catastrophe fracture of cutting tool also happens in this case at high cutting speed and high feeding rate.

When the cutting speed is kept as constant, the feed rate varies from 0.05 mm/rev to 0.30 mm/rev. The area of adhered Ti increases accordingly. When the cutting speed increases, the size of the crater area increases and the size of the adhesion area of Ti becomes smaller. This is because when the cutting speed increases, the temperature of the tool surface will become higher, and will promote the temperature-controlled wear, such as the diffusion wear. In diffusion wear mechanism, the elements in the cutting tool, such as C, W, and Co, may diffuse from the cutting tool and lead to the formation of more smooth area.

Further, the amount of workpiece volume cut affects the wear mechanisms. The thickness of adhesion of Ti decreases when the stock removal volume increases from 10 to 30 cm^3. More outer surface of the adhesion area will be abraded by the chip when the cutting volume increases. Thus, the increase of the feed rate leads to the increase of the area of adhesion. When the cutting speed increases, the area of adhesion will decrease and the width and depth of the crater will increase.

4.4 MAJOR INTERACTIONS BETWEEN WEAR MECHANISMS

This section serves to explain the major interactions between dominant wear mechanisms.

4.4.1 Interaction #1 (at Low Cutting Velocities)

When the cutting tool cuts the workpiece at low cutting velocities, only an adhered layer of mostly Ti is observed in addition to smaller quantities of the other workpiece elements, Al and V. At low cutting speeds (for all feed rates), the weight percentage of Ti, Al, and V are about 90%, 6%, and 4%, respectively (matching the workpiece weight percentage). As the feed rate increases, the area of this adhered (predominantly) Ti layer increases as shown in Figure 4-29, where the adhered layer area is the largest for the highest feed rate of 0.30 mm/rev.

There is also some diffusion of the cutting tool elements (W, C, Co) into the workpiece material, *i.e.*, *(i)* into the chips as well as *(ii)* into the adhered Ti layer. At low temperatures around 500°C [61], the diffusion coefficient of C is much larger than that of W and Co. Hence, more C diffuses from the cutting tool to the *(i)* chips, as well as to the *(ii)* adhesion layer on the tool, compared to W and Co. This C is deposited further along the tool by the

edge of the passing chips as shown in Figure 4-29 and Figure 4-30 (b). This is the only way the C can reach that area. Further, from Figure 4-30 (b) – (d), it is observed that the distribution of C is more abundant and uniform in the adhesion layer compared to the distribution of W and Co. There is a possibility that the observed W and Co in the EDX maps in Figure 4-30 (c) and (d) are actually being captured through holes on the adhesion layer. This possibility can be excluded due to the significantly different observed concentrations of W and Co between the unworn and adhesion areas; this difference in concentrations is insignificant in the case of C. Further, the small amounts of W and Co observed in the adhesion layer are not at the same locations as the detected C, thus signifying that these are not holes in the adhesion layer, but rather different amounts of diffused W, C, and Co from under the adhesion layer into the adhesion layer. Also, the temperature is not high enough for large-rate diffusion to happen at a low surface speed of 30 m/min, regardless of the feed rate. Therefore, no crater is observed at low cutting velocities.

Thus, at low cutting velocities (temperatures), an adhered layer of mostly Ti is observed (which increases with feed), and diffusion of (mostly) C occurs from the tool *(i)* to the chips as well as *(ii)* to the adhered-layer on the tool.

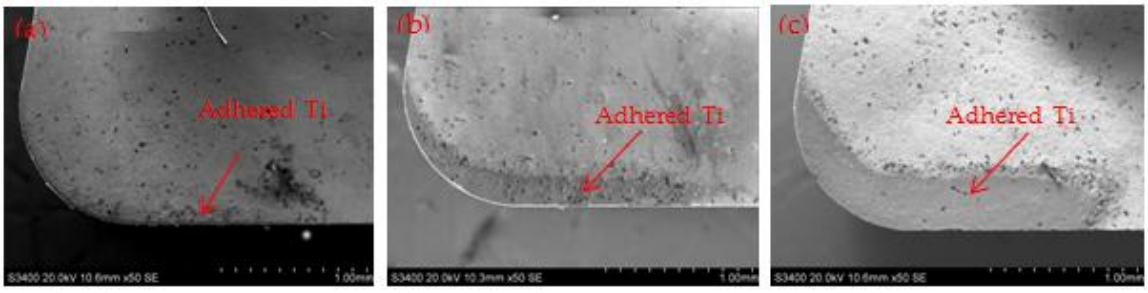

Figure 4-29 SEM images of cutting tool when cutting speed is 30m/min (lowest speed) and feed rate is (a) 0.05 mm/rev, (b) 0.15 mm/rev, and (c) 0.30 mm/rev. The red arrow points to the adhered Ti. From (a) to (c), the area of adhered Ti is increasing with the increase of the feed rate.

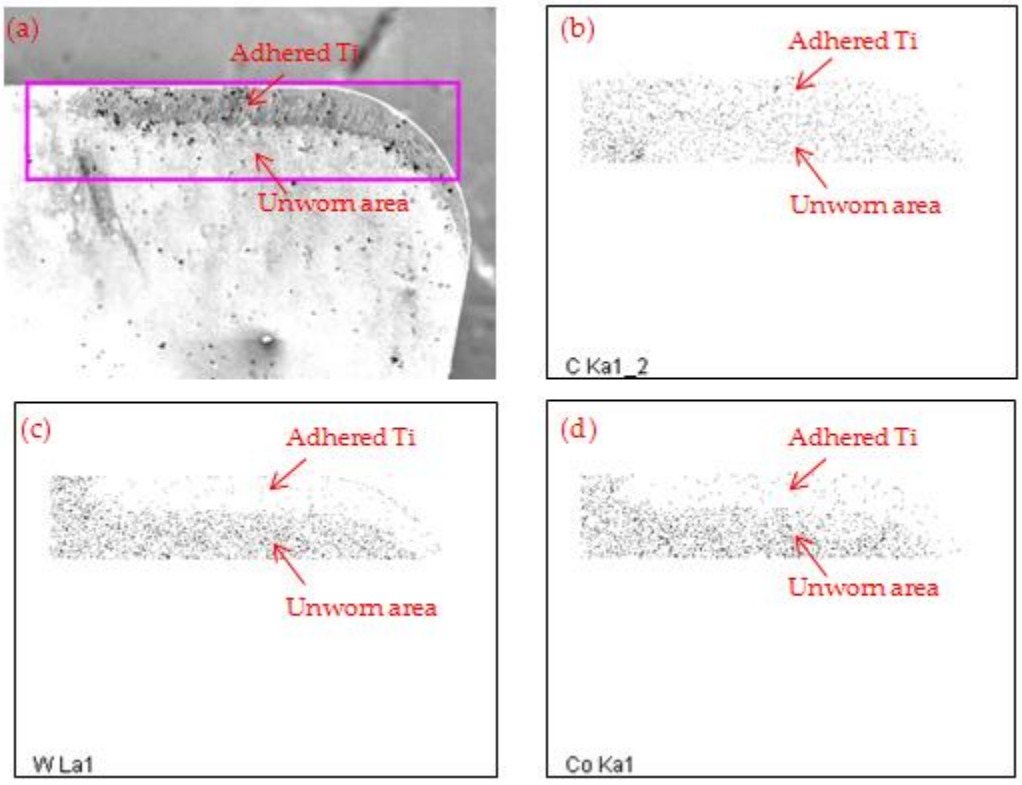

Figure 4-30 (a) SEM image of cutting tool when cutting speed is 30m/min and feed rate is 0.15 mm/rev. The pink square shows the selected area for EDS analysis. (b), (c), and (d) are the elemental distribution of C, W, and Co element in selected area by EDS, separately.

4.4.2 Interaction #2 (at Medium and High Cutting Velocities)

When the cutting tool cuts the workpiece at medium and high cutting velocities, there are series of events happen in sequence. A sample area is used to analyze these events, as shown in Figure 4-31. Figure 4-32 is the schematic figure of the worn surface of the cutting tool. Figure 4-31 (b) is the sketch map for this chosen area seen from different views. Next, each event is explained individually in the following.

1. First, a crater is formed due to (1) high-temperature diffusion of Cobalt from the tool to the chip [1], and (2) loss of WC grains due to the sliding action of the chip on the rake face of the tool [1]. The diffusion coefficient of Co is $8 \times 10^{-4} mm^2/s$ while the coefficient of WC is $1.05 \times 10^{-8} mm^2/s$. Therefore, the diffusion of Co accounts for the primary contribution to the diffusion wear and diffusion of C and W is weak comparatively. This is in good agreement with the autoradiographic studies by Cook et. al. [62]. After large amount of Co diffuses to the chip, the contact area between WC grains become smaller without the binding from Co. Then, the WC grain will be carried away by the chip. Next, the crater is formed, which includes the idealized areas 1, 2, and 3 in Figure 4-31 (b). Area 4 is the unworn WC-Co surface.
2. When the cutting continues, the second event happens in which Ti from the workpiece start to adhere to the crater. Until T_2, an adhesion layer formed on the crater surface. This is shown in Figure 4-31, in which areas 1 and 3 is already covered by the adhesion of Ti.
3. When the cutting process continues, the adhesion layer will start to wear away by sliding wear and continuing diffusive wear.
4. Until T4, the surface appearance is shown in Figure 4-31 (c). It is clear that more adhesion layer is worn away and some new adhesion layer formed on the crater. Meanwhile, the diffusive wear progresses.
5. From T4 to T5, the adhesion layer is further worn away as shown in Figure 4-31 (d).

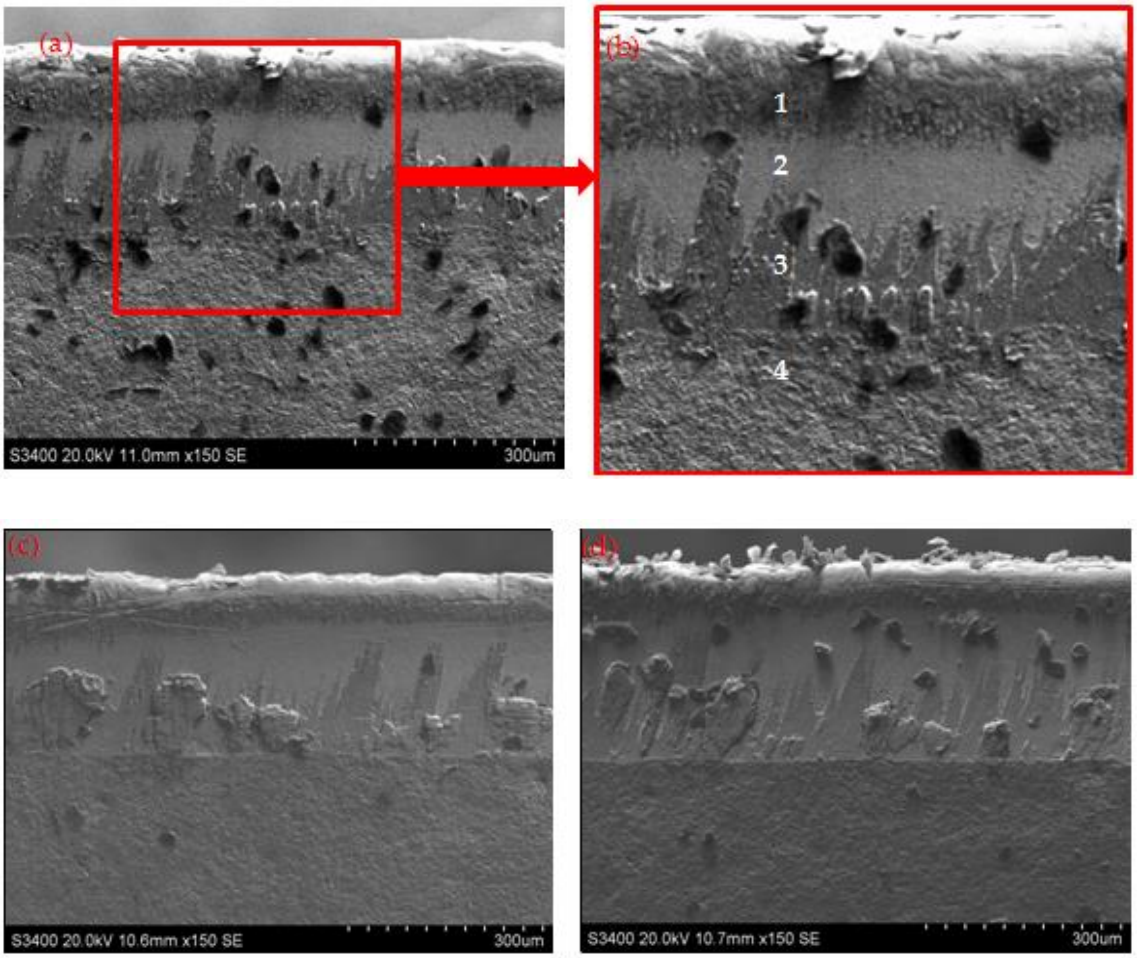

Figure 4-31 (a) SEM image of cutting tool when cutting speed is 120m/min and feed rate is 0.15 mm/rev (volume 1); (b) amplified part of (a); (c) SEM image when cutting speed is 120m/min and feed rate is 0.15 mm/rev (volume 2) and (d) SEM image of cutting tool when cutting speed is 120m/min and feed rate is 0.15 mm/rev (volume 3)

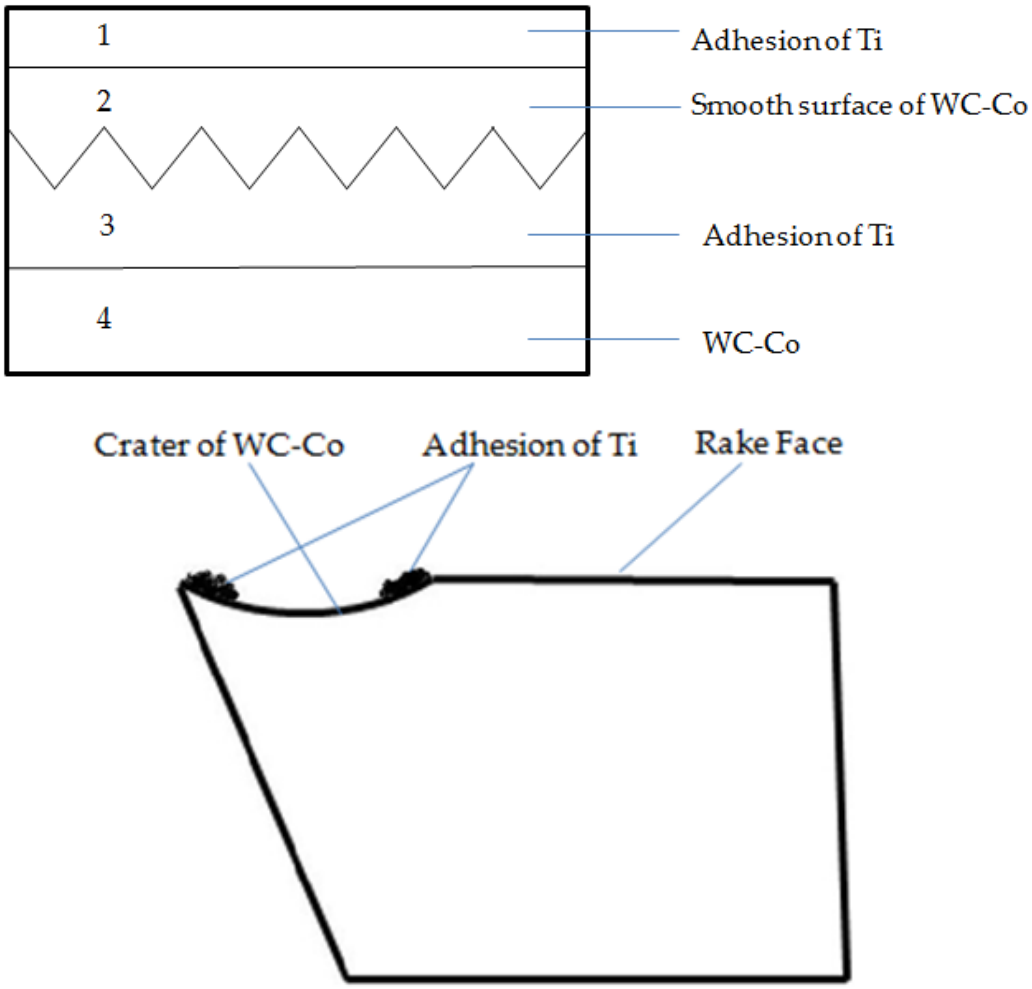

Figure 4-32 Sketch map of worn surface of WC-Co (top view), and Sketch map of worn surface (side view)

These events can also be listed as a flow chart, which is shown in Figure 4-33. It is observed that the depth of the crater increases when the cutting process continues.

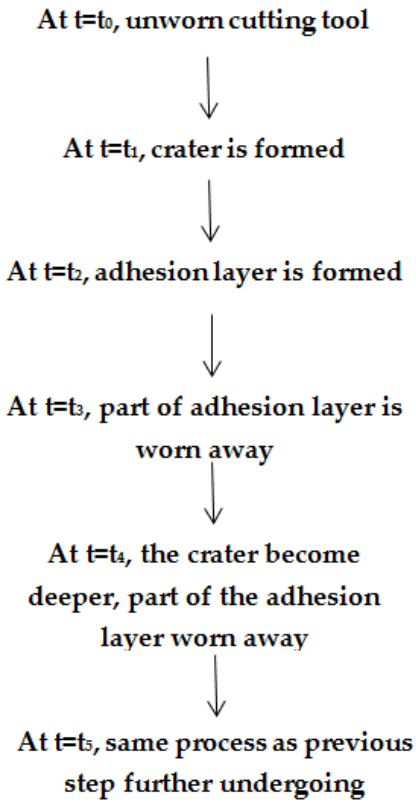

Figure 4-33 Flow chart of interaction #2

4.4.3 Interaction #3 (C Pullout and Deposition at Low Feed Rates)

When the cutting tool cuts the workpiece at high cutting velocities and low feed rates, interactions between the dominant wear mechanisms result in carbon pullout from the tool body and its deposition on the tool surface – this is the third interaction observed.

When the chip slides on the rake face with high velocity, high temperatures are generated. At high temperatures, the diffusion coefficients of W, C, and Co are close to each other. At this temperature, the pullout of WC resulting from Co diffusion, play a more important role than the diffusion of W and C. Although the diffusion coefficient of Co is slightly lower than those of W and C, the Co diffusion makes the WC grains more exposed to the chips, and

weakens the attachment between these peripheral WC grains and the rest of the tool body. These WC particles are removed by the sliding chip and a crater is formed. As cutting progresses, the Ti from the workpiece starts to adhere to the crater and forms an adhered layer on the crater close to the cutting edge. This adhered layer will separate the contact between the tool surface and chip and decrease the temperature in the tool in that region. This will prevent the crater from increasing to some extent. Due to this lower temperature, the diffusion rate of elements from the tool to the chip are decreased, especially for W and Co [61]. However, at lower temperatures, the diffusion coefficient of C is much higher than that of W or Co, and hence C will diffuse from the tool to adhered layer, which explains the C build-up at the tool edge as shown in Figure 4-34. Further, part of this C deposition can be carried by the chip to the tool body, which can be seen in Figure 4-34 as the C discoloration. The elemental distribution in EDS in Figure 4-35 can verified the SEM image. The distribution of C matches that in SEM image. From SEM and EDS, there is no indication of the formation of a stable TiC layer as discussed in [63].

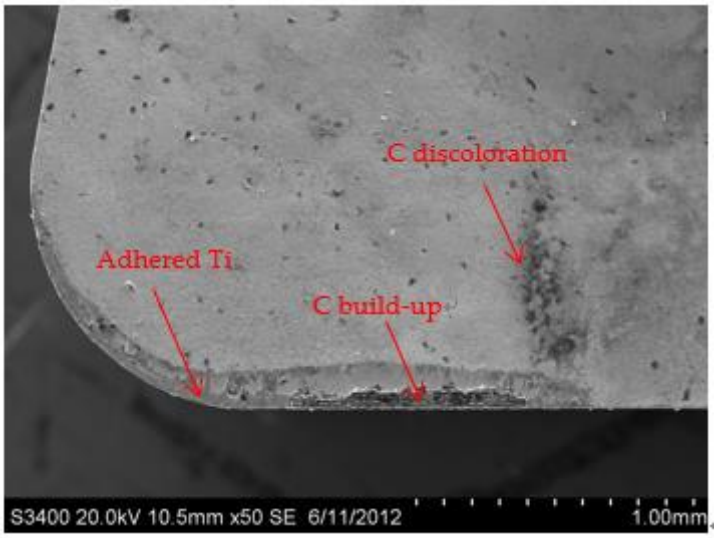

Figure 4-34 SEM images of cutting tool when cutting speed is 120m/min and feed rate is 0.05 mm/rev. The regions of adhesive Ti, C build-up, and C discoloration are pointed.

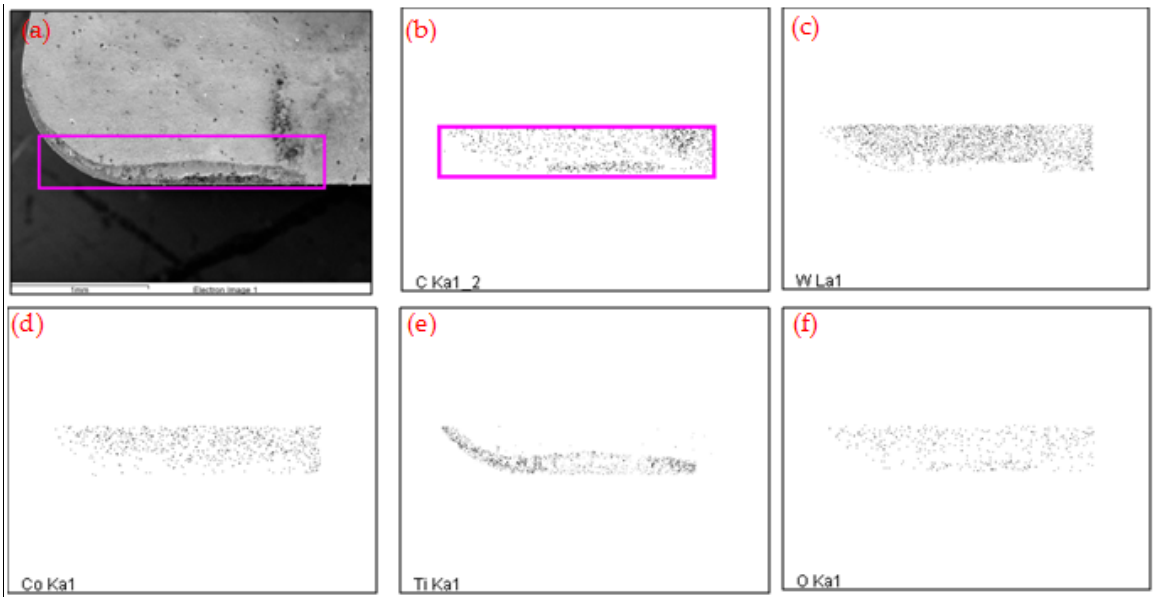

Figure 4-35 (a) SEM image of cutting tool when cutting speed is 120m/min and feed rate is 0.05 mm/rev. The pink square shows the selected area for EDS analysis. (b), (c), (d), (e), (f) are the EDS image of selected area of C, O, Ti, Co, and W element, which show the elemental distribution

4.5 MAPPING OF MAJOR WEAR MECHANISM INTERACTIONS

After analyzing and identifying the worn surface of WC-Co at different conditions, three kinds of interactions between the wear mechanisms at different conditions are obtained. In this section, the mapping of wear mechanisms and the mapping of interactions between wear mechanisms are shown in Figure 4-36 and Figure 4-37 respectively.

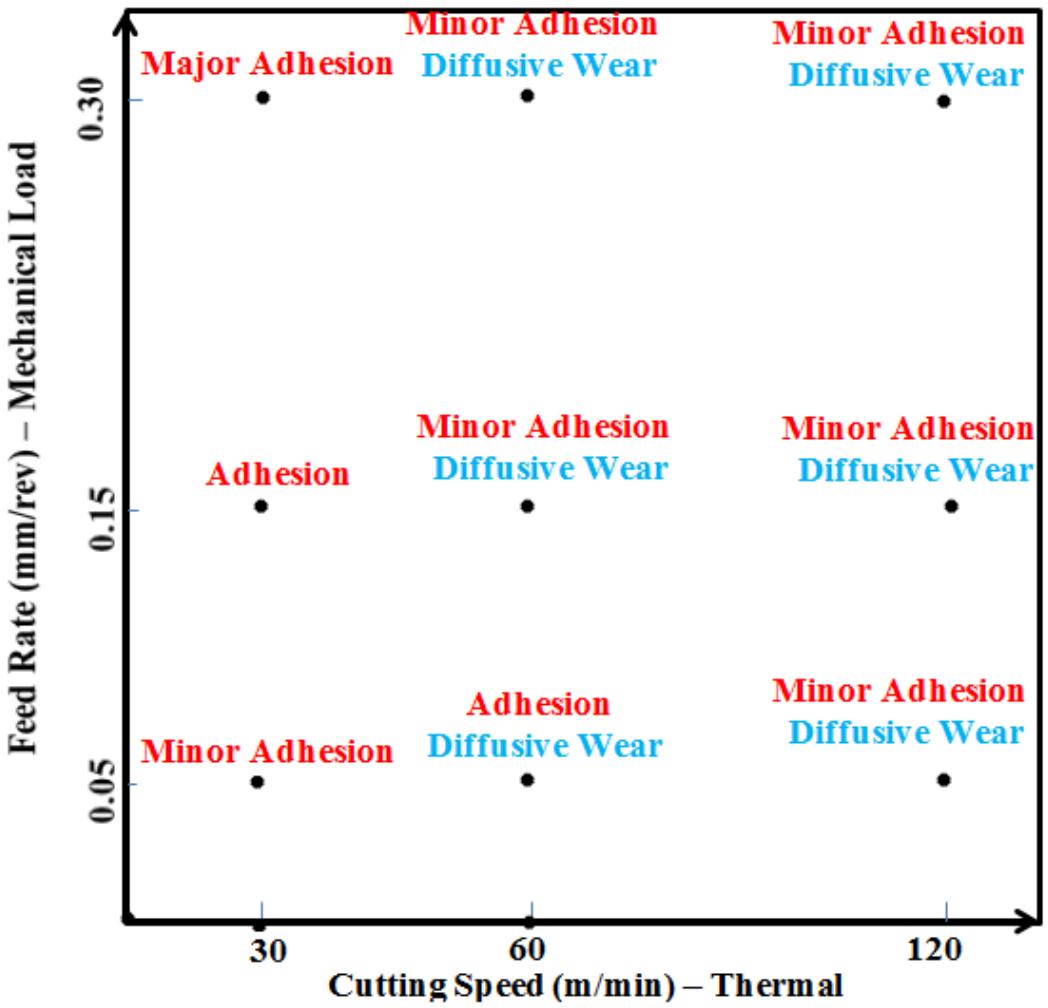

Figure 4-36 Mapping of wear mechanisms at different conditions

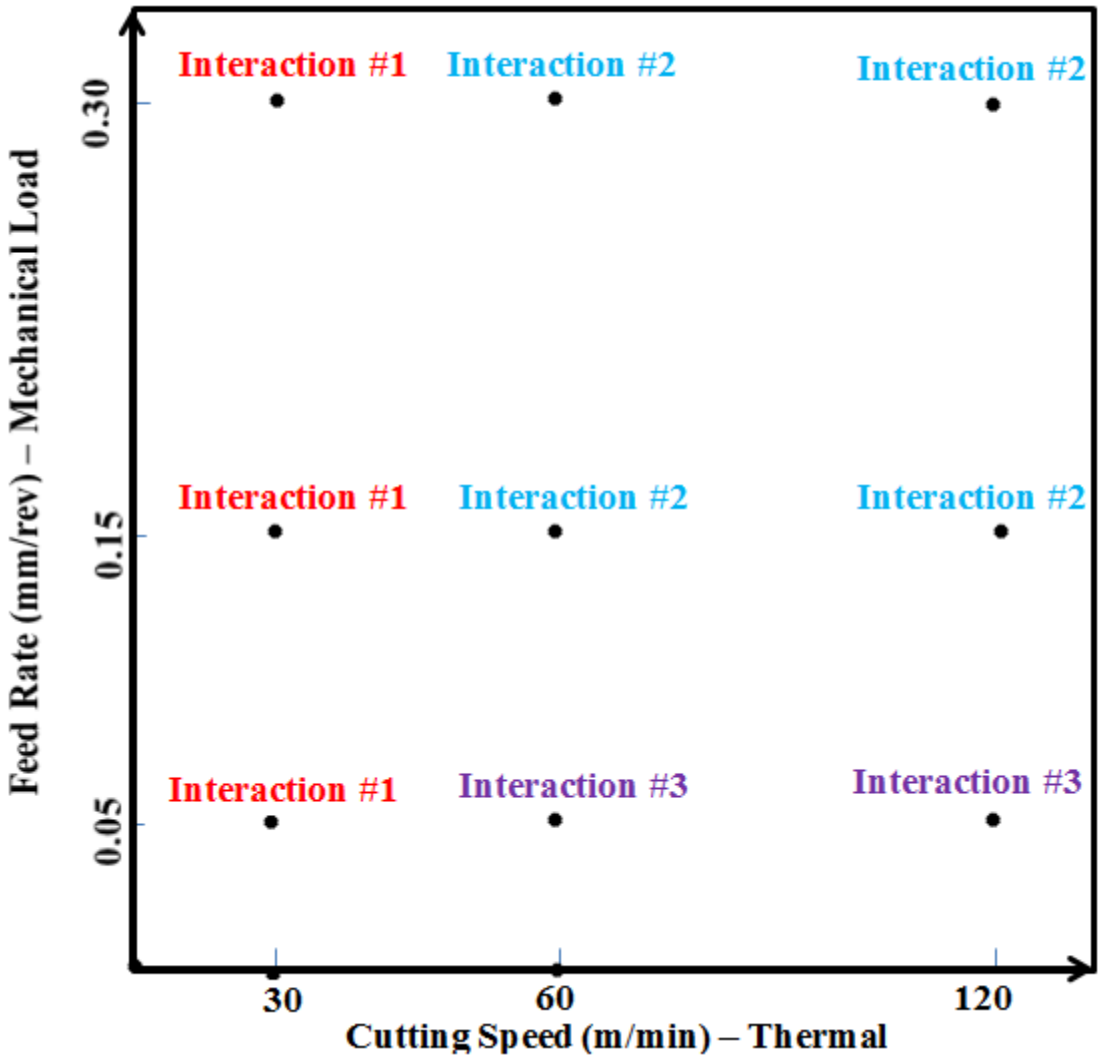

Figure 4-37 Mapping of interactions between the wear mechanisms at different conditions

Figure 4-36 shows the mapping of the wear mechanisms, which indicates the transition of wear mechanisms. Adhesion occurs at low cutting speed and all feed rates. At low feed rate, the area of adhesion layer is smaller. As the feed rate increases, the area of adhesion layer increases correspondingly. When the cutting speed increases, diffusive wear mechanisms appears and part of the adhesion layer is worn away. Figure 4-37, which is based on the discussion in Section 4.4, shows the mapping of the interactions between the wear

mechanisms. At low cutting speed and all feed rates, Interaction #1 occurs. At medium and high cutting speeds, Interaction #3 occurs. At medium and high cutting speeds and feed rates, Interaction #2 occurs. Interaction #2 has the largest wear rate.

5. CONFIRMING MAJOR WEAR MECHANISMS INTERACTIONS THROUGH TRIBOMETRIC TESTS (RQ2)

This chapter discusses the design of tribometric bench tests to confirm the wear mechanism interactions in terms of fundamental material behavior. Generally, according to the structure and function of the tribosystem to be studied, the tribotests can be grouped by machinery field test, machinery bench tests, tribosystem tests, components bench tests, model tests, and laboratory tests [64]. In our case, tribosystem tests and tribometric bench tests are our research objects, which are to identify and analyze the interactions between wear mechanisms in a machining tribosystem, and to confirm the fundamental physicochemical material interaction behavior through tribometric tests. Since the design of the tribometric bench tests are used to simulate the wear mechanisms and the interaction among them in the tribosystem, the design has to meet a sufficient similarity in the basic tribological parameters between the tribosystem tests and tribometric bench tests. These parameters may include materials/lubricant/environment combination, connected materials properties, cutting speed, feed rate, temperature, cutting time, and so on.

The basic characteristics and relevant parameters of the tribosystem tests and tribometric bench tests in our study are shown in Figure 5-1.

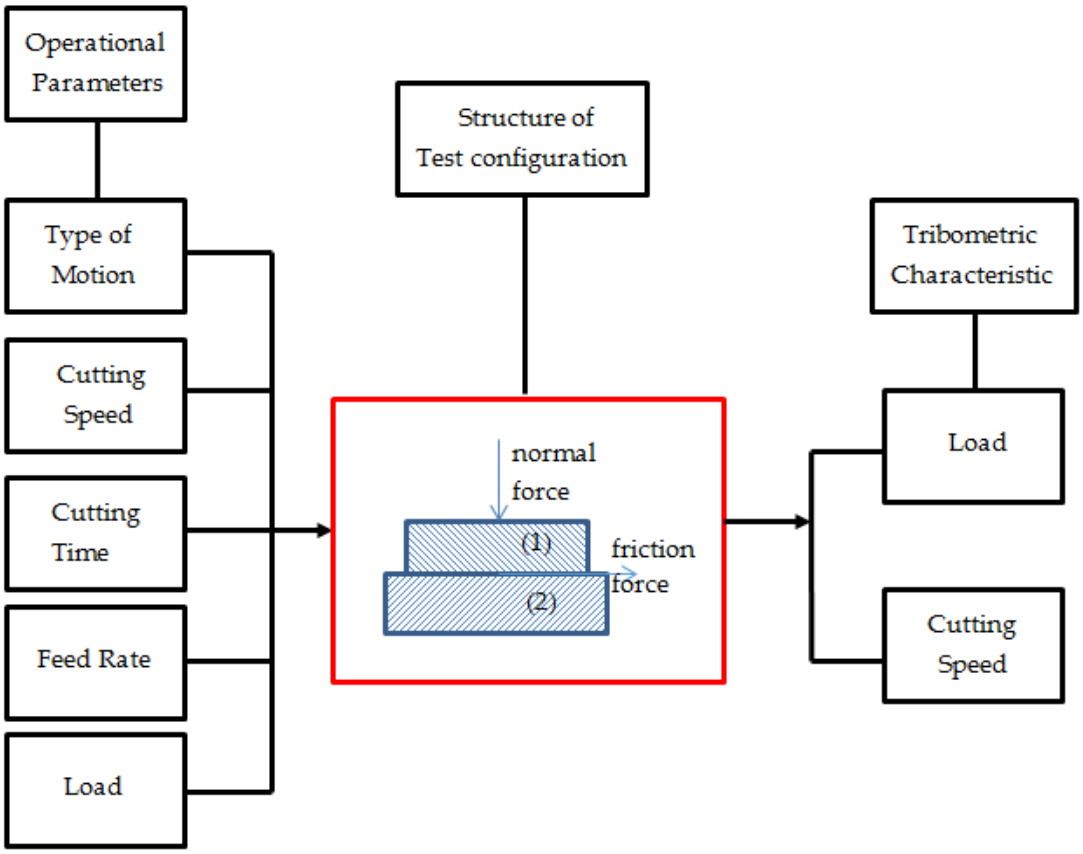

Figure 5-1 Basic characteristics and parameters of tribosystem and tribometer

5.1 MATCHING THE MACHINING TRIBOSYSTEM TESTS TO BENCH TESTS

5.1.1 Parameters of the Machining Tribosystem

The parameters of tribosystem play an important role in the wear process. It may affect the interaction among the wear mechanisms and the transition of the dominant wear mechanisms. The basic and relevant parameters of the tribosystem are given below.

For the (field-level) machining tribosystem:

1. Triboelement 1: rake face of WC-Co cutting tool;
2. Triboelement 2: (shiny) underside of Ti-6Al-4V chip

3. Geometry of the test configuration: It is shown in Figure 5-2.

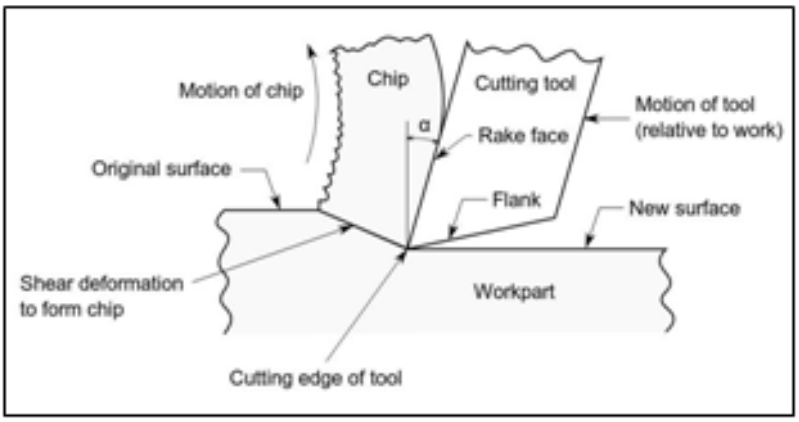

Figure 5-2 Description of the geometry of the test configuration [65].

4. Materials characteristics and properties:

    a. WC-Co: Fine WC particles are the major constituent, which are relatively hard and brittle, and the minor constituent is a cobalt-rich binder phase which is relatively soft and ductile and account for 10.2 % [14].

    b. Ti-6Al-4V: High fracture resistance, high resistance to corrosion, it can maintain high strength at elevated temperatures. However, it also has some disadvantages, such as low modulus of elasticity, high chemical reactivity and low thermal conductivity [7]. The low thermal conductivity results in the majority of the generated heat flowing into the tool edge (80%) [8], and wear out the cutting tool faster. These properties of WC-Co and Ti-6Al-4V are summarized in Table 5-1.

Table 5-1 The physical and chemical properties of WC-Co and Ti-6Al-4V [12, 15, 16]

	WC-Co	Ti-6Al-4V
Composition	10.2% Co, 89.8% WC	90% Ti, 6% Al, 4% V
Density (g/cm3)	14.96	4.42
Hardness (HV)	1675	349
Young's Modulus (GPa)	580 [16]	114
Ultimate Tensile Strength (MPa)	1440	950

5. Interfacial element: Air (no lubrication).
6. Environmental medium: dry air.
7. Motion: sliding motion between the rake face of cutting tool and the chip.
8. Load: The load for each process conditions combination is different. Further, these loads vary during the cut both periodically due to the adiabatic shear banding process as well as due to tool wear. The maximum cutting and feed forces recorded from a force-sensor integrated tool are given below in Table 5-2 for each process condition.

Table 5-2 The forces applied and resultant stress at different conditions.

Feed rate (mm/rev)	Cutting speed (m/min)	Chip velocity (m/min)	Max cutting force (N)	Max feed force (N)	Resultant Force (N)	Shear angle (degrees)
0.05	30	9.79	172.55	247.95	302.08	17.42
0.05	60	18.65	161.91	246.19	294.66	16.67
0.05	120	44.48	215.41	265.27	341.71	19.54
0.15	30	7.10	294.29	606.57	674.19	12.94
0.15	60	14.66	290.7	578.83	647.73	13.33
0.15	120	32.51	302.2	537.09	616.27	14.68
0.30	30	5.61	418.07	1107.99	1184.24	10.34
0.30	60	13.86	468.2	990.73	1095.79	12.65
0.30	120	74.92	2350	1331	2700.75	30.24

9. Sliding Speed: In the turning tests, three cutting speed are used, which are 30 m/min, 60 m/min, and 120 m/min. As the cutting speed changes, the rake angle (α) is constant, which is -6°. However, the shear angle (φ) changes as a function of rake angle and friction angle (β), as given in the Equation (5.2). From this the chip velocities are calculated (Equation 5.1).
10. The chip formation process in orthogonal turning is illustrated in Figure 5-3.

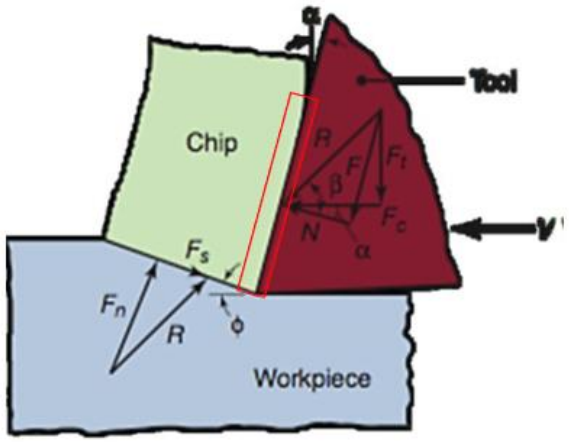

Figure 5-3 Schematic illustration of orthogonal turning. The red rectangle shows the contact area between the chip and the rake face of tool. N is the normal force, F is the friction force along the contact area of chip and tool, F_t is the thrust force, F_C is the cutting force. R is the resultant force. α is the rake angle, and φ is the shear angle.[5]

The normal force and speed of chip are calculated, which are shown in Table 5-3. The speed of chip is calculated by the following formulas,

$$V_C = V * \frac{\sin\varphi}{\cos(\varphi-\alpha)} \qquad (5.1)$$

$$\varphi = 45 + 1/2(\alpha - \beta) \qquad (5.2)$$

Here, V_C is speed of chip, V is cutting speed, φ is shear angle, α is rake angle, and β is the angle shown in Figure 5-3.

The contact area is calculated by two methods, which are by ImageJ and by equation. The equation is expressed as

$$\sigma_c = \frac{N}{l\,d} \qquad (5.3)$$

Here, N is speed of chip, l is contact length between the chip and rake face of cutting tool, d is the depth of cut. There is some approximation in this equation. In our case, the calculation of contact area is conducted by ImageJ, which gives a more accurate result. One example is given in Figure 5-4, in which the contact area at cutting speed 30 m/min and feed rate 0.30 mm/rev is 0.833 mm^2.

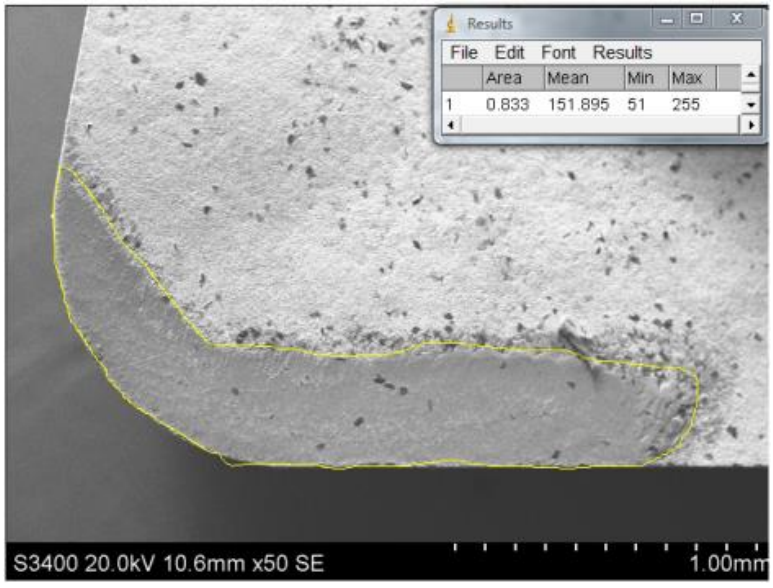

Figure 5-4 The measurement of contact area by ImageJ

Table 5-3 The normal force, friction force and speed of chip at different conditions

Feed rate(mm/rev)	Cutting speed (m/min)	Normal force at chip-rake interface (N)	Chip velocity (m/min)	Contact area (mm^2)	Contact Stress (MPa)
0.05	30	197.52	9.79	0.09	2146.98
0.05	60	186.76	18.65	0.12	1518.35
0.05	120	241.96	44.48	0.18	1314.99
0.15	30	356.08	7.10	0.41	866.38
0.15	60	349.61	14.66	0.41	842.44
0.15	120	356.69	32.51	0.31	1158.07
0.30	30	531.60	5.61	0.86	618.14
0.30	60	569.19	13.86	0.82	696.69
0.30	120	2476.25	74.92	N/A	N/A

5.1.2 Parameters of Ball-On-Disc Tribometric Tests

Bench tests are usually used to simulate the tribological behavior of a practical tribosystem and try to simplify the conditions and parameter in the tribosystem. Currently, the common bench tests used for WC-Co / Ti-6Al-4V tribosystems include pin-on-disc, ball-on-disc, and block-on-ring tribometers [32, 51, 54, 55]. In this study, the ball-on-disc is adopted.

The basic characteristics and relevant parameters of ball-on-disc test are given below.

1. Triboelement 1: Ball
2. Triboelement 2: Disc
3. Geometry of the test configuration: Figure 5-5 shows the schematic illustration of ball-on-disc test.
4. Interfacial element: Air and no lubrication.
5. Environmental medium: dry air.

6. Motion: sliding motion between the ball and the disk. A ball is stationary against rotating disc.
7. Maximum load: 5N.

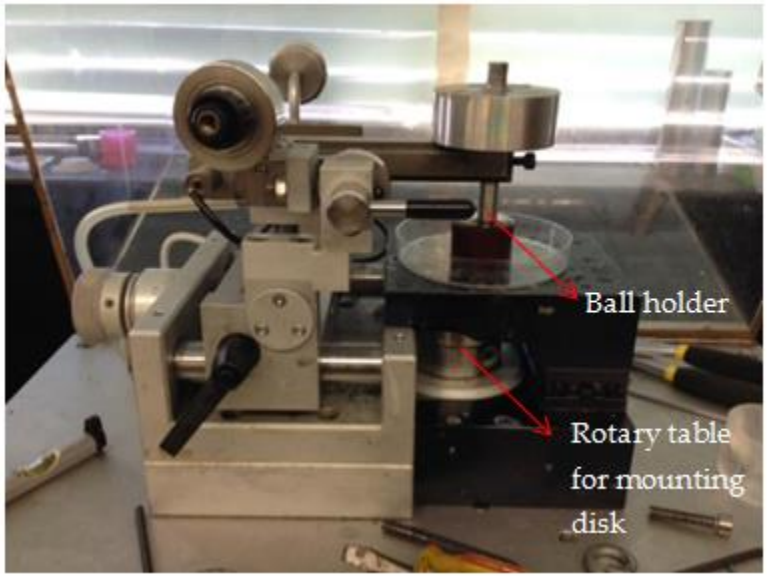

Figure 5-5 Schematic illustration of ball-on-disc test. The ball is stationary and the disc is rotating.

5.1.3 Calculation of Tribometric Parameters

Since a tribometer is made to simulate the tribological behavior of a tribosystem, there should be a sufficient similarity between the operational parameters of the tribosystem and tribometer. The value of parameters in the machining tests will be scaled to the corresponding parameters in the tribometer tests. The scaling process is given in the following.

First, the stress between the ball and disc is needed to be calculated. A rule that contact stress between chip and rake face of cutting tool in the tribosystem equal to the stress between the ball and disc [13] is followed. The contact stress in the tribosystem can be obtained by the normal stress and the contact area. Then this contact stress is used to

calculate the contact force and radius of the contact area between the ball and disc by using the Herztian equations [66].

$$k = 9/16[(1 - \upsilon_1{}^2) + \frac{E_1}{E_2}(1 - \upsilon_2{}^2)] \qquad (5.4)$$

Where k is an elastic mismatch factor, υ_1 is Poisson ratio of Ti-6Al-4V, υ_2 is the Poisson ratio of WC-Co, E_1 is the elastic modulus of Ti-6Al-4V, E_2 is the elastic modulus of WC-Co.

$$a^3 = \frac{4kPR}{3E_1} \qquad (5.5)$$

Where a is the radius of contact area, P is normal load, R is the radius of WC-Co ball.

$$P_m = \frac{P}{\pi a^2} \qquad (5.6)$$

Where P_m is the mean contact pressure.

By combining these equations above, the forces in tribometer tests and radiuses of contact area for some representative cases are shown in Table 5-4. Due to the forces higher than the limit of the tribometer (5N), the forces are scaled into the limit as the value of P` by divided by 10. Here, 7 typical tests of 9 are conducted in tribometer tests.

Table 5-4 Data of the radius of contact area and normal force

Machining Test Condition			Sliding speed	a (radius of the contact area)	P (Normal force)	P` (P/10)
Test number	Feed rate (mm/rev)	Cutting speed (m/min)	(m/min)	(mm)	(N)	(N)
1	0.05	60	18.6	0.11	48.2	4.8
2	0.05	120	44.5	0.09	31.3	3.1
3	0.15	30	7.1	0.06	9.0	0.9
4	0.15	60	14.7	0.06	8.2	0.8
5	0.15	120	32.5	0.08	21.4	2.1
6	0.30	30	5.6	0.04	3.3	0.3
7	0.30	60	13.9	0.05	4.7	0.5

5.2 OBSERVATIONS FROM TRIBOMETRIC TESTS

After the ball-on-disc tests, the worn balls are characterized by SEM and EDS. In these experiments, major and observed wear mechanisms on WC-Co are adhesion of Ti-6Al-4V, C pullout. From the SEM image, the adhesion of Ti can be seen on the cutting tool.

5.2.1 At Low Cutting Velocities

Figure 5-6 shows the SEM image of the worn surface of ball when rotating speed is 30 m/min and normal load is 1 N, which corresponds to the turning test at cutting speed 30 m/min and feed rate 0.15 mm/rev. From this figure, adhesion layer can be seen and also some black discoloration is shown on the surface. Figure 5-7 shows the EDS images of composition of elements of the ball. From the EDS images, it is clear that the adhesion layer is mainly Ti and the discoloration element is C. These features of the worn surface agree well with that in the turning test at same condition.

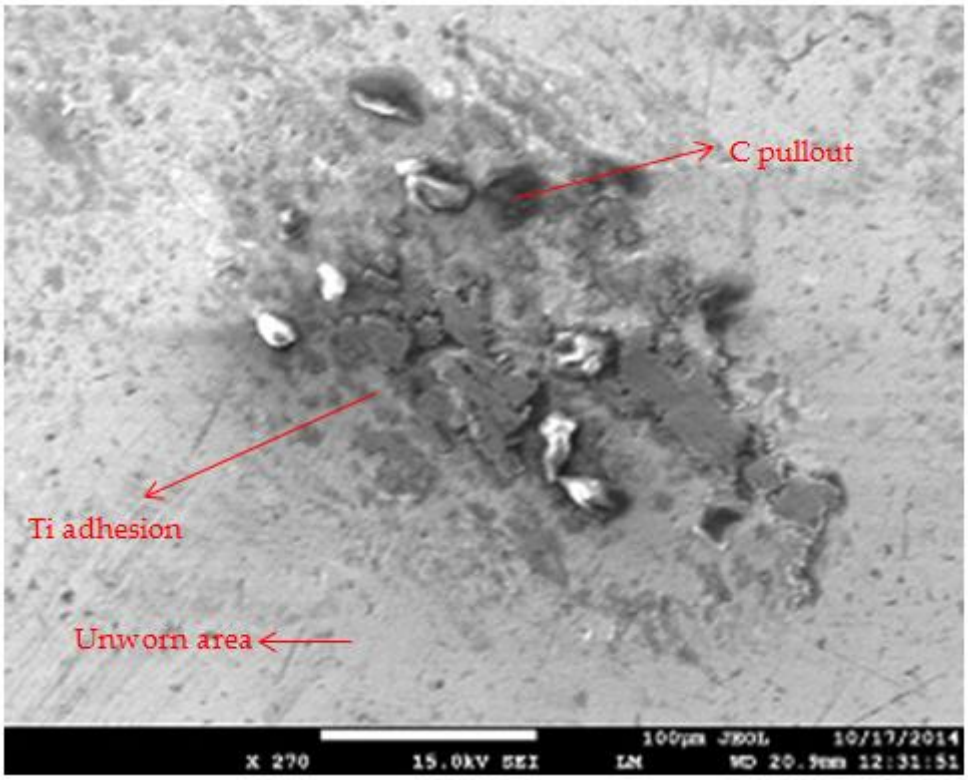

Figure 5-6 SEM image of the worn surface of ball when rotating speed is 30m/min and the normal load is 0.9 N

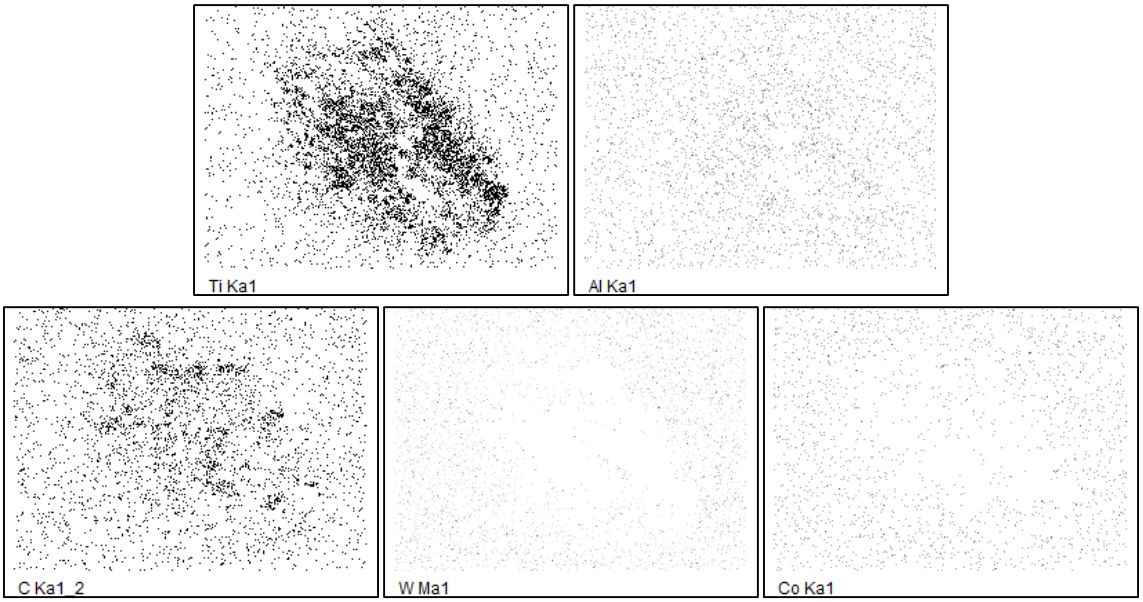

Figure 5-7 EDS images of composition of elements of the ball when rotating speed is 30 m/min and the normal load is 0.90 N. The elements are Ti, Al, C, W, and Co from left to right.

Figure 5-8 shows the SEM image of the worn surface of ball when rotating speed is 30 m/min and normal load is 0.3 N, which corresponds to the turning test at cutting speed 30 m/min and feed rate 0.30 mm/rev. Figure 5-9 shows the EDS images of composition of elements of the ball. These two figures show the similar surface features as those at rotating speed is 30 m/min and normal load is 1 N. This means that this difference of normal load does not provide much difference on the wear mechanisms.

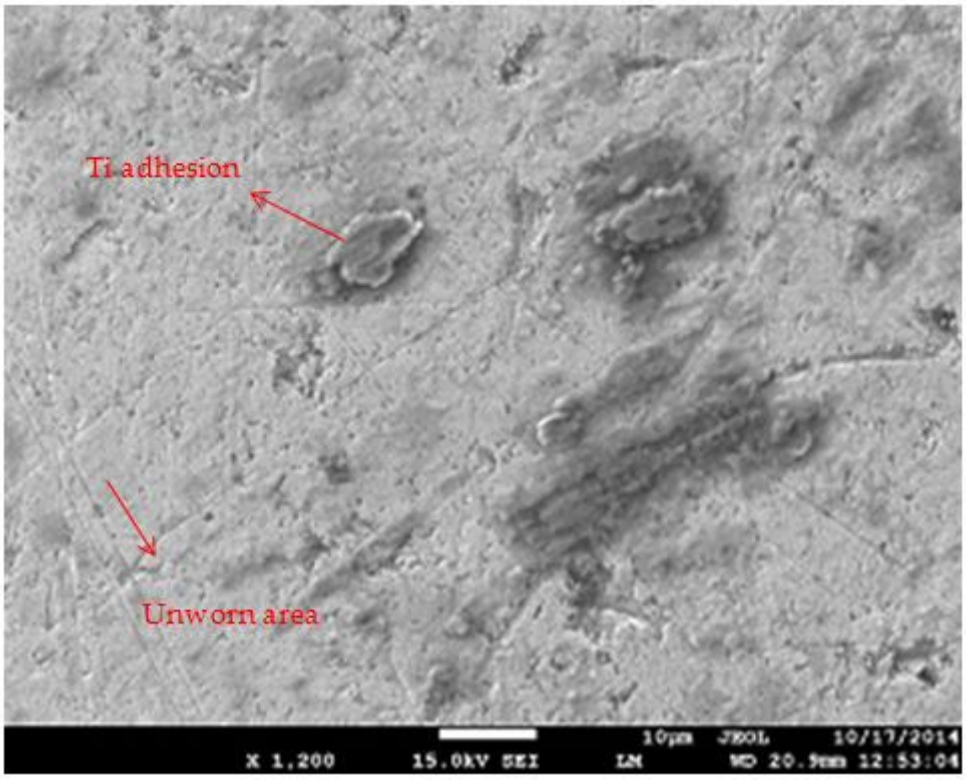

Figure 5-8 SEM image of the worn surface of ball when rotating speed is 30m/min and the normal load is 0.3 N.

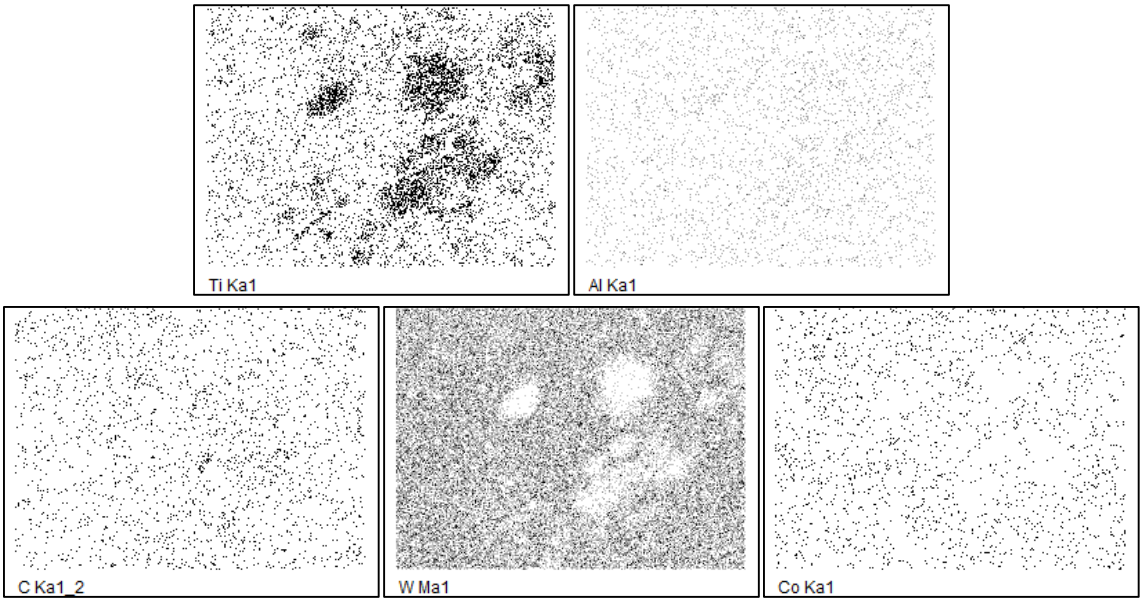

Figure 5-9 EDS images of composition of elements of the ball when rotating speed is 30 m/min and the normal load is 0.3 N. The elements are Ti, Al, C, W, and Co from left to right.

5.2.2 At Medium Cutting Velocities

Next, let us take a look at these wear mechanisms occurred at medium cutting velocity. Figure 5-10 shows the SEM image of the worn surface of ball when rotating speed is 60m/min and normal load is 5 N, which corresponds to the turning test at cutting speed 60 m/min and feed rate 0.05 mm/rev. From this figure, it can be seen that adhesion layer can be seen and also some black discoloration is shown on the surface. Figure 5-11 shows the EDS images of composition of elements of the ball. From the EDS images, it is clear that the adhesion layer is mainly Ti and the discoloration element is C. These features of the worn surface agree well with that in the turning test at same condition.

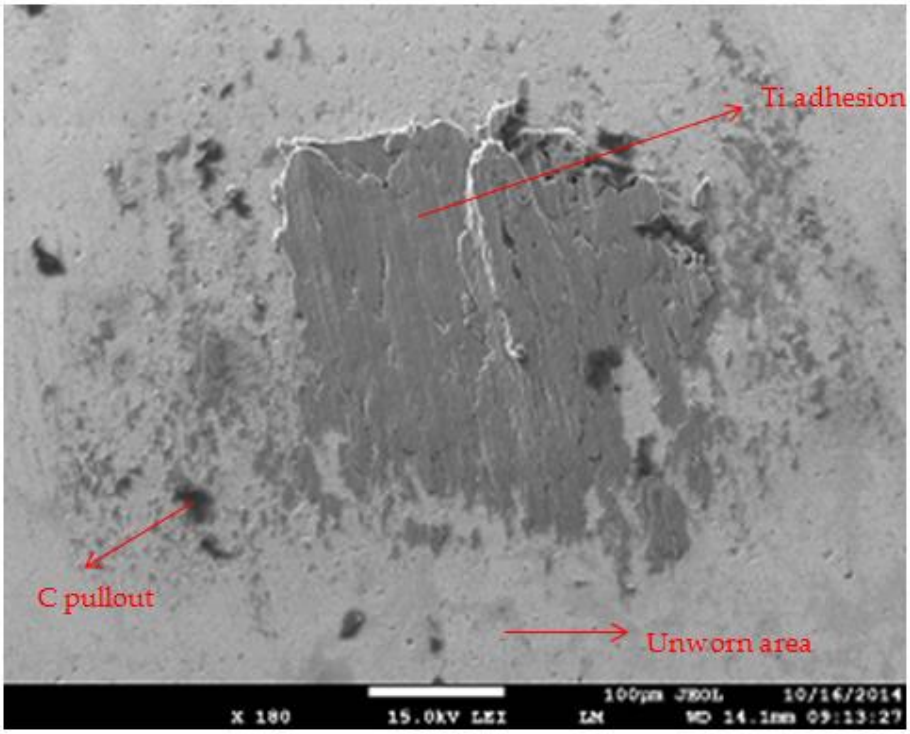

Figure 5-10 SEM images of the worn surface of ball when rotating speed is 60m/min and normal load is 5 N.

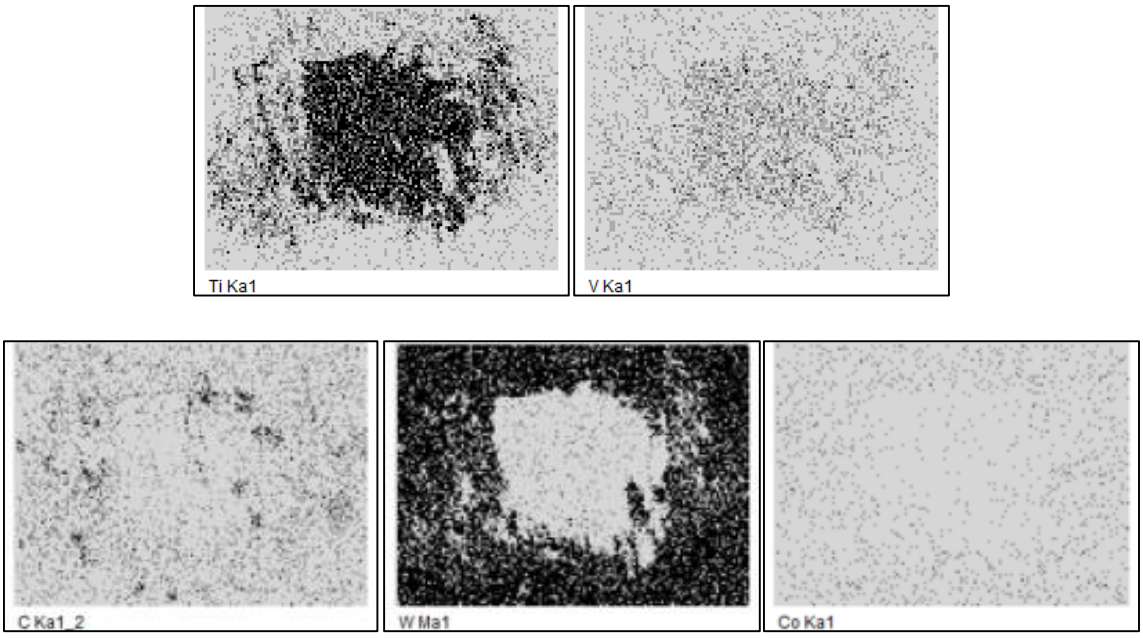

Figure 5-11 The EDS images of composition of elements of the ball when rotating speed is 60 m/min and normal load is 5 N. The elements are Ti, V, C, W, and Co from left to right.

Figure 5-12 and Figure 5-13 show the SEM image and EDS mappings of the worn surface of ball when rotating speed is 60 m/min and normal load is 0.8 N, which corresponds to the turning test at cutting speed 60 m/min and feed rate 0.15 mm/rev. These features of the worn surface agree well with the previous one at cutting speed 60 m/min and normal load 5 N.

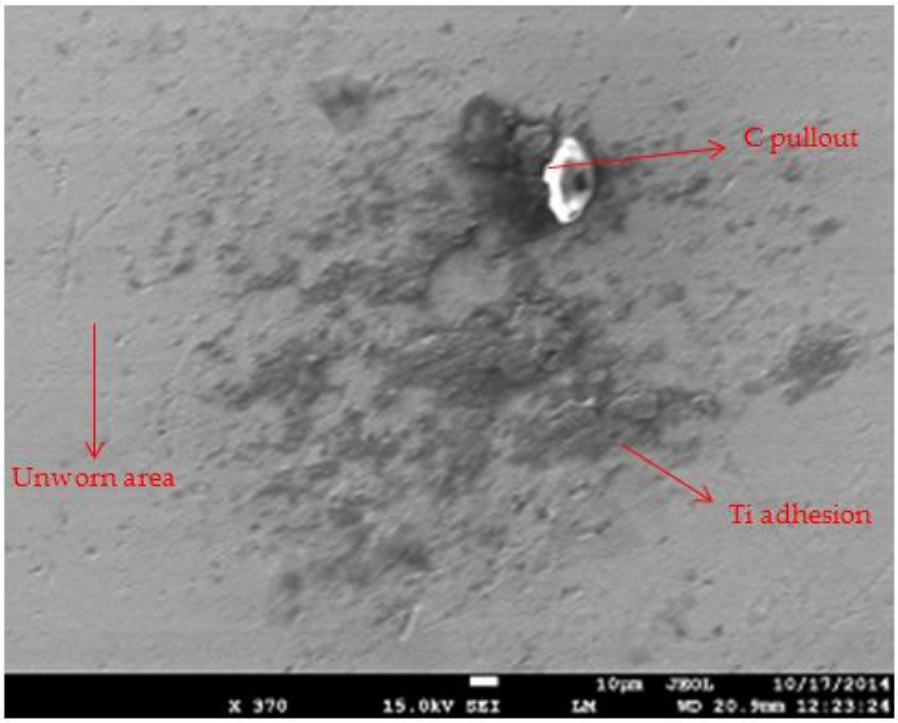

Figure 5-12 SEM images of the worn surface of ball when rotating speed is 60m/min and the normal load is 0.8 N.

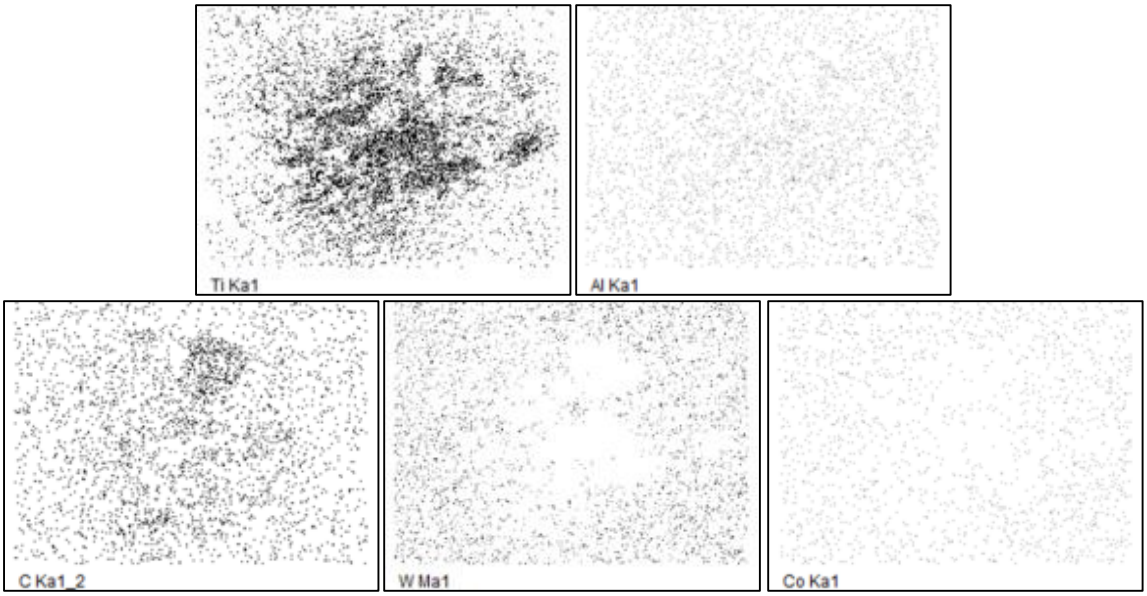

Figure 5-13 EDS images of composition of elements in cutting tool when cutting speed is 60 m/min and the normal load is 0.8 N. The elements are Ti, Al, C, W, and Co from left to right.

Figure 5-15 shows the SEM image of the worn surface of ball when rotating speed is 60m/min and normal load is 0.5 N, which corresponds to the turning test at cutting speed 60 m/min and feed rate 0.30 mm/rev. These features of the worn surface agree well with the previous one at cutting speed 60 m/min and normal load 5 N. Figure 5-15 shows the EDS images of composition of elements of the ball. From the EDS images, it is clear that the adhesion layer is mainly Ti and the discoloration element is C. These features of the worn surface agree well with that in the turning test at same condition.

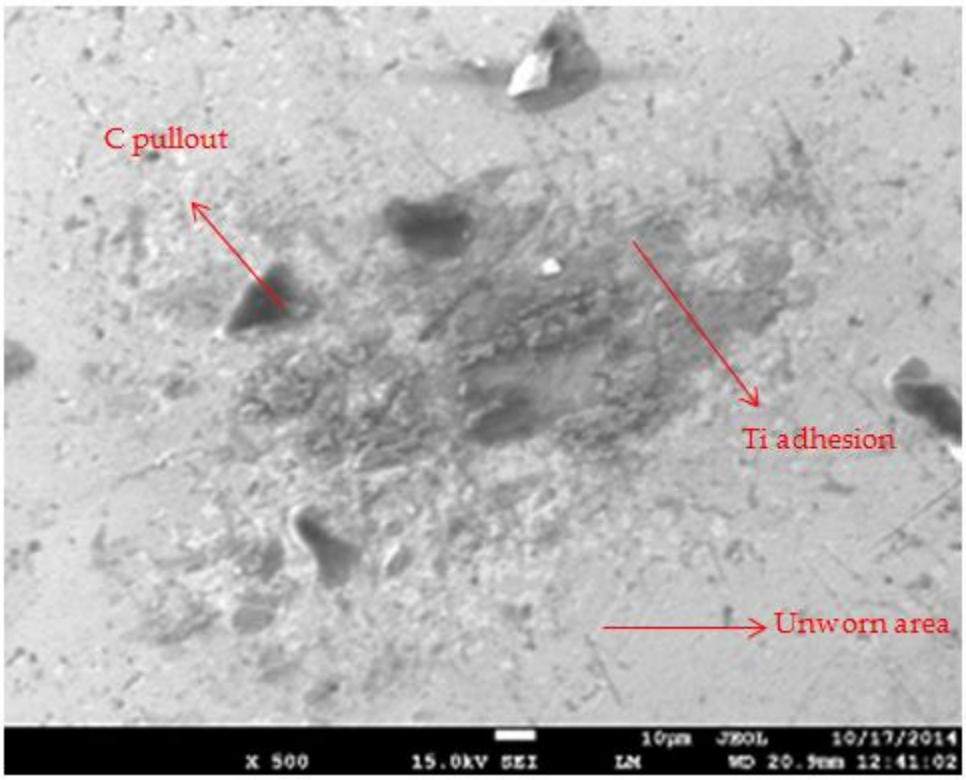

Figure 5-14 SEM images of the worn surface of ball when rotating speed is 60m/min and normal load is 0.5 N.

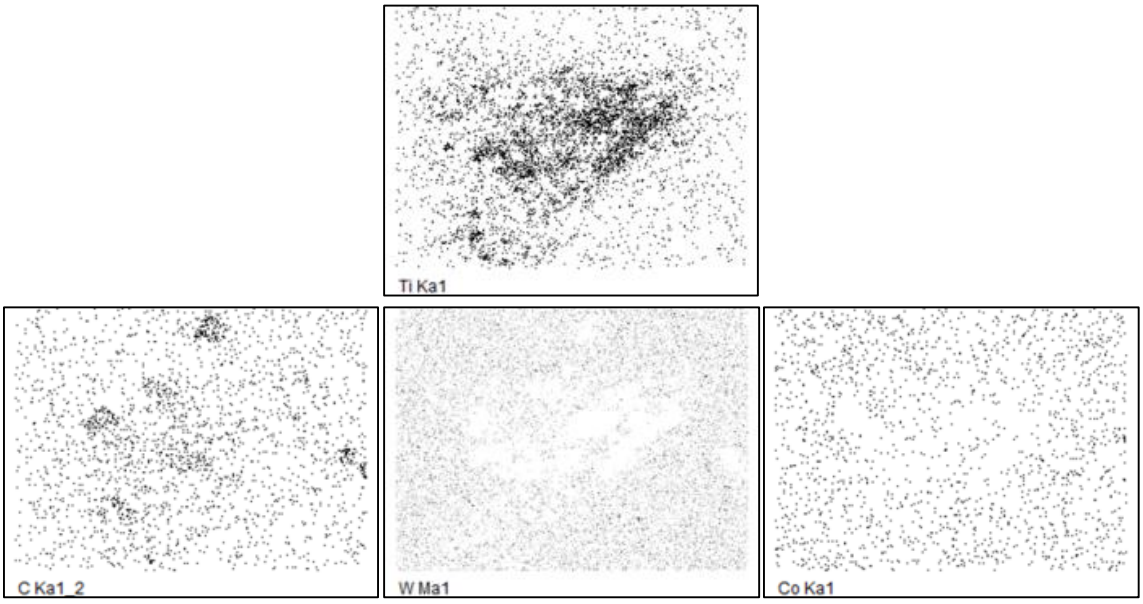

Figure 5-15 EDS images of composition of elements in cutting tool when cutting speed is 60 m/min and the normal load is 0.5 N. The elements are Ti, C, W, and Co from left to right.

5.2.3 At High Cutting Velocities

Next, let us take a look at these wear mechanisms occurred at high cutting velocity. Figure 5-16 shows the SEM image of the worn surface of ball when rotating speed is 120m/min and normal load is 3 N, which corresponds to the turning test at cutting speed 120 m/min and feed rate 0.05 mm/rev. From this figure, it can be seen that adhesion layer can be seen and also some black discoloration is shown on the surface. Figure 5-17 shows the EDS images of composition of elements of the ball. From the EDS images, it is clear that the adhesion layer is mainly Ti and the discoloration element is C. These features of the worn surface agree well with that in the turning test at same condition.

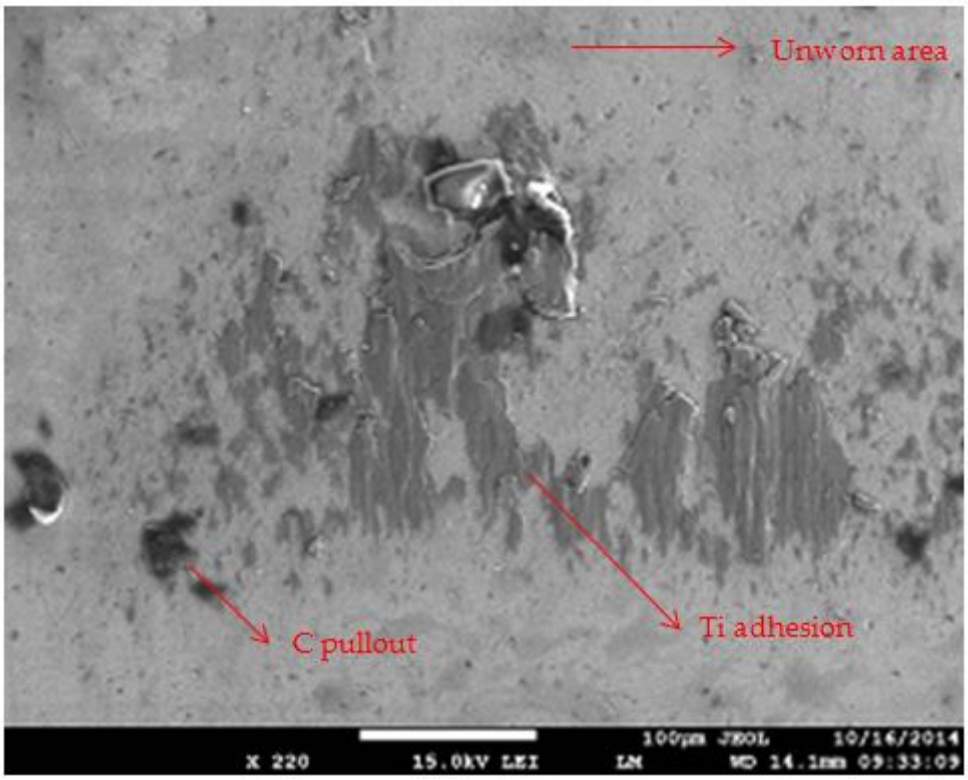

Figure 5-16 SEM images of the worn surface of ball when rotating speed is 120m/min and normal load is 3 N.

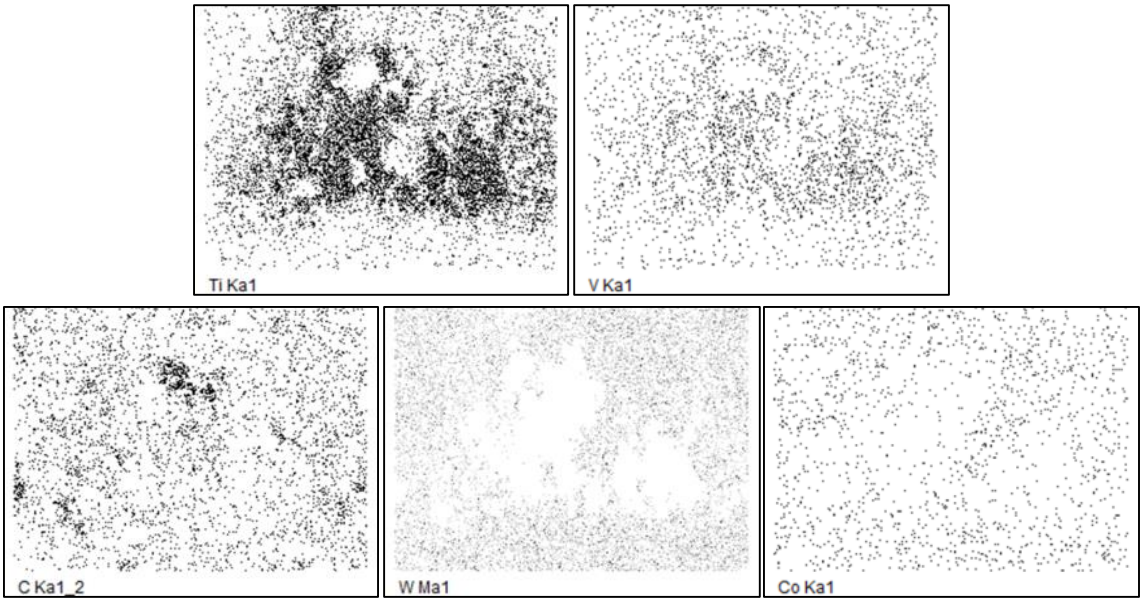

Figure 5-17 EDS images of composition of elements in cutting tool when cutting speed is 120 m/min and the normal load is 3 N. The elements are Ti, V, C, W, and Co from left to right.

Next, let us take a look at these wear mechanisms occurred at medium cutting velocity. Figure 5-18 shows the SEM image of the worn surface of ball when rotating speed is 120m/min and normal load is 2 N, which corresponds to the turning test at cutting speed 120 m/min and feed rate 0.15 mm/rev. From this figure, it can be seen that adhesion layer can be seen and also some black discoloration is shown on the surface. Figure 5-19 shows the EDS images of composition of elements of the ball. From the EDS images, it is clear that the adhesion layer is mainly Ti and the discoloration element is C. These features of the worn surface agree well with that in the turning test at same condition.

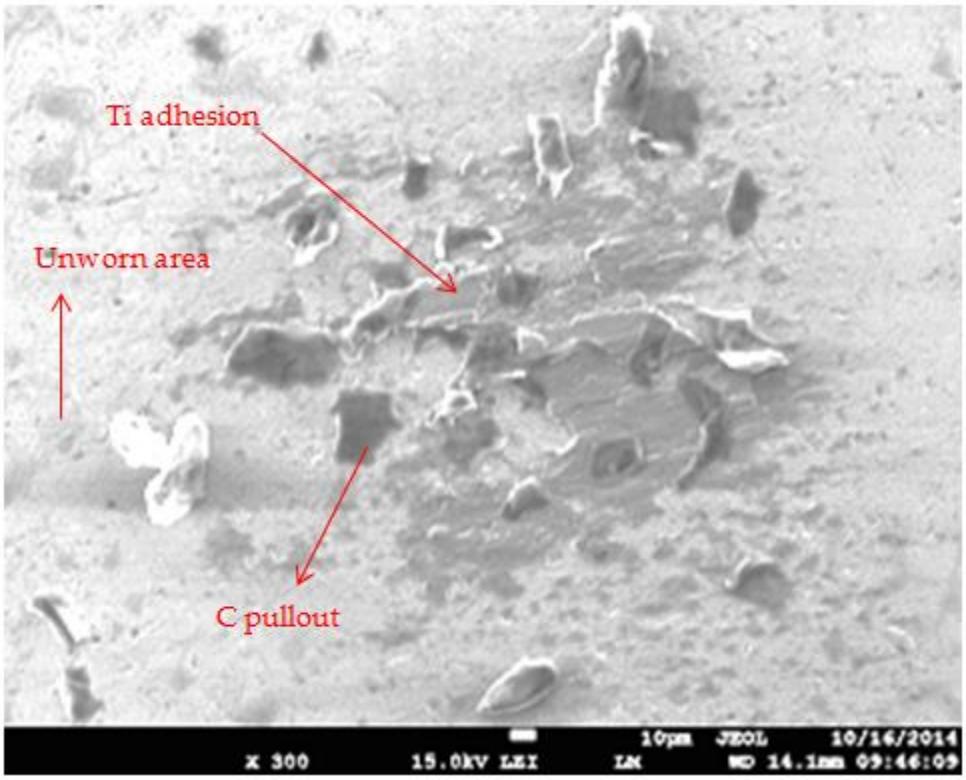

Figure 5-18 SEM images of the worn surface of ball when rotating speed is 120m/min and normal load is 2 N.

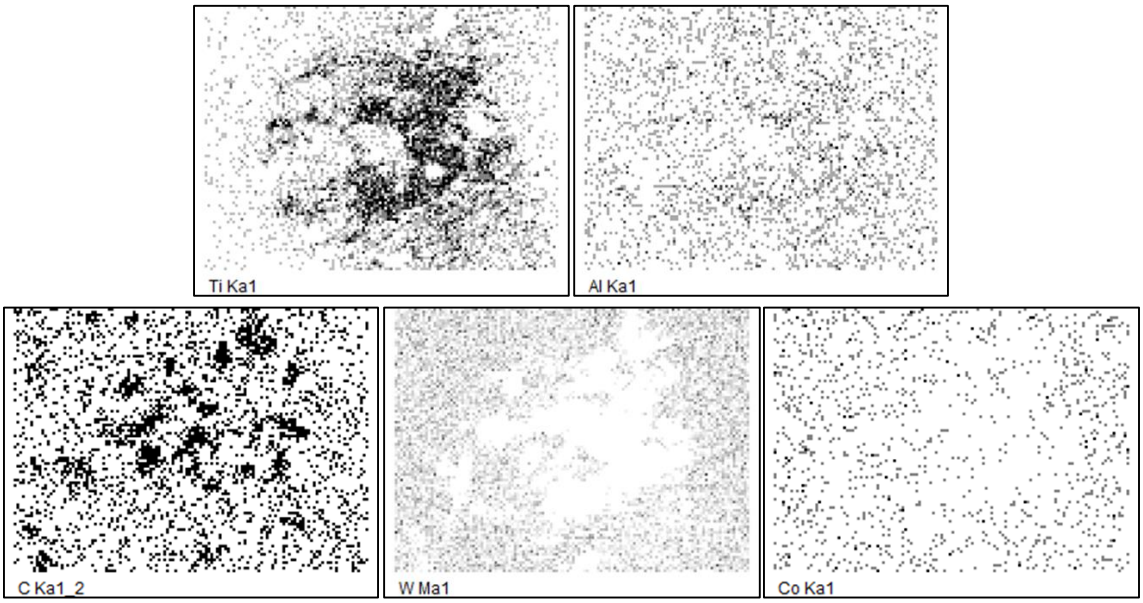

Figure 5-19 EDS images of composition of elements in cutting tool when cutting speed is 120 m/min and the normal load is 2 N. The elements are Ti, V, C, W, and Co from left to right.

5.3 COMPARISON OF WEAR MECHANISM INTERACTION OBSERVATIONS

The seven tribometric bench tests were conducted at low, medium, and high velocity counterparts of machining cutting speeds. Due to the tribometer equipment limitations, the forces had to be scaled. When examining the SEM images and EDS maps of the WC-Co ball, the following major observations were obtained. When considering major wear mechanisms, adhesion and carbon pullout were the main mechanisms observed. When considering major wear mechanism interactions, interaction #1 (adhesion of Ti and diffusion of C into the adhered layer at low velocities) and interaction # 3 (C pullout and deposition at low feed rates) were observed across all velocities of testing. Ti adhesion and the migration of carbon into this adhered titanium layer, which are the characteristics of interaction #1, were observed at all the velocities of bench testing – this confirms interaction #1. Also, adhesion, carbon pullout and deposition, which are the characteristic of interaction #3, were also observed – this confirms the partial occurrence of interaction #3. It is to be noted that crater formation was not expected to be observed in ball-on-disc tribometric testing since the mechanics of chip formation in the cutting process is a different from the sliding contact simulated on the bench tests. Thus, the observance of these interactions in the tribometric testing level confirms the material pair response.

6. CONTROLLING WEAR MECHANISM INTERACTIONS FOR TOOL LIFE OPTIMIZATION (RQ3)

This chapter conducts a preliminary investigation on how machining operational parameters can be controlled to manipulate wear mechanism interactions so as to increase the life of the cutting tool. For this, from experiment results and their analyses, the amount of material lost from the tool body can be roughly estimated on the basis of each wear mechanisms interaction. This is obtained by examining the 3D surface profile to the worn surface of the tool by a non-contact optical surface profiler (white light interferometer).

A representative scenario of estimating the relative amount of material worn away from the tool surface is shown in Figure 6-1. By drawing a suitable line (AB) on the 3D point cloud map of the worn surface of the tool, the associated surface profile (height variations) of the surface is obtained. By quantifying the constituent dimensions, a relative estimate of the material lost due to each major wear mechanism as well as interaction type can be obtained.

On examining the 3D surface profile of the worn cutting tools, it is observed that the volume loss on the tool due interaction #2 is significantly more than that of interaction #1 and interaction #3. This is evident since the volume lost on the tool due to crater formation is much more than that due to carbon pullout as well as any possible adhesive wear when the adhered layer is removed by mechanical action. Thus, the occurrence of interaction #2 or the interaction associated with crater formation needs to be minimized.

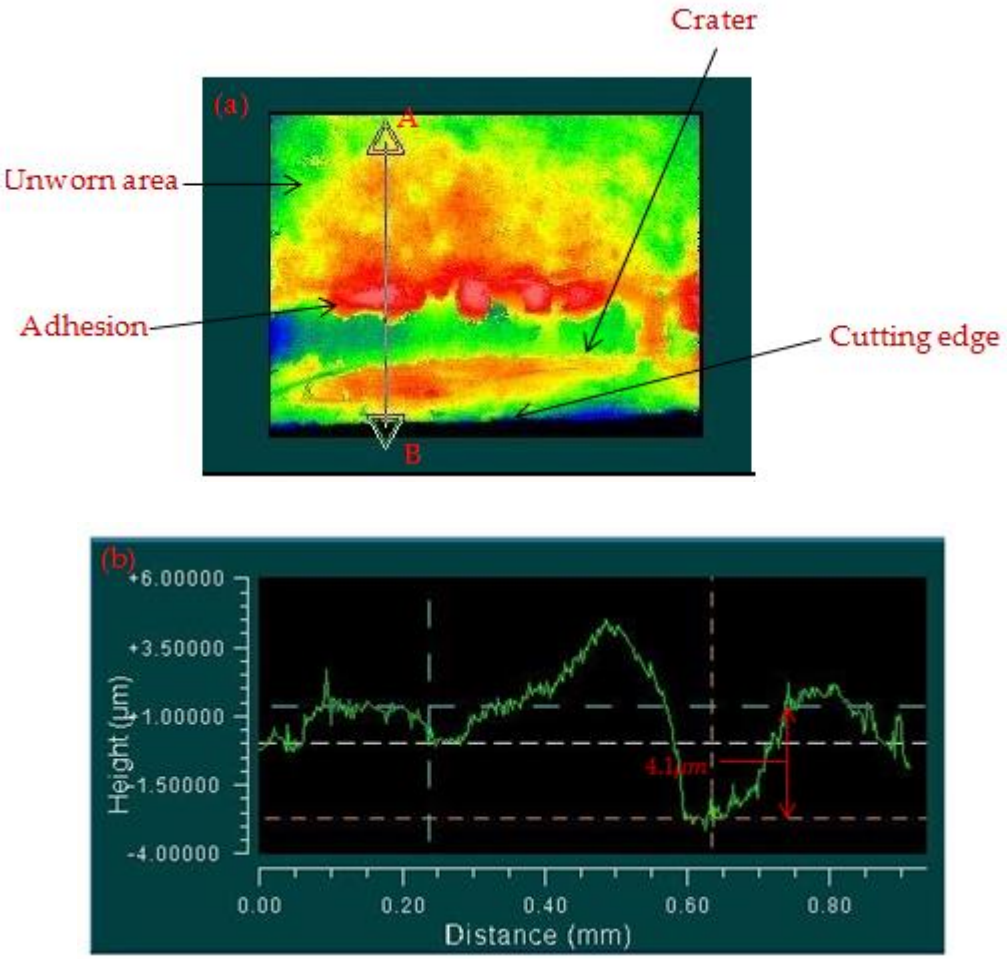

Figure 6-1 (a) 3D image of worn cutting tool (b) Surface profile curve along AB.

For machining, high materials removal rate (MRR) of the workpiece is desired. The MRRs of all nine turning tests are shown in Figure 6-2.

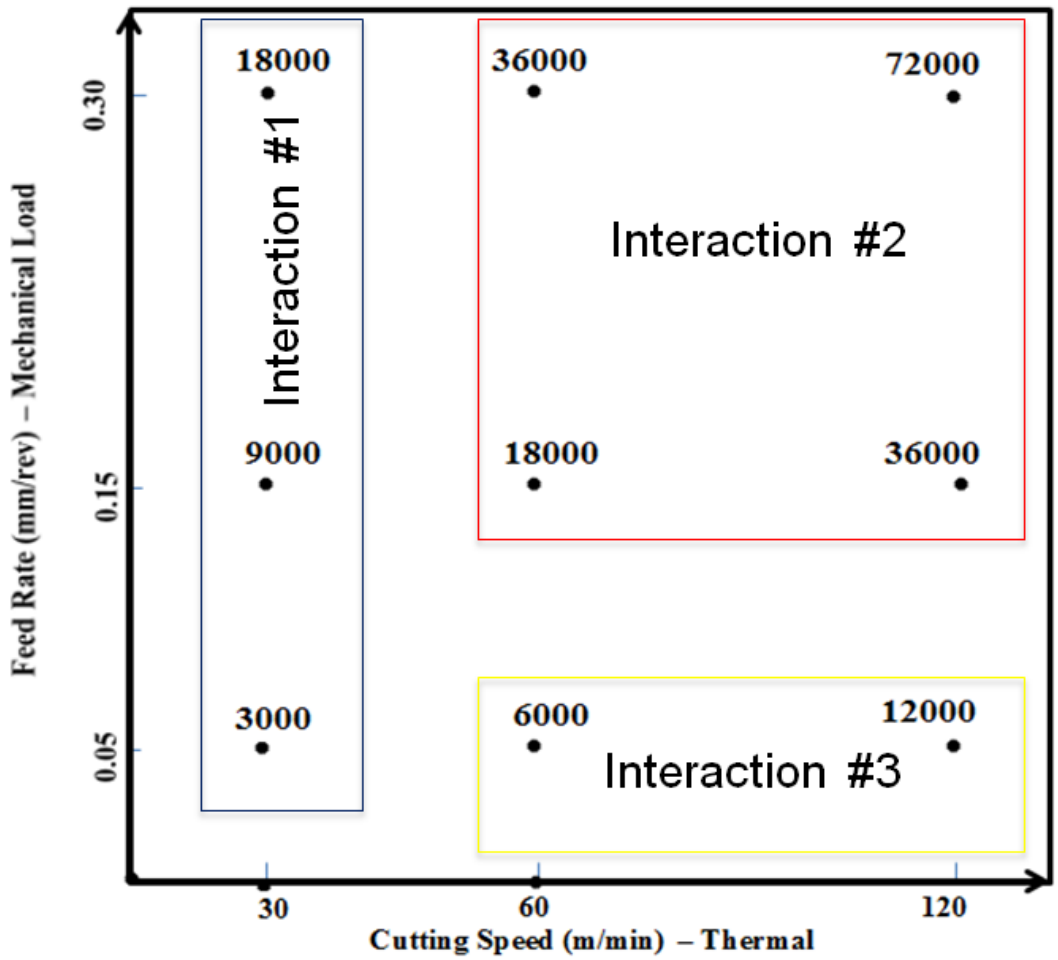

Figure 6-2 Materials removal rate (MRR) during 9 turning tests. (Unit:mm^3/min)

From the view of MRR, the highest MRR can be obtained at high cutting speed and high feed rates, in which interaction #2 occurs. However, this will largely reduce the tool life, which is not desired since this will require more frequent tool changes. This leaves the remaining two interactions (#1 and #3). On comparing these, interaction #1 (low cutting speed and high feed rate) and interaction #3 (high cutting speed and low feed rate) are essentially better operational conditions in terms of net productivity (*i.e.*, balancing cycle time and tool changing time). Between these, the operational condition of the highest cutting speed (120 m/min) is not really preferred due to a greater chance of too failure due to the

associated higher temperatures. Further, on comparing the material removal rates in each condition, this high cutting speed and low feed rate combination has a lower MRR (12,000 mm^3/min) than the high feed rate and low cutting speed combination (18,000 mm^3/min), and hence this operational condition combination is a better one choose for higher tool life and hence net productivity.

7. CONCLUSIONS

Through the above research work involving WC-Co / Ti-6Al-4V tribosystem analysis through machining and tribometric bench tests, major wear mechanisms and interactions between these wear mechanisms have been studied. It was observed that no single wear mechanism occurred individually and that a number of major wear mechanism interactions contributed to the final wear state of the tool.

In the machining tests, three major interactions between wear mechanisms have been identified by their unique features. Interaction #1 occurs at low cutting velocities (temperatures), in which an adhered layer of mostly Ti is observed (whose area increases with feed), and diffusion of (mostly) C occurs from the tool body into *(i)* to the chips as well as *(ii)* to the adhered titanium layer on the tool. Interaction #2 occurs at medium and high cutting velocities, in which a series of events eventually lead to a smooth crater and an adhesion layer of titanium is formed on top of it. Interaction #3 occurs at low feed rates, in which both of C pullout and an adhesion layer formed.

When conducting counterpart ball-on-disc tribometric bench tests to appropriately match the conditions in the machining process in terms of load and speed and to further study the associated material behavior, two of the above interactions were observed. This suggests that such interaction phenomena are intrinsic to the material pair even at scaled force levels.

Following this, the three major wear mechanism interactions were ranked in terms of the amount of tool material work away which was relatively estimates through the 3D surface profiler maps. As a result, interaction #2 was suggested to be avoided, and the other two interactions (#1 and #3) were ranked accordingly to provide competitive material removal rates while maintaining a lower tool wear rates.

Thus, this research work helped provide a better understanding of the interactions between major wear mechanisms in the WC-Co / Ti-6Al-4V machining tribosystem, and recommendations for improving tool life from a mechanism interactions perspective.

REFERENCES

1. Hua, J., Shivpuri, R., A Cobalt Diffusion Based Model for Predicting Crater Wear of Carbide Tools in Machining Titanium Alloys, *Journal of Engineering Materials and Technology*, 2005. 127(1): p. 136-144.

2. Pirso, J., Letunovitš, S., Viljus, M., Friction and Wear Behaviour of Cemented Carbides. *Wear*, 2004. 257(3–4): p. 257-265.

3. Gahr, K., *Microstructure and Wear of Materials.* Elsevier, 1987.

4. Shaw, M., *Metal Cutting Principles.* Oxford Univerisity Press, Oxford, UK, 2004.

5. Kalpakjian, S., Schmid, S., *Manufacturing Processes for Engineering Materials,* Prentice Hall, Upper Saddle River, NJ, 2003.

6. Sandvik Coromant, *Metalcutting Technical Guide*, 2012.

7. Nabhani, F., Machining of aerospace titanium alloys. *Robotics and Computer-Integrated Manufacturing*, 2001. 17(1–2): p. 99-106.

8. Konig, W., Applied Research on the Machinability of Titanium & Its Alloys. *Proc. AGARD Conf. Advanced Fabrication Processes*, 1979. p. 256.

9. Hadzley, A., Finite Element Model of Machining with High Pressure Coolant for Ti-6Al-4V Alloy. P*rocedia Engineering*, 2013. 53(0): p. 624-631.

10. Matikainen, V., Abrasion, Erosion and Cavitation Erosion Wear Properties of Thermally Sprayed Alumina Based Coatings. *Coatings*, 2014. 4(1): p. 18-36.

11. Kuttolamadom, M., Mears, L., Kurfess, T., Choragudi, A., Investigation of the Machining of Titanium Components for Lightweight Vehicles. SAE 2010 World Congress, 2010.

12. Kuttolamadom, M., Prediction of The Wear & Evolution of Cutting Tools in a Carbide / Ti-6Al-4V Machining Tribosystem by Volumetric Tool Wear Characterization & Modeling., Ph.D. Thesis, Clemson University, Clemson, SC, 2012.

13. Astakhov, V., *Tribology of Metal Cutting.* Elsevier, 2006.

14. Upadhyaya, G., *Cemented Tungsten Carbides - Production, Properties, and Testing,.* William Andrew Publishing, United States, 1998.

15. Titanium Information Group, Properties of Titanium Alloys - Ti6Al4V Grade 5, July 30, 2002. *http://www.azom.com/article.aspx?ArticleID=1547.*

16. ASM, *ASM Engineering Materials Reference Book,* 2nd edition, ASM International, 1989, p. 182.

17. Bhushan, B., *Modern Tribology Handbook,* CRC Press, 2000.

18. ASM, *Friction, Lubrication, and Wear Technology.* ASM Handbook, Vol-18.

19. Dmitri Kopeliovich, Mechanisms of Wear, July 2014. *http://www.substech.com/dokuwiki/doku.php?id=mechanisms_of_wear&s=adhesive%20wear*

20. Archard, J., Contact and Rubbing of Flat Surfaces. *J. Appl. Phys.*, 1953. 24: p. 981.

21. ASTM, *Standard Terminology Relating to Wear and Erosion*. Annual Book of Standards. Vol. 03.02. 1987.

22. Stachowiak, G., Andrew W., *Engineering Tribology (3rd Edition),* Butterworth-Heinemann, 2005.

23. Hirst, J., The Wear of Metals under Unlubricated Conditions. *Proc. Roy. Soc.*, 1956. 236: pp. 397-410.

24. Ohnuki, A., Deformation Processing. *JSLE Transactions*, 1983. 28: p. 53-56.

25. Trent, E., *Metal Cutting.* Butterworth-Heinemann, Oxford, UK, 1977.

26. Crosskey, M., M., A Modeling Study of Diffusion Wear of Carbide Tools in Titanium Machining. *Proceedings of the COMSOL Conference,* 2007.

27. Gekonde, H., Subramanian, S., Tribology of tool–chip interface and tool wear mechanisms. *Surface and Coatings Technology*, 2002. 149(2–3): p. 151-160.

28. Odelros, S., *Tool Wear in Titanium Machining*, Master's Thesis, Uppsala University, Sweden, 2012.

29. SLTE, Wear Mechanisms. 2008. *http://www.stle.org/resources/lubelearn/wear/#mechanisms.*

30. Sasada, T., Oike M., Emori, N., The Effect of Abrasive Grain Size on The Transition between Abrasive and Adhesive Wear. *Wear*, 1984. 97(3): p. 291-302.

31. Okonkwo, P., The Effect of Temperature on Sliding Wear of Steel-Tool Steel Pairs. *Wear*, 2012. 282–283(0): p. 22-30.

32. Kagnaya, T., Wear Mechanisms of WC–Co Cutting Tools from High-speed Tribological Tests. *Wear*, 2009. 267(5–8): p. 890-897.

33. Paul, J., Wear Mapping and Wear Characterization Methodology, *Mechanical Tribology*. 2004, CRC Press, UK.

34. Wang, S., Mild-to-severe Wear Transition and Transition Region of Oxidative Wear in Steels. *Wear*, 2013. 306(1–2): p. 311-320.

35. So, H., Chen, H., Chen, L., Extrusion Wear and Transition of Wear Mechanisms of Steel. *Wear*, 2008. 265(7–8): p. 1142-1148.

36. Yang, Q., Senda, T., Ohmori, A., Effect of Carbide Grain Size on Microstructure and Sliding Wear Behavior of HVOF-sprayed WC–12% Co Coatings. *Wear*, 2003. 254(1–2): p. 23-34.

37. Wang, Y., Hsu, S., The Effects of Operating Parameters and Environment on The Wear and Wear Transition of Alumina. *Wear*, 1996. 195(1–2): p. 90-99.

38. Xu, H., Jahanmir, S., Transitions in the mechanism of material removal in abrasive wear of alumina. *Wear*, 1996. 192(1–2): p. 228-232.

39. Cho, S., The Transition from Mild to Severe Wear in Alumina during Sliding. *Acta Metallurgica et Materialia,* 1992. 40(1): p. 185-192.

40. Kato, K., Classification of Wear Mechanisms/Models. *Proceedings of the Institution of Mechanical Engineers, Part J: Journal of Engineering Tribology*, 2002. 216(6): p. 349-355.

41. Falex.com, *The Four-Ball Wear Test Machine,* http://www.falex.com/equipment.html

42. ASTM, Standard Test Method for Wear Preventive Characteristics of Lubricating Grease (Four-Ball Method). ASTM, 2008. D 2266-91.

43. ASTM, Standard Test Method for Wear Testing with a Pin-on-Disk Apparatus. ASTM, 2010. G 99-05.

44. ASTM, Standard Test Method for Ranking Resistance of Materials to Sliding Wear In Block-on-Ring Wear Test Using Micro-Tribometer. ASTM, 2009. G 77-98.

45. ASTM, Standard Test Method for Linearly Reciprocating Ball-on-Flat Sliding Wear. ASTM, 2010. G 133-05.

46. Sen, U., S., Yilmaz, F., Effect of Process Time on The Tribological Properties of Boronized GGG-80 Ductile Cast Iron. *Industrial Lubrication and Tribology,* 2005. 57(6): p. 243-248.

47. Kennedy, D., Methods of Wear Testing for Advanced Surface Coatings and Bulk Materials. *Journal of Materials Processing Technology*, 1998 (77): p. 246-253.

48. Advanced Engine Technology Ltd., Taber Abrasor, http://www.sabreen.com/SabreenArticlePDAprMay05.pdf

49. Falex.com, Falex Air Jet Erosion Test Machine, http://www.falex.com/pdf/FalexAirJetErosion.pdf

50. Maruyama, T., Yokouchi, A., Difference in Preventive Mechanism for Fretting Wear between Oil and Grease Lubrication*. 2014STLE nnual Meeing & Exhibition*, 2014.

51. Van Acker, K., et al., Influence of Tungsten Carbide Particle Size and Distribution on The Wear Resistance of Laser Clad WC/Ni Coatings. *Wear*, 2005. 258(1–4): p. 194-202.

52. Rutherford, K., Hutchings, I., A Micro-abrasive Wear Test, with Particular Application to Coated Systems. *Surface and Coatings Technology*, 1996. 79(1–3): p. 231-239.

53. Voitik, R., Realizing Bench Test Solutions to Field Tribology Problems by Utilizing Tribological Aspect Number*,* Tribology - Wear Test Selection for Design and Application, Ruff A.W and Bayer, R.G., eds., American Society for Testing and Materials, Conshohocken, PA, 1993, ASTM STP 1199, pp. 45-59..

54. Zhao, W., Li, L., Friction and Wear Properties of WC-Co Cemented Carbide Sliding against Ti-6Al-4V Alloy in Nitrogen Gas*. Advanced Materials Research*, 2011. 188: p. p. 49-54.

55. Xu, W., Friction and Wear Properties of Ti-6Al-4V/WC-Co in Cold Atmospheric Plasma Jet. *Applied Surface Science*, 2012. 259(0): p. 616-623.

56. Stachowiak, G.W., *Experimental Methods in Tribology.* Elsevier, 2004.

57. Sandvik, Cemented Carbide, Sandvik New Developments & Applications. *Sandvik Hard Materials*, 2005.

58. ASM, *ASM Handbook Volume 12: Fractography.* ASM International, 1992.

59. Hertzberg, R., *Deformation & Fracture Mechanics of Engineering Materials.* John Wiley & Sons, Inc., NY, USA, 1996.

60. Joshi, V., *Titanium Alloys: An Atlas of Structures and Fracture Features.* CRC Press, 2006.

61. Zhang, S., Investigation on Diffusion Wear during High-speed Machining Ti-6Al-4V Alloy with Straight Tungsten Carbide Tools. *The International Journal of Advanced Manufacturing Technology,* 2009. 44(1-2): p. 17-25.

62. Cook, N., Nayak, P., Development of Improved Cutting Tool Materials. *U.S. Air Force Technical Report,* AFML-TR-69-185, 1969.

63. Hartung, P., *Tool Wear in Titanium Machining.* MIT Press, 1981.

64. Czichos, H., *Tribology: A Systems Approach to The Science and Technology of Friction, Lubrication and Wear*. Elsevier, North-holland, 1978.

65. Burns, T., Materials Modeling: Shear Band Formation in Bulk Metallic Glasses. *Mathematical Modeling in Industry XVII*, 2013.

66. Fischer-Cripps, A., The Hertzian Conatact Surface. *Journal of Materials Science,* 1999. 34: p. 129-137.